Chapter 2
Wire Ropes Under Tensile Load

2.1 Stresses in Straight Wire Ropes

2.1.1 Global Tensile Stresses

The wires in straight wire ropes under tensile load are mainly strained by tensile stresses. The real tensile stress in the wires will not be considered in most cases. Instead of this the stress condition will be normally characterised globally by the rope tensile stress (nominal tensile stress). This global rope tensile stress is

$$\sigma_z = \frac{S}{A}.$$

In this, S is the rope tensile force and A is the wire rope cross-section, that means the sum of the cross sections of all wires in the rope with the diameters δ_i is

$$A = \frac{\pi}{4} \sum \delta_i^2.$$

A very practical form for the tensile rope stress is the diameter related tensile rope force

$$S/d^2.$$

S is again the tensile rope force and d is the nominal rope diameter. This diameter related tensile rope force S/d^2 has the advantage that both factors S and d are well defined and well known for the rope maker and rope user. A further advantage is that in most cases the calculation result encludes in its deviation the deviation of the rope diameter.

K. Feyrer, *Wire Ropes*, DOI: 10.1007/978-3-642-54996-0_2,

2.1.2 Real Stresses

The real stress in wires of the layer k is named σ_{tk} in opposition to the (global) rope tensile stress σ_z. The real wire tensile stress σ_{tk} is bigger than the rope tensile stress σ_z. In addition to the tensile stresses, the wires in ropes under tensile force are strained by bending and torsion stresses and normally slightly by pressure. The stresses in all the individual wires are different:

- Systematically according to the different lay angles of the wire and the strand layers and
- Unsystematically because wires or strands very often are lying loosely on their base and therefore do not start to take up the load from the beginning by increasing the tensile force of the rope.

The unsystematic working stresses may be bigger in some cases than the systematic ones. Of course, they cannot be calculated but their influence can always be observed especially in the rope endurance under fluctuating tensile forces.

Conditions for calculating wire stresses
The working stresses will be determined in the following chapter. Thereby, an ideal wire rope will be presupposed:

- The wire rope is of perfect geometry.
- The wires are without self-contained stresses.
- No wires or strands are loose, so that all wires start to bear when the wire rope will be under a slight tensile force.
- All stresses remain in the elastic region.

The self-contained stresses of the wires resulting from their manufacture have no importance in the case of static loads. In case of fluctuating loading, they influence the endurance like an increasing or a decreasing of the middle stress.

2.1.3 Basic Relation for the Wire Tensile Force in a Strand

A tensile force loading a strand induces a torque because of the helix form of the wires. Therefore the strand will be turning if the strand ends are not secured against this. In practical usage, the turning of strands and ropes must be prevented because otherwise the strand loosens its structure and because of this very unequal stresses would be induced in the wires. For normal ropes, the turning can be only prevented securing the rope ends. In so-called non-rotating ropes, the turning is more or less prevented because the torque of different right or left wound wire layers or strand layers compensate each other. In the following it will be presupposed that the turning of the strands and ropes are prevented.

For one wire, the portion of the tensile strand force S_i in strand axis direction and the corresponding portion of the circumference force U_i out of torque act as

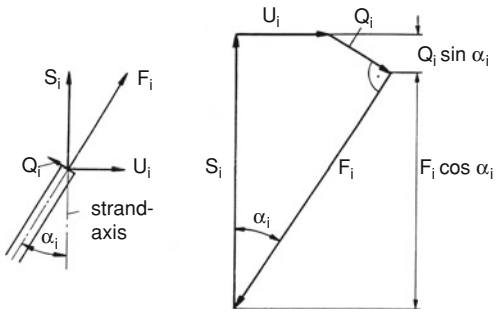

Fig. 2.1 Forces on the wire of a strand

outer forces on the single wire in the wire layer i of a strand. The division of the strand tensile force and torque in the wire forces S_i and U_i will be described later on. For the present, S_i and U_i will be presupposed as known.

Both outer forces S_i and U_i on a wire must be in balance with the inner forces, the wire tensile force F_i and the wire shear force Q_i. The forces on a wire of a wire layer i are shown in Fig. 2.1. From these, using σ_i for the lay angle, both of the following equations can be derived

$$F_i = \frac{S_i - Q_i \cdot \sin \alpha_i}{\cos \alpha_i} \tag{2.1}$$

and

$$U_i = F_i \cdot \sin \alpha_i - Q_i \cdot \cos \alpha_i. \tag{2.2}$$

The shear force Q_i of a wire of layer i is caused by the bending and torsion of this wire, of course geometrically limited by the rope extension. As was first presented by Berg (1907), the shear force of a wire in layer i is

$$Q_i = \frac{\sin \alpha_i}{r_i} . \left(M_{\mathrm{b},i} \cdot \cos \alpha_i - M_{\mathrm{tor,i}} \cdot \sin \alpha_i \right) \tag{2.3}$$

with the wire winding radius $r_{W,i} = r_i$, the bending moment $M_{\mathrm{b},i}$ around the binormal and the torque $\mathrm{M_{tor,i}}$ around the wire axis. With this the tensile force in a wire of the wire layer i is

$$F_i = \frac{S_i}{\cos \alpha_i} - \frac{\sin^2 \alpha_i}{r_i \cdot \cos \alpha_i} \cdot \left(M_{\mathrm{b,i}} \cdot \cos \alpha_i - M_{\mathrm{tor,i}} \cdot \sin \alpha_i \right). \tag{2.4}$$

According to Berg (1907), the portion of the strand torsion moment caused by a wire of the wire layer i is

$$M_i = F_i \cdot r_i \cdot \sin\alpha_i - Q_i \cdot r_i \cdot \cos\alpha_i + M_{\mathrm{b,i}} \cdot \sin\alpha_i + M_{\mathrm{tor,i}} \cdot \cos\alpha_i. \tag{2.5}$$

The most recent equations for bending and torsion moment for a wire of the wire layer i were developed by Czitary (1952) as follows

$$M_{\mathrm{b},i} = E_i \cdot J_i \cdot \left(\frac{\sin^2\alpha_i}{r_i} - \frac{\sin^2\alpha_{0i}}{r_{0i}} \right) \tag{2.6}$$

and

$$M_{\mathrm{tor},i} = G_i \cdot J_{\mathrm{p}i} \cdot \left(\frac{\sin\alpha_i \cdot \cos\alpha_i}{r_i} - \frac{\sin\alpha_{0i} \cdot \cos\alpha_{0i}}{r_{0i}} \right). \tag{2.7}$$

In addition to the known symbols, there is E_i the elasticity module, G_i the shear module, J_i the equatorial and $J_{\mathrm{p}i}$ the polar moments of inertia of a wire in the wire layer i. The index 0 means the state before loading by a tensile force. As before, the parameters without the index 0 show the loaded state.

The portion of the strand torque for one wire of the wire layer i can be calculated from (2.3), (2.5)–(2.7)

$$M_i = F_i \cdot r_i \cdot \sin\alpha_i - M_{\mathrm{b,i}} \cdot \sin\alpha_i \cdot \left(1 + \cos^2\alpha_i\right) + M_{\mathrm{tor},i} \cdot \cos^3\alpha_i. \tag{2.8}$$

Both of the moments $M_{\mathrm{b}i}$ and $M_{\mathrm{t}i}$ are very small, because the lay angle and the winding radius alter only slightly under the tensile load. Therefore, the shear force Q_i is also very slight. As demonstrated by Czitary (1952), both moments and the shear force can be neglected for the calculation of the wire tensile force F_i. This neglect only results in a very minimal deviation. With this, out of (2.1) the simple relation for the tensile force in a wire in the layer i depicted in Fig. 2.2 is

$$F_i = \frac{S_i}{\cos\alpha_i} \tag{2.9}$$

and the circumference force out of (2.2) is

$$U_i = F_i \cdot \sin\alpha_i$$

or

$$U_i = S_i \cdot \tan\alpha_i. \tag{2.10}$$

According to (2.4), the portion of the strand torque for a wire in the layer i is now

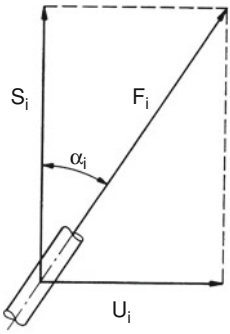

Fig. 2.2 Tensile force of a strand wire neglecting the small shear force

$$M_i = F_i \cdot r_i \cdot \sin \alpha_i$$

or

$$M_i = S_i \cdot r_i \cdot \tan \alpha_i \tag{2.11}$$

These equations from Berg (1907) have since been used by nearly all researchers, as for example Heinrich (1937), Costello (1997), Costello and Sinha (1977b). Only Dreher (1933), who first did extensive investigations into wire rope torsion has introduced a basic equation deviating from (2.9). But Dreher's equation is of no value for use with real wire ropes as Heinrich (1942) has already shown. Dreher's equation is only true for a simple wire helix not supported by a strand centre.

A length-related radial force exists between the wire helix and the centre wire or a wire layer (or between a helix strand and the core) in a wire rope under a tensile force. The length-related radial force (when neglecting the bending moment and torque) is

$$q_i = \frac{F_i}{\rho_i} = \frac{F_i \cdot \sin^2 \alpha_i}{r_i}. \tag{2.12}$$

2.1.4 Wire Tensile Stress in the Strand or Wire Rope

2.1.4.1 Wire Tensile Stress in Strand or Spiral Rope

The first to work out a partition of the wire rope tensile force in wire tensile forces was Benndorf (1904). The following determination of the tensile stress follows his work. Out of the last chapter with (2.9), the wire tensile force component in strand axe direction (neglecting the small shear force) is

$$S_i = F_i \cdot \cos \alpha_i.$$

The strand tensile force is the sum of all wire tensile force components

$$S = \sum_{i=0}^{n} z_i \cdot S_i = \sum_{i=0}^{n} z_i \cdot F_i \cdot \cos \alpha_i \tag{2.13}$$

In addition to the known symbols, n is the number of wire layers counted from the inside with $n = 0$ for the centre wire and z_i is the number of wires in the wire layer i.

For the following, it will be presupposed that the strand cross-section rests plane if the strand with the length l_S is elongated with Δl_S by a tensile force. The elongation can now be calculated and, from this, the tensile force of all the wires. The tensile force of a wire in a wire layer i is

$$F_i = \frac{\Delta l_i}{l_i} \cdot E_i \cdot A_i. \tag{2.14}$$

l_i is the wire length, Δl_i the wire elongation, E_i the elasticity module and A_i the cross-section of a wire in the wire layer i. The extension of that wire is

$$\varepsilon_i = \frac{\Delta l_i}{l_i}. \tag{2.15}$$

With l_S for the length of the strand, the length of the wire is

$$l_i = \frac{l_\mathrm{S}}{\cos \alpha_i}. \tag{2.16}$$

In Fig. 2.3, the unwound wire about the strand axis is shown before and after the strand elongation. Therefore, when the failures of higher classification are neglected, then the wire elongation is

$$\Delta l_i = (\Delta l_S - \Delta u_i \cdot \tan \alpha_i) \cdot \cos \alpha_i$$

or

$$\Delta l_i = \Delta l_S \cdot \cos \alpha_i - \Delta u_i \cdot \sin \alpha_i. \tag{2.17}$$

The contraction of the winding radius respectively the circumference in relation to the wire extension—that transverse contraction ratio can also be designated as "Poisson's ratio" of the wire helix—is

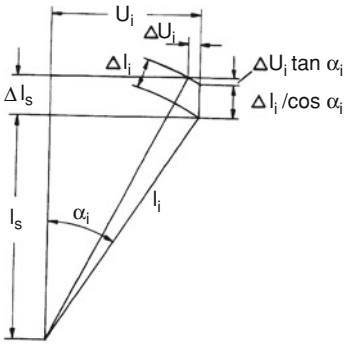

Fig. 2.3 Elongation of a strand wire

$$v_i = \frac{\Delta u_i / u_i}{\Delta l_i / l_i}.$$

Here u_i is the winding circumference and Δu_i its contraction. Using this and (2.15), the contraction of the winding circumference is

$$\Delta u_i = \varepsilon_i \cdot v_i \cdot u_i$$

and with $u_i = l_i \cdot \sin \alpha_i$ is

$$\Delta u_i = \varepsilon_i \cdot v_i \cdot l_i \cdot \sin \alpha_i. \tag{2.18}$$

Using (2.17) and (2.18), the wire elongation is then

$$\Delta l_i = \Delta l_S \cdot \cos \alpha_i - \varepsilon_i \cdot v_i \cdot l_i \cdot \sin^2 \alpha_i$$

or

$$\Delta l_i + \Delta l_i \cdot v_i \cdot \sin^2 \alpha_i = \Delta l_S \cdot \cos \alpha_i.$$

Following this, the elongation of a wire in the wire layer i is

$$\Delta l_i = \frac{\Delta l_S \cdot \cos \alpha_i}{1 + v_i \cdot \sin^2 \alpha_i}. \tag{2.19}$$

This equation together with (2.14) and (2.16) supplies the tensile force of a wire in the wire layer i as a function of the strand elongation

$$F_i = \frac{\Delta l_S \cdot \cos^2 \alpha_i}{l_S \cdot \left(1 + v_i \cdot \sin^2 \alpha_i\right)} \cdot E_i \cdot A_i \tag{2.20}$$

or its component in the direction of the strand

$$S_i = \frac{\Delta l_S \cdot \cos^2 \alpha_i}{l_S \cdot \left(1 + v_i \cdot \sin^2 \alpha_i\right)} \cdot E_i \cdot A_i. \tag{2.20a}$$

Using (2.13) the strand tensile force is

$$S = \frac{\Delta l_S}{l_S} \cdot \sum_{i=0}^{n} \left(\frac{z_i \cdot \cos^3 \alpha_i}{1 + v_i \cdot \sin^2 \alpha_i} \cdot E_i \cdot A_i \right). \tag{2.21}$$

The tensile force in a wire of a specific wire layer k is found by combining (2.20) and (2.21) with the elimination of $\Delta l_S / l_S$

$$F_k = \frac{\frac{\cos^2 \alpha_k}{1 + v_k \cdot \sin^2 \alpha_k} \cdot E_k \cdot A_k}{\sum_{i=0}^{n} \left(\frac{z_i \cdot \cos^3 \alpha_i}{1 + v_i \cdot \sin^2 \alpha_i} \cdot E_i \cdot A_i \right)} \cdot S. \tag{2.22}$$

The tensile stress in this wire is

$$\sigma_{tk} = \frac{F_k}{A_k} = \frac{\frac{\cos^2 \alpha_k}{1 + v_k \cdot \sin^2 \alpha_k} \cdot E_k}{\sum_{i=0}^{n} \left(\frac{z_i \cdot \cos^3 \alpha_i}{1 + v_i \cdot \sin^2 \alpha_i} \cdot E_i \cdot A_i \right)} \cdot S. \tag{2.23}$$

2.1.4.2 Wire Tensile Stress in Stranded Ropes

As before, the same derivation can be used for the stranded rope by now observing a strand as a wire. The wire layers keep the counting index i and a certain wire layer the index k, whereas the strand has the respective indices j and l. The total number of wire layers in a strand is n_W and the total number of strand layers is n_s.

The wire rope tensile force is according to (2.13)

$$S = \sum_{j=0}^{ns} F_j \cdot z_j \cdot \cos \beta_j$$

and with the strand tensile force

$$F_j = \sum_{i=0}^{n_{wj}} F_{ij} \cdot z_{ij} \cdot \cos \alpha_{ij}$$

the wire rope tensile force is

$$S = \sum_{j=0}^{n_S} z_j \cdot \cos \beta_j \cdot \sum_{i=0}^{n_{wj}} F_{ij} \cdot z_{ij} \cdot \cos \alpha_{ij}. \tag{2.24}$$

According to (2.20), the wire tensile force in the wire layer i of the strand j is

$$F_{ij} = \frac{\Delta l_j}{l_j} \cdot \frac{\cos^2 \alpha_{ij}}{1 + v_{ij} \cdot \sin^2 \alpha_{ij}} \cdot E_{ij} \cdot A_{ij} \tag{2.25}$$

and according to (2.19) and the wire rope length $L = l_j \cdot \cos \beta_j$

$$\frac{\Delta l_j}{l_j} = \frac{\Delta L}{L} \cdot \frac{\cos^2 \beta_j}{1 + v_j \cdot \sin^2 \beta_j}. \tag{2.26}$$

Then, using (2.25) and (2.26), the tensile force of a wire ij is

$$F_{ij} = \frac{\Delta L}{L} \cdot \frac{\cos^2 \beta_j}{1 + v_j \cdot \sin^2 \beta_j} \cdot \frac{\cos^2 \alpha_{ij}}{1 + v_{ij} \cdot \sin^2 \alpha_{ij}} \cdot E_{ij} \cdot A_{ij}. \tag{2.27}$$

Using (2.27) and (2.24), the wire rope tensile force is

$$S = \frac{\Delta L}{L} \cdot \sum_{j=0}^{n_S} \left(z_j \cdot \frac{\cos^3 \beta_j}{1 + v_j \cdot \sin^2 \beta_j} \cdot \sum_{i=0}^{n_{wj}} z_{ij} \cdot \frac{\cos^3 \alpha_{ij}}{1 + v_{ij} \cdot \sin^2 \alpha_{ij}} \cdot E_{ij} \cdot A_{ij} \right). \tag{2.28}$$

Combining (2.27) and (2.28) by eliminating $\Delta L/L$, the tensile force in the certain wire k in the strand l is

$$F_{kl} = \frac{\dfrac{\cos^2 \beta_l}{1 + v_l \cdot \sin^2 \beta_l} \cdot \dfrac{\cos^2 \alpha_{kl}}{1 + v_{kl} \cdot \sin^2 \alpha_{kl}} \cdot E_{kl} \cdot A_{kl} \cdot S}{\sum_{j=0}^{n_s} \left(z_j \cdot \dfrac{\cos^3 \beta_j}{1 + v_j \cdot \sin^2 \beta_j} \cdot \sum_{i=0}^{nw} z_{ij} \cdot \dfrac{\cos^3 \alpha_{ij}}{1 + v_{ij} \cdot \sin^2 \alpha_{ij}} \cdot E_{ij} \cdot A_{ij} \right)} \tag{2.29}$$

and the tensile stress in that wire is

$$\sigma_{tkl} = \frac{F_{kl}}{A_{kl}}. \tag{2.30}$$

2.1.4.3 Influence of the Poisson Ratio

The Poisson ratio (transverse contraction ratio) for steel $v_i = 0.3$ can also be used for the steel wire helix in the strands. Because the length-related radial force between the wires is very small, the reduction of the wire diameter and winding

radius or circumferences in the strands, in the spiral ropes and in the strands of the stranded ropes are practically only caused by the elongation of the wires. This is especially true for the most frequently used parallel lay ropes.

The transverse contraction ratio of the strand helix v_j in stranded ropes is difficult to estimate. Especially in wire ropes with a fibre core, this "Poisson ratio" is very large. In any case of fluctuating force, there is a great part of the rope contraction and the rope elongation remaining.

The influence of the Poisson ratio of the wires and the "Poisson ratio" of the winding radius or circumferences of wires on the calculated distribution of the wire tensile forces is normally not very large. For strands, the influence reduces with the increasing number of wires. For a parallel wire strand with 19 wires, the calculated stress of the outer wires is at the most 2 % more and that of the centre wire 3 % less if the Poisson ratios are neglected.

The influence of the Poisson ratios of wires and of winding circumferences of wires and strands on the wire tensile stress is also small for the stranded ropes. This is true for ropes with steel cores because the "Poisson ratio" v_j is also small. For ropes with fibre cores, the contraction can be quite large. However, the influence on the distribution of tensile forces of the strands is small.

However, unlike with the calculation of the wire tensile stresses, the "Poisson ratio" v_j must used as precisely as possible if the equations given here are to be used later on to calculate the additional stresses, the rope elongation or the rope elasticity module. The Poisson ratio $v = 0.3$ can continue to be used for the strands and spiral wire ropes. But that is not valid for the strand helix (strand axis) in stranded ropes.

The cross-section of fibre cores and their effective diameter are very greatly reduced under the effect of the length-related radial force of the bearing strands. This is also true to a lesser extent for wire ropes with steel cores especially for wire ropes with several strand layers especially if the strand layers lie parallel. The "Poisson ratio" of the strand winding radius of these wire ropes is not constant as it depends on the wire rope stress. The "Poisson ratio" of the stranded wire ropes can generally only evaluated by measurement and not by calculation.

2.1.4.4 Wire Tensile Stress Neglecting the Poisson Ratios

If the tensile force of the wires in strands or wire ropes is calculated by neglecting the "Poisson ratios", the equations are much simpler. The tensile force in a strand is in this case

$$S = \frac{\Delta l_S}{l_S} \cdot \sum_{i=0}^{n_W} z_i \cdot \cos^3 \alpha_i \cdot E_i \cdot A_i \tag{2.21a}$$

and the tensile force in the wire k is

$$F_k = \frac{\cos^2 \alpha_k \cdot E_k \cdot A_k}{\sum_{i=0}^{n_W} Z_i \cdot \cos^3 \alpha_i \cdot E_i \cdot A_i} \cdot S. \tag{2.22a}$$

By neglecting the contraction, the tensile force of the stranded rope is

$$S = \frac{\Delta L}{L} \cdot \sum_{j=0}^{n_S} \left(z_j \cdot \cos^3 \beta_j \cdot \sum_{i=0}^{n_{Wj}} z_{ij} \cdot \cos^3 \alpha_{ij} \cdot E_{ij} \cdot A_{ij} \right) \tag{2.28a}$$

and the tensile force in the wire k of the strand l is

$$F_{kl} = \frac{\cos^2 \beta_l \cdot \cos^2 \alpha_{kl} \cdot E_{kl} \cdot A_{kl}}{\sum_{j=0}^{n_S} \left(z_j \cdot \cos^3 \beta_j \cdot \sum_{i=0}^{n_{wj}} z_{ij} \cdot \cos^3 \alpha_{ij} \cdot E_{ij} \cdot A_{ij} \right)} \cdot S. \tag{2.29a}$$

The wire tensile stresses in the spiral rope and in the stranded rope are

$$\sigma_{tk} = \frac{F_k}{A_k} \quad \text{and} \quad \sigma_{tkl} = \frac{F_{kl}}{A_{kl}}.$$

All wires have nearly the same tensile stress if a wire rope has a fibre core and the same lay angle for all wire layers (except, of course, the centre wires in the strands which have a higher stress than the other wires). This common tensile stress is

$$\sigma_t = \frac{S}{A \cdot \cos \alpha \cdot \cos \beta}. \tag{2.31}$$

This equation was previously given by Wiek (1980). In the outer wires, the tensile stress is a little smaller than as calculated in (2.31).

Example 2.1: *Wire tensile stress in spiral wire ropes*

Calculation of the tensile stress in the wires of the open spiral wire rope 1 × 37 according to Fig. 2.4 with the global wire rope tensile stress $\sigma_z = 300$ N/mm^2.

The tensile force of the spiral rope, is

$$S = A_m \cdot \sigma_z = (1.431 + (6 + 12 + 18) \cdot 1.227) \cdot \sigma_z = 45.61 \cdot 300 = 13{,}680\,\text{N}.$$

Using (2.23), the tensile stress in the centre wire is

$$\sigma_{t0} = \frac{45.61 \cdot \sigma_z}{1.431 + \frac{0.9703^3}{1 + 0.3 \cdot 0.2419^2} \cdot (6 + 12 + 18) \cdot 1.227} = \frac{45.61}{41.09} \cdot \sigma_z$$

$$\sigma_{t0} = 1.110 \cdot \sigma_z = 333\,\text{N/mm}^2.$$

With the same Eq. (2.23), the tensile stress in the wires of the layers 1, 2 and 3 with the same lay angle $\alpha = 14°$ is

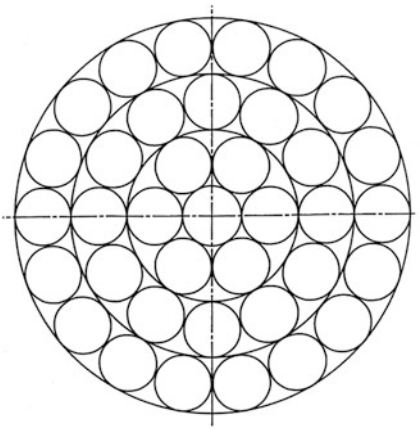

Fig. 2.4 Cross-section of a spiral rope 1 × 37, wire diameters $\delta_0 = 1.35$ mm, $\delta_1 = \delta_2 = \delta_3 = 1.25$ mm; wire cross sections $A_0 = 1.431$ mm^2, $A_1 = A_2 = A_3 = 1.227$ mm^2; lay angles $\alpha_1 = 0°$, $\alpha_1 = 14°$, $\alpha_2 = -14°$, $\alpha_3 = 14°$

$$\sigma_{t,1,2,3} = \frac{\dfrac{0.9703^2}{1 + 0.3 \cdot 0.2419^2} \cdot 45.61 \cdot \sigma_z}{41.09}$$
$$\sigma_{t,1,2,3} = 1.027 \cdot \sigma_z = 308\,\text{N/mm}^2.$$

2.1.5 Additional Wire Stresses in the Straight Spiral Rope

A straight spiral rope respectively a straight strand becomes longer and thinner under a tensile force. The wire helix will be deformed and—beside the tensile stress—there exist bending stresses, torsion stresses and radial pressures from the small length-related radial force of the wires. The bending and torsion stresses have to be calculated from the alteration in the space curve of the wire.

The space curve of a wire in a straight strand is in parameter form

$$\begin{aligned} x &= -r \cdot \sin\varphi \\ y &= r \cdot \cos\varphi \\ z &= \frac{r}{\tan\alpha} \cdot \varphi. \end{aligned} \tag{2.32}$$

φ is the angle of rotation (running angle), α the lay angle and $r_W = r$ the wire winding radius, Fig. 2.5. The lay length is

$$h_W = \frac{2 \cdot \pi \cdot r}{\tan\alpha}.$$

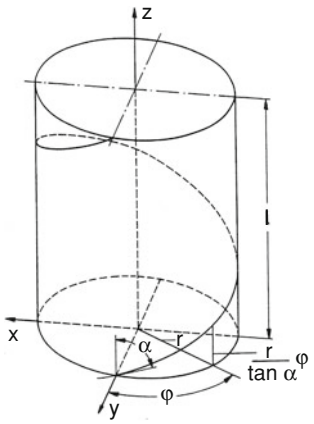

Fig. 2.5 Wire space curve in a straight spiral rope

Although the moments M_b and M_{tor} out of (2.6) and (2.7) can be neglected in calculating the wire tensile force, the bending and torsion stresses resulting from these moments can be considerable. The stresses come from the change of the curvature K and the winding T.

The curvature K of a space curve is in parameter form according to (2.32) with the curvature radius ρ

$$K = \frac{1}{\rho}$$

$$K = \sqrt{\frac{(x'^2 + y'^2 + z'^2) \cdot (x''^2 + y''^2 + z''^2) - (x' \cdot x'' + y' \cdot y'' + z' \cdot z'')^2}{(x'^2 + y'^2 + z'^2)^3}}. \tag{2.33}$$

The winding T shows how strongly the space curve differs from the osculating plane in the neighbourhood of a point. The winding is

$$T = \rho^2 \cdot \frac{\begin{vmatrix} x' & y' & z' \\ x'' & y'' & z'' \\ x''' & y''' & z''' \end{vmatrix}}{(x'^2 + y'^2 + z'^2)^3}. \tag{2.34}$$

For the simple case of a wire in a straight strand or spiral rope with the wire winding radius r, the curvature radius ρ is

$$\rho = \frac{r}{\sin^2 \alpha} \tag{2.35}$$

and the winding

$$T = \frac{\sin \alpha \cdot \cos \alpha}{r}. \tag{2.36}$$

The stresses in the wires induced by the alteration of the wire curvature are of special interest. Together with the tensile stresses, they determine the endurance of the strand or spiral rope in the case of fluctuating tensile force.

The bending stress is

$$\sigma_b = \left(\frac{1}{\rho} - \frac{1}{\rho_0}\right)\frac{\delta}{2}E \tag{2.37}$$

or with (2.35)

$$\sigma_b = \left(\frac{\sin^2\alpha}{r} - \frac{\sin^2\alpha_0}{r_0}\right)\frac{\delta}{2}E. \tag{2.37a}$$

The torsion stress is

$$\tau = (T - T_0)\frac{\delta}{2}G \tag{2.38}$$

and with (2.36)

$$\tau = \left(\frac{\sin\alpha\cos\alpha}{r} - \frac{\sin\alpha_0\cos\alpha_0}{r_0}\right)\frac{\delta}{2}G. \tag{2.38a}$$

In addition to the symbols already known, δ is the wire diameter. The index 0 is again of value for the initial state and the symbols without indices designate the state under the effect of tensile force. E is again the elasticity module and G is the shear module. The bending and torsion stresses were first calculated by Schiffner (1986).

Example 2.2: *Additional stresses in a spiral rope*

Calculation of the bending and torsion stresses in the wires of an open spiral rope according Fig. 2.4 with the global wire rope stress $\sigma_z = 300$ N/mm^2 (neglecting the influence of the point pressure between the crossing wires).

The winding radius under the effect of the tensile force is (neglecting the small higher tensile stress in the centre wire) with $\sigma_t = \sigma_{t,1,2,3}$

$$r_i = r_{0i}\left(1 - \nu\frac{\sigma_t}{E}\right) = r_{0i}\left(1 - 0.3\frac{308}{196{,}000}\right) = 0.99953 r_{0i}$$

and the lay angle

$$\sin\alpha = \sin\alpha_0 \cdot \frac{1 - \nu\cdot\frac{\sigma_t}{E}}{1 + \frac{\sigma_t}{E}} = \sin\alpha_0 \cdot \frac{1 - 0.3\cdot\frac{308}{196,000}}{1 + \frac{308}{196{,}000}}.$$

$$\alpha_0 = 14^\circ; \quad \sin\alpha_0 = 0.24192; \quad \cos\alpha_0 = 0.97030$$

$$\sin\alpha = 0.9980 \cdot \sin\alpha_0 = 0.9980 \cdot 0.24192 = 0.24144$$

$$\cos\alpha = 0.97042.$$

According to (2.37a), the bending stress in the wires of the different wire layers is

$$\sigma_{bi} = \left(\frac{0.9980^2 \cdot \sin^2 \alpha_0}{0.99953 \cdot r_{0i}} - \frac{\sin^2 \alpha_0}{r_{0i}} \right) \cdot \frac{\delta}{2} \cdot E = 0.00354 \cdot \frac{0.2419^2}{r_{0i}} \cdot \frac{1.25}{2} \cdot 196{,}000$$

$$\sigma_{bi} = \frac{25.4}{r_{0i}}.$$

According to (2.38a), the torsion stress is

$$\tau_i = \left(\frac{0.23430}{0.99953 \cdot r_{0i}} - \frac{0.23473}{r_{0i}} \right) \cdot \frac{1.25}{2} \cdot 76{,}000 = \frac{15.2}{r_{0i}}.$$

Then with $r_{01} = 1.3$ mm, $r_{02} = 2.55$ mm, $r_{03} = 3.8$ mm, the bending stresses are

$$\sigma_{b1} = 19.4 \text{ N/mm}^2; \quad \sigma_{b2} = 9.9 \text{ N/mm}^2; \quad \sigma_{b3} = 6.7 \text{ N/mm}^2$$

and the torsion stresses are

$$\tau_1 = 11.7 \text{ N/mm}^2; \quad \tau_2 = 6.0 \text{ N/mm}^2; \quad \tau_3 = 4.0 \text{ N/mm}^2.$$

As shown in the example, the additional wire stresses in spiral ropes are not very large.

2.1.6 Additional Wire Stresses in Straight Stranded Ropes

The wires of straight stranded wire ropes under tensile force are loaded like the wires in spiral ropes by bending and torsion stresses. Besides that, they are loaded with a second tensile stress caused by friction between the wires in the bent strands, Schmidt (1965). The additional stresses will be evaluated using the space curves of the strands and the wires.

According to (2.32), the equations for the space curve of the strand axis in a straight stranded rope are

$$\begin{aligned} x_S &= -r_S \cdot \sin \varphi_S \\ y_S &= r_S \cdot \cos \varphi_S \\ z_S &= \frac{r_S}{\tan \beta} \varphi_S \end{aligned} \tag{2.39}$$

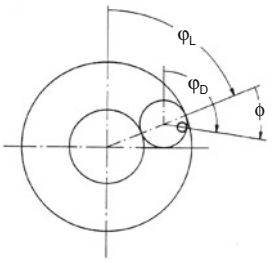

Fig. 2.6 Winding angle of a wire in the wire rope cross section, normative phase angle Φ

with r_S for the strand winding radius, β for the strand lay angle and φ_S for the angle of rotation of the strand helix. The strand lay length is

$$h_S = \frac{2 \cdot \pi \cdot r_S}{\tan \beta}.$$

Andorfer (1983) derived analytically the equations for the space curve of the double helix of the wire in the straight stranded rope as done before by Bock (1909) using a kinematic method and later on by Wolf (1984) using a vectoral method. The wire winding radius r stands perpendicular on the strand axe helix and the ratio between the wire winding angle φ_W and the strand winding angle φ_S is constant, $\varphi_W/\varphi_S = \text{const}$. Schiffner (1986) pointed out that this constant ratio practically always occurs if the clearance between the wires is—as usual—very small.

The constant ratio between both winding angles φ_W and φ_S is only valid if they both start from $\varphi_W = \varphi_S = 0$. The constant ratio of the winding angles is therefore better described by

$$m^* = \frac{h_S}{h_W \cdot \cos \beta}.$$

That means in any one strand lay length h_S there are m^* wire lay lengths h_W. With $m = m^* \pm 1$ is

$$\varphi_W \pm \varphi_S = m \cdot \varphi_S = \Phi.$$

Bock (1909) nominated Φ as normative phase angle. After $\Phi = 2\pi$, a wire element has the same position as for $\Phi = 0$, Fig. 2.6. The positive sign has to be set for ordinary lay ropes and the negative for lang lay ropes.

To include the case of any phase of φ_W and φ_S a constant winding angle of the wire helix φ_{W0} or shorter φ_0 will be added. Then it is

$$\varphi_W \pm \varphi_S + \varphi_0 = m \cdot \varphi_S + \varphi_0.$$

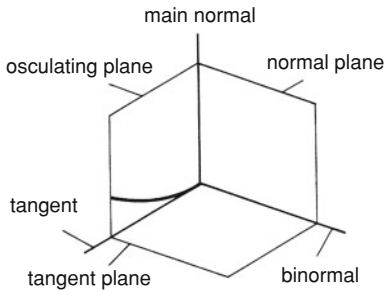

Fig. 2.7 Moving trihedral (tangent, main normal and binormal) of a space curve

With this, for the space curve for a wire in a straight stranded wire rope, the equations of Andorfer (1983) are in parameter form

$$\begin{aligned} x &= -r_S \cdot \sin\varphi_S \\ &\quad - r_W \cdot [\cos(\varphi_0 + m \cdot \varphi_S) \cdot \sin\varphi_S + \sin(\varphi_0 + m \cdot \varphi_S) \cdot \cos\beta \cdot \cos\varphi_S] \\ y &= r_S \cdot \cos\varphi_S \\ &\quad + r_W \cdot [\cos(\varphi_0 + m \cdot \varphi_S) \cdot \cos\varphi_S - \sin(\varphi_0 + m \cdot \varphi_S) \cdot \cos\beta \cdot \sin\varphi_S] \\ z &= \frac{h_S}{2 \cdot \pi} \cdot \varphi_S - r_W \cdot \sin(\varphi_0 + m \cdot \varphi_S) \cdot \sin\beta. \end{aligned} \tag{2.40}$$

The Eq. (2.37) for the bending stress can only used for the strand center wires of stranded ropes. For the lay wires in the strands this simple equation is not valid, because the curvature plane turns around the wire axis against the wire. Determinant for the change of bending stress is therefore not only the change of the curvature radius ρ but also the turning angle γ_k so that the maximum bending stress occurs in another fibre of the wire. Leider (1977) presented firstly this fact in case of bending a strand. Schiffner (1986)—respecting this—calculated the wire bending and torsion stresses by changing the space curve in a stranded rope under the action of the wire rope tensile force. Depending on the small rope elongation and diameter reduction under rope tensile forces these stresses are also small (Fig. 2.7).

The effect of the turning angle γ_k on the wire bending stress can be demonstrated for the case when a strand is bent over a sheave. For the straight strand the curvature radius of a lay wire is $\rho_0 = r_W/\sin^2\alpha$. For the bent strand Wiek (1981) and with a small correction Leider (1977) have derived the curvature radius ρ of lay wires for the different position of the wire element in relation to the sheave axis. As turning angle Leider (1977) has used the angle between the main normals but Schiffner (1986) found, that the angle between the osculating plane before changing and the main normal after changing is correct for the turning angle

$$\gamma_k = \arcsin \frac{A \cdot a + B \cdot b + C \cdot c}{\sqrt{(A^2 + B^2 + C^2) \cdot (a^2 + b^2 + c^2)}} \tag{2.41}$$

with

$$\begin{aligned} A &= y_0' \cdot z_0'' - z_0' \cdot y_0'' \\ B &= z_0' \cdot x_0'' - x_0' \cdot z'' \\ C &= x_0' \cdot y_0'' - y_0' \cdot x_0'' \end{aligned}$$

and

$$\begin{aligned} a &= y' \cdot (x' \cdot y'' - y' \cdot x'') - z' \cdot (z' \cdot x'' - x' \cdot z'') \\ b &= z' \cdot (y' \cdot z'' - z' \cdot y'') - x' \cdot (x' \cdot y'' - y' \cdot x'') \\ c &= x' \cdot (z' \cdot x'' - x' \cdot z'') - y' \cdot (y' \cdot z'' - z' \cdot y''). \end{aligned}$$

The equation for the osculating plane is

$$A \cdot (X - x_0) + B \cdot (Y - y_0) + C \cdot (Z - z_0) = 0$$

and for the main normal

$$\frac{X - x}{a} = \frac{Y - y}{b} = \frac{Z - z}{c}.$$

X, Y and Z are the coordinates of the centre of the moving trihedral for the space curve for which the bending stress is considered. The parameter equations x_0, y_0 and z_0 present the space curve before changing, and x, y and z afterwards.

The maximum change of bending stress resulting from the space curve change is

$$\sigma_b = \frac{\delta}{2} \cdot E \cdot \left(\frac{1}{\rho} \cdot \cos(\psi_{max} - \gamma_k) - \frac{1}{\rho_0} \cdot \cos \psi_{max} \right). \tag{2.42}$$

The turning angle ψ_{max} for the virtual fibre with the maximum stress change is determined by

$$\psi_{max} = \arctan \left(\frac{\sin \gamma_k}{\cos \gamma_k - \dfrac{\rho}{\rho_0}} \right). \tag{2.43}$$

Following Schiffner (1986), the calculation of the torsion stress has to be adjusted on the space curve with the winding

$$T^* = \frac{\mathrm{d}\varphi_\mathrm{w} \cdot \cos\alpha}{\mathrm{d}s} = \frac{h_\mathrm{S} \cdot \cos\alpha}{h_\mathrm{W} \cdot \cos\beta} \frac{1}{\sqrt{x'^2 + y'^2 + z'^2}}.$$

Then according to (2.38), the torsion stress from the winding change is

$$\tau = \left(T^* - T_0^*\right) \cdot \frac{\delta}{2} G.$$

When loaded by a tensile force, the wires elongate and contract. The strands will be bent up like the wires in the straight strand under a tensile force. The wires displace each other under the strand bending in core direction. The friction between the wires induces a secondary tensile stress in the wires. Andorfer (1983) calculates this secondary tensile stress to be as Schmidt (1965) first indicated.

When the rope tensile force increases, the secondary tensile force increases in the strand wire of the wire rope from the outside to the inside in the opposite direction to the displacement. The displacement is restricted to the half lay length of the strand wires. The resulting wire tensile force is bigger than the mean tensile force in the wire sections lying directly on the core and smaller than that of the outer wire sections. Contrary to the statement of Andorfer (1983), this is also valid for ordinary lay ropes as well. The force induced by friction will be called secondary tensile force although the force can be either tensile or compression.

On the other hand, the secondary tensile force reverses its direction when the rope tensile force decreases so that the resulting tensile force in the inner wire sections is smaller and in the outer wire sections bigger than the mean wire tensile force. The rope force reversal increases the wire stress amplitude in the case of wire ropes loaded with fluctuating tensile forces.

The secondary tensile stress in a straight stranded rope can reach a considerable size. This stress is especially responsible for the fact that well-lubricated stranded wire ropes have a longer endurance under fluctuating tensile force than unlubricated ones. The lubrication reduces the friction and because of that the secondary tensile stress.

Supplementary to the fluctuating tests, Wang (1989) calculated the stresses in a simple stranded rope ordinary lay FC-6 × 7-sZ with the diameter 12.2 mm. At about the half endurance for the lower wire rope stress $\sigma_{\mathrm{z\ unt}} = 100\ \mathrm{N/mm^2}$ (with the indices of Wang) the rope extension is $\varepsilon_{\mathrm{sunt}} = 1.5\ \%$ and the lateral contraction $\varepsilon_{\mathrm{q\ unt}} = 5.2\ \%$ and for the upper wire rope stress $\sigma_{\mathrm{z\ oben}} = 675\ \mathrm{N/mm^2}$ the rope extension is $\varepsilon_{\mathrm{s\ oben}} = 5.8\ \%$ and the lateral contraction $\varepsilon_{\mathrm{q\ oben}} = 9.8\ \%$. For this rope with fibre core between the lower and the upper rope tensile force the transverse contraction ratio is $\nu = 1.69$ for the rope diameter and $\nu = 1.88$ for the winding radius of the strand axis.

Wang (1989) presented the results of his calculation, done with the relatively high friction coefficient $\mu = 0.25$, in Fig. 2.8. The (global) rope tensile stress range is $2\sigma_{\mathrm{za}} = 575\ \mathrm{N/mm^2}$ between 100 and 675 $\mathrm{N/mm^2}$. After Fig. 2.8 the maximum range of longitudinal stresses in the fibres of the lay wires is

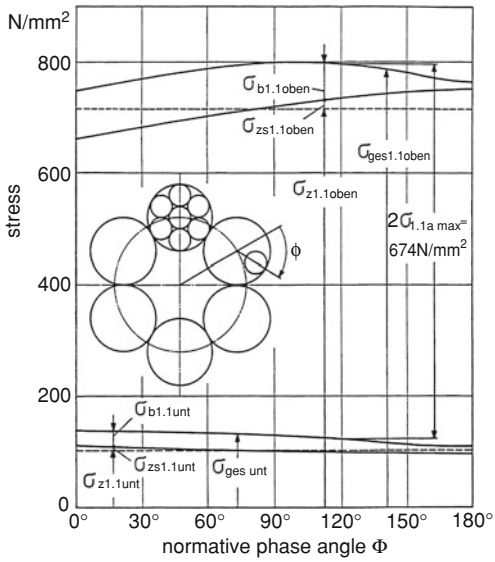

Fig. 2.8 Longitudinal stresses in the lay wires of a wire rope FC + 6 × 7 *sZ* under fluctuating forces, Wang (1989)

$2\sigma_{1.1a\ max} = 674\ N/mm^2$. That is 17.2 % more than the range of the rope tensile stress $2\sigma_{za}$.

In addition to the longitudinal stresses the wires will be stressed by torsion, pressure and to a small extent by wear and corrosion. Supplementary to this, secondary bending stresses occur in wire ropes with crossing wire layers or crossing strand layers. All these stresses are systematically unavoidable.

In any case, higher stresses occur unsystematically in some wires because of the unevenly distributed wire tensile forces. This uneven distribution coming from the fabrication and the handling of the wire ropes cannot be totally avoided. The calculated stresses compared with the strength show "what is possible in the ideal case and gives the limit that a rope construction can reach but never exceed," Donandt (1950).

Jiang et al. (1997) and Wehking and Ziegler (2004) recently calculated the stresses in a tensile loaded strand 1 + 6 by the finite element method. In contrast to the analytic method presented here, this method includes the pressure between the centre wire and the lay wires. The maximum stress in the lay wires has nearly the same size as in the analytical calculation but is a little further away from the analytical maximum, the inner wire edge. In his dissertation Ziegler (2007) extended the finite element calculations on strands 1 × 19 and 1 × 37.

2.2 Wire Rope Elasticity Module

2.2.1 Definition

The elongation behaviour of materials under the effect of mechanical stresses is described by elasticity modules. The elongation of a wire rope depends, of course, on elasticity module for wire materials, but the wire rope elasticity module describing wire rope elongation differs from the wire elasticity module. The rope stress-extension curve is not linear. Therefore, for a certain wire rope, the wire rope elasticity module is not constant but depends on the tensile stresses.

As far as strands and spiral ropes are concerned, there is only minimal non-linearity and this can be neglected in most cases. The wire rope elasticity module for these ropes can be calculated approximately using analytical methods (see Sect. 2.2.2), but this is not true for stranded ropes as their rope elasticity modules can only be evaluated by measurements, and—because of the non-linear stress-extension curve—the wire rope elasticity module resulting from these measurements can only be given with a correct definition of the loading.

The main rope elasticity modules which are of importance for practical usage are:

- $E_S(\sigma_{lower}, \sigma_{upper})$ as secant between both of the wire rope stresses with a load reverse at the beginning stress (this is especially the case for fluctuating tensile stresses) and, as a special case of this,
- $E_S(0, \sigma_{upper})$ with the lower stress 0.

Here, and in the following, the stresses refer to the wire rope stresses $\sigma_z = S/A$ with the rope tensile force S and the metallic cross-section A of all rope wires. The index z normally used for the global wire rope stress is left out here for simplification ($\sigma_{z,lower} = \sigma_{lower}$ and $\sigma_{z,upper} = \sigma_{upper}$).

The rope elasticity modules defined in this way are always meant if they have not been described expressly in a different way. Here it is important that a stress reverse takes place at the starting stress. The rope elasticity module as secant between two points on a stress–elongation curve (without stress reverse at the beginning) is of no practical importance.

The tangent elasticity module defined by a tangent on the stress-extension curve will be only used in special cases. But later on this tangent elasticity module E_t will be used as an assisting parameter for evaluating the stress-extension curve to find out the rope elasticity module $E_S(\sigma_{lower},\sigma_{upper})$, see Sect. 2.2.3. The measurements of the stress-extension curves for this have always been taken between the lower stress $\sigma_{lower} = 0$ and the upper rope stress $\sigma_{upper} = 800$ N/mm^2. Because of this, it is not necessary to show either of these end stresses in the symbol of the tangent elasticity module. The tangent elasticity module (as assisting parameter) on the stress-extension curves between the rope tensile stresses 0 and 800 N/mm^2 in the up-and-down direction are therefore given by the symbols where only the rope tensile stress in the tangent point is nominated:

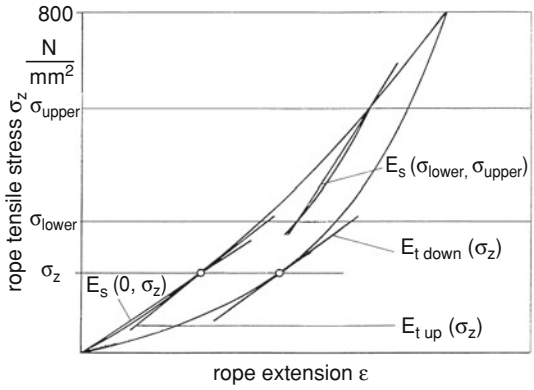

Fig. 2.9 Definitions of the wire rope elasticity modules used

- $E_{t,up}$ (σ_z) rope elasticity module as tangent on the stress-extension curve in the up direction at the rope tensile stress σ_z
- $E_{t,down}$ (σ_z) rope elasticity module as tangent on the stress-extension curve in the down direction at the rope tensile stress σ_z

The rope elasticity modules in the different definitions used here are shown in Fig. 2.9.

2.2.2 *Rope Elasticity Module of Strands and Spiral Ropes, Calculation*

As already mentioned, the non-linearity of the stress-extension curve is relatively small for strands and spiral ropes. There is also only a small increase of the rope elasticity module with the number of loadings. The smaller the number of wires in the rope, the more likely this is to be true. Buchholz and Eichmüller (1988) found that there was only the very small difference of $\Delta E = 600$ N/mm^2 between the first, second and third measurements with an almost constant rope elasticity module $E_S = 198{,}000$ N/mm^2. Taking all these observations into consideration, it is possible to make reliable calculations for the rope elasticity module for strands and spiral ropes with a small number of wires. A method of calculation was first devised for this by Hudler (1937).

The calculation can be done with the help of the equations from Sect. 2.1. The rope elasticity module is by definition

$$E_S = \frac{\sigma_z}{\varepsilon}.$$

With (2.21) for the tensile stress and the definition of the strand extension

$$\varepsilon = \frac{\Delta l_S}{l_S},$$

the rope elasticity module for strands and spiral ropes is

$$E_S = \frac{1}{A}\sum_{i=0}^{n} \frac{z_i \cdot \cos^3 \alpha_i}{1 + v_i \cdot \sin^2 \alpha_i} \cdot E_i \cdot A_i. \tag{2.44}$$

Poisson's ratio can be set $v = v_i = 0.3$ for all wire diameters and winding radii in steel spiral ropes because the length-related force between the wire layers is small and the lateral contraction is almost only caused by the tensile stress in the wires.

Example 2.3: *Elasticity module of an open spiral rope according to* Fig. 2.4

According to (2.44) the rope elasticity module is

$$E_S = \frac{196{,}000}{45.61} \cdot \left(1.431 + \frac{(6 + 12 + 18) \cdot 0.9703^3 \cdot 1.227}{1 + 0.3 \cdot 0.2419^2}\right)$$
$$E_S = 177{,}000 \text{ N/mm}^2.$$

The rope elasticity module for strands and spiral ropes calculated by (2.44) is independent from the rope tensile stress. But in reality this rope elasticity module always depends slightly on the stress level and it is always a little smaller than the one calculated. This means, the smaller the stress level and the higher the number of wires in the rope, the bigger the difference. The calculated rope elasticity module can only be reached approximately with a strong pre-stressing.

A reference value for the elasticity modules of closed spiral ropes for bridges which have not been pre-stressed is given in Fig. 2.10 by DIN 18809. This shows elasticity modules with different definitions:

- E_g rope elasticity module for the first loading up to the permanent load
- E_p rope elasticity module for the traffic load
- E_A rope elasticity module for defining the rope length
- E_B rope elasticity module during bridge erection

2.2.3 Rope Elasticity Module of Stranded Wire Ropes

Because of its lateral contraction, the rope elasticity module of stranded ropes cannot be calculated in the same way as that of strands or spiral ropes. The lateral contraction of the stranded ropes depends on a large unknown quantity at the tensile stress level. Therefore, the elasticity module of stranded ropes can only be evaluated by taking measurements.

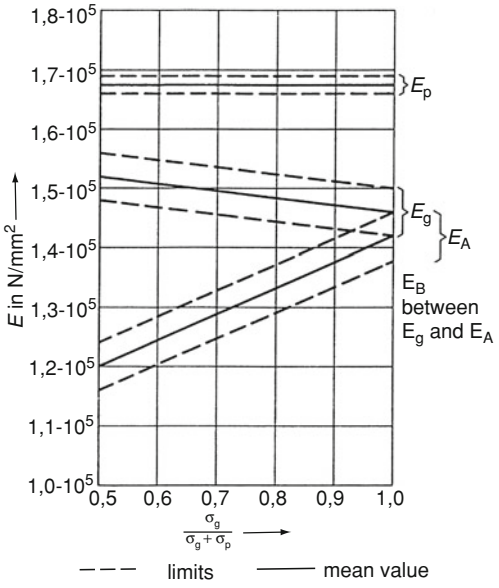

Fig. 2.10 Reference value for rope elasticity modules of locked coil ropes, DIN18809

Wyss (1957) and Jehmlich (1985) have made series of measurements. They distinguished between a total rope elasticity module starting from the stress 0 (first loading) and the rope elasticity module between two stresses after a longer rope working time. An important contribution to what is known about the rope elasticity module was made by Hankus (1976, 1978, 1989). He measured the elongation of many ropes of different constructions with fibre and steel cores with the first loading as well as after loading repeatedly in an up-and-down direction. He used these measurements to evaluate the rope elasticity module as secant starting from the stress $\sigma_z = 0$ with multi-dimensional linear regression calculations. He also evaluated the rope elongation after it had been loaded for a long time.

The following remarks about the rope elasticity module relate mostly to the Stuttgart tests conducted by Feyrer and Jahne (1990). These tests were done with nearly all types of construction for round stranded wire ropes. A lot of the tests were carried out by the students listed in the previous article.

2.2.3.1 Stress-Extension Curves

The measurements of stress-extension curves—which form the basis of the evaluation for rope elasticity modules—have always been taken in the same manner. The rope elongation ΔL is measured for a rope length of $L = 2{,}000$ mm with two inductive elongation meters on the right and left of the rope as seen in Fig. 2.11. The results of these measurements are recorded for the first loading cycle up to

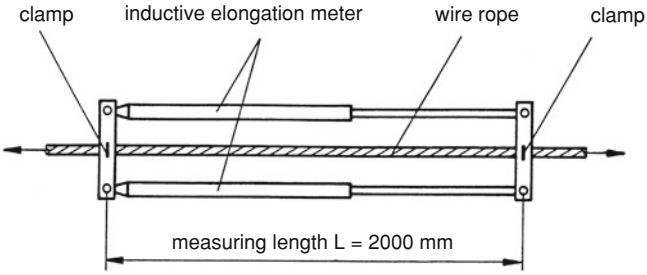

Fig. 2.11 Arrangement for measuring the wire rope elongation, Feyrer and Jahne (1990)

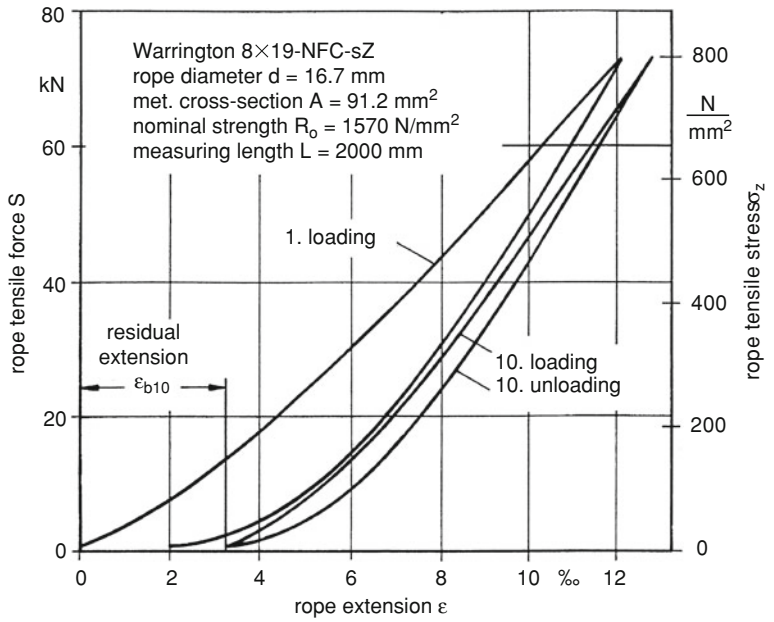

Fig. 2.12 Stress-extension curves for a stranded wire rope with fibre core, Feyrer and Jahne (1990)

rope tensile stress $\sigma_z = 800$ N/mm^2 and after nine loadings between $\sigma_z = 0$ and $\sigma_z = 800$ N/mm^2 for the tenth loading and unloading.

The nine loading cycles should give nearly the same compression of the rope structure as is found in practice after some time under working conditions (of course with smaller tensile stresses and a greater number of loading cycles). It will be anticipated here that after ten loading cycles the mean residual extension is 4 % with a large deviation. A residual extension of approximately the same size was found for wire ropes running over sheaves after 2 % of their life time as Woernle (1929) already noticed. However a residual extension of 3 % was measured again

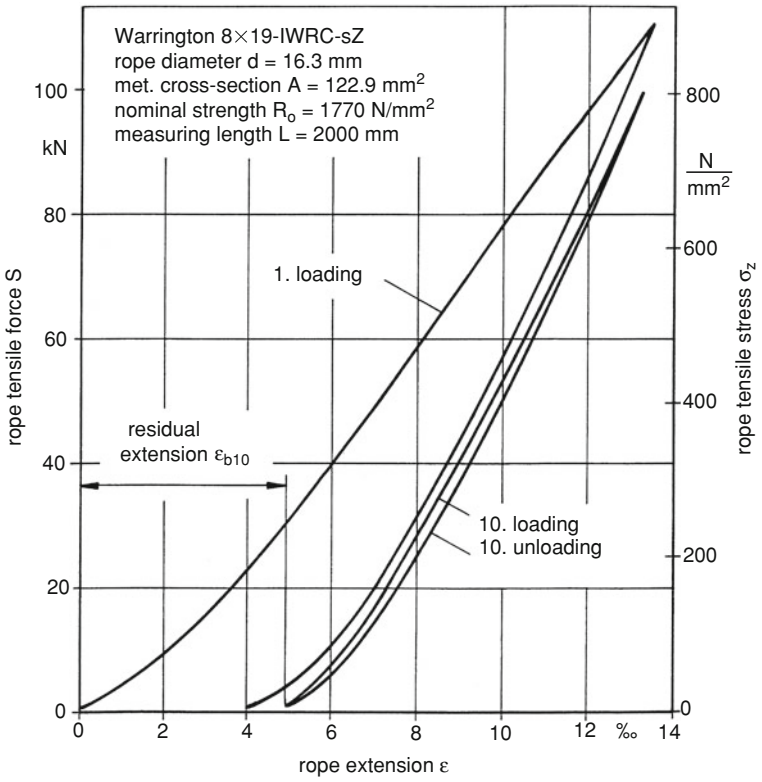

Fig. 2.13 Stress-extension curves for a stranded wire rope with steel core, Feyrer and Jahne (1990)

for elevator ropes FC-8 × 19 after a long period of operation under these ten loading cycles.

In Fig. 2.12, the stress-extension curves are presented for a wire rope with a fibre core under the first and the tenth loading and unloading. This figure shows the typical progressive increase of tensile stress arising as the rope extends. Especially for wire ropes with a fibre core, a large progressive increase and hysteresis for loading and unloading occurs. The progressive form of the rope stress-extension curve has its origin in the lateral contraction of the stranded ropes. In ropes with fibre cores, this is especially large and nonlinear.

The stress-extension curves of wire ropes with steel cores are given as an example in Fig. 2.13. This also shows the progressive increase of the stress when a rope with a steel core becomes extended. Normally, this is not as large as in the case of wire ropes with fibre cores. However, in this special case, the residual extension is greater. The stress-extension curve is always different for loading and unloading. The enclosed area in the hysteresis loop is a mark of the inner frictional work of the wire rope.

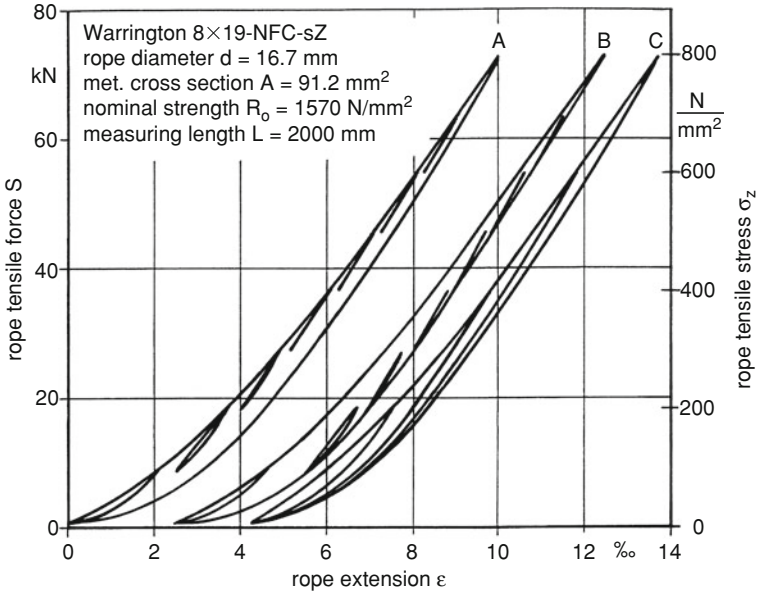

Fig. 2.14 Stress-extension curves with loading between different stresses, Feyrer and Jahne (1990)

Figure 2.14 shows the stress-extension curves for the loading and unloading of the wire rope from Fig. 2.12 after the tenth loading cycle. Between the rope tensile stresses 0 and 800 N/mm^2, the tensile stress changes in small steps. In loop A, the tensile stress increases starting from $\sigma_z = 0$ in steps of $\Delta\sigma_z = 100$ N/mm^2 and reduces the stress at every level reached in a small stress loop $\sigma_{upper} - \sigma_{lower} = \Delta\sigma_z = 100$ N/mm^2. The two lowest partial loops still show a clear hysteresis, but the others do not.

Loop B is again loaded in stress steps of $\Delta\sigma_z = 100$ N/mm^2 but now starting from $\sigma_z = 800$ N/mm^2 in a "down" direction. The two lowest partial loops show a clear hysteresis as in loop A. The partial loops for the same stresses σ_{lower} and σ_{upper} in the loops A and B are practically parallel. They represent the rope elasticity modules E_S (σ_{lower}, σ_{upper}).

In loop C some partial loops of stress-extension curves are shown, starting from $\sigma_z = 0$ to the upper stresses $\sigma_{upper} = 200$, 400 and 600 N/mm^2. The loading curves are the same for all upper stresses. The unloading curves from these upper stresses can be taken approximately as a part of the entire unloading curve from the upper stress 800–0 N/mm^2, turned around the point for $\sigma_z = 0$.

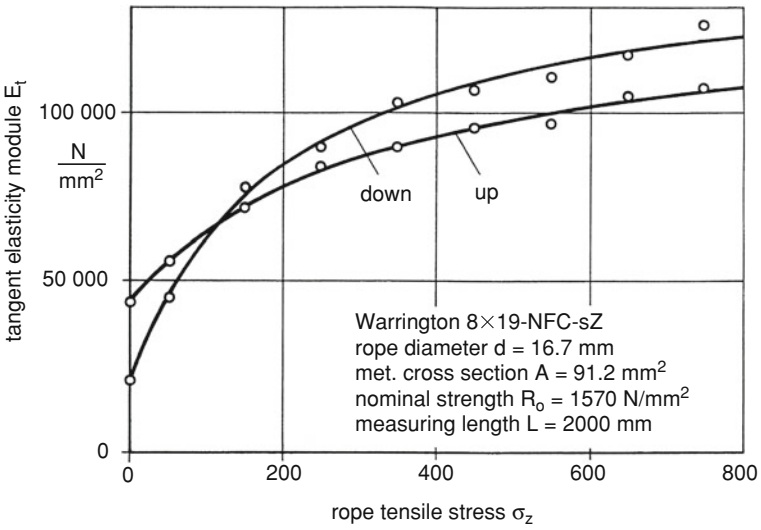

Fig. 2.15 Assistant parameter: tangent elasticity module E_t, Feyrer and Jahne (1990)

2.2.3.2 Assistant Parameter: Tangent Elasticity Module

The stress-extension curves of the different wire ropes measured between the rope tensile stresses 0 and 800 N/mm^2—as seen in Figs. 2.12 and 2.13—will be used to evaluate the rope elasticity module E_S (σ_{lower}, σ_{upper}). The calculation based on the rope tangent module has the advantage of being very precise. The tangent module has been taken point-for-point from the stress-extension curves. Figure 2.15 gives an example of the tangent module based on the diagram in Fig. 2.12 after the tenth loading and unloading. It should be realised here that the tangent module depends strongly on the rope tensile stress and the direction of the loading or unloading.

Common linear regression calculation was used to work out the rope tangent module from numerous wire ropes. After a number of trials, the best regression equation was found to be

$$E_t(\sigma_z) = C_0 + \frac{C_1}{\sigma_z + A} + \sum_{i=2}^{n} C_i \cdot x_i. \tag{2.45}$$

The constant A in the equation has to be worked out by iteration, but this does not cause a problem when using computers. The wire rope construction is characterised by the variables x_i. For example $x_2 = 0$ is set for 6-strand ropes and $x_2 = 1$ is set for 8-strand ropes. Separate regression calculations have been done for ropes with fibre cores, ropes with steel cores and for spiral round strand ropes, and also, of course, both for loading and unloading.

With a common constant

$$B = C_0 + \sum_{i=2}^{n} C_i \cdot x_i \quad \text{and with} \quad C = C_1,$$

the tangent elasticity module for the rope tensile stress σ_z on the stress-extension curve between the tensile stresses $\sigma_z = 0$ and 800 N/mm^2 in an "up-and-down" direction is

$$E_t(\sigma_z) = B + \frac{C}{\sigma_z + A}. \tag{2.46}$$

The constants *A*, *B* and *C* are listed in Tables 2.1 and 2.2. The constant *B* for wire ropes with fibre-covered steel cores in Table 2.1 has been changed unlike constant *B* in Feyrer and Jahne (1990).

2.2.3.3 Rope Elasticity Module with the Lower Tensile Stress $\sigma_z = 0$

The extension ε of a wire rope is

$$\varepsilon = \int \frac{1}{E_t(\sigma_z)} \cdot d\sigma_z.$$

Using (2.46), the extension of a wire rope between the two stresses σ_{lower} and σ_{upper}—in the stress-extension curve coming from $\sigma_z = 0$—in the "up" direction—is

$$\varepsilon = \int_{\sigma_{lower}}^{\sigma_{upper}} \frac{1}{B_{up} + \frac{C_{up}}{\sigma_z + A_{up}}} \cdot d\sigma_z = \int_{\sigma_{lower}}^{\sigma_{upper}} \frac{\sigma_z + A_{up}}{B_{up} \cdot \sigma_z + A_{up} \cdot B_{up} + C_{up}} \cdot d\sigma_z$$

and after integration

$$\varepsilon = \frac{\sigma_{upper} - \sigma_{lower}}{B_{up}} - \frac{C_{up}}{B_{up}^2} \cdot \ln \frac{\sigma_{upper} + A_{up} + C_{up}/B_{up}}{\sigma_{lower} + A_{up} + C_{up}/B_{up}}. \tag{2.47}$$

According to (2.47), the important rope elasticity module with the lower stress $\sigma_{lower} = 0$ and the upper stress σ_{upper} is

$$E_S(\sigma_z) = E_S(0, \sigma_z) = \frac{\sigma_z}{\varepsilon}$$

or

Table 2.1 Constants *A*, *B* and *C* for calculating the elasticity module in N/mm^2 of round stranded ropes, Feyrer and Jahne (1990)

Rope condition	Core	Coefficient of determination Standard deviation	Constant *A*	Constant *C*	Constant *B*					
					6-strand wire layers			8-strand wire layers		
					1	2	3	1	2	3
New up	NFC	64 %	161	−10,700,000	118,000	102,000	101,000	116,000	100,000	99,000
	SFC	14,000			112,000	96,000	95,000	110,000	94,000	93,000
	IWRC	75 %	81	−5,140,000	120,000	105,000	104,000	103,000	88,000	87,000
	PWRC	13,000			137,000	122,000	121,000	120,000	105,000	104,000
	ESWRC				126,000	111,000	110,000	109,000	94,000	93,000
	EFWRC				108,000	93,000	92,000	91,000	76,000	75,000
Ten times loaded up	NFC	82%	161	−14,400,000	152,000	141,000	138,000	149,000	138,000	135,000
	SFC	11,000			141,000	130,000	127,000	138,000	127,000	124,000
	IWRC	89%	131	−12,500,000	160,000	149,000	147,000	149,000	138,000	136,000
	PWRC	10,000			163,000	152,000	150,000	152,000	141,000	139,000
	ESWRC				156,000	145,000	143,000	145,000	134,000	132,000
	EFWRC				145,000	134,000	132,000	134,000	123,000	121,000
Ten times loaded down	NFC	89 %	192	−25,500,000	177,000	166,000	163,000	174,000	163,000	160,000
	SFC	11,000			166,000	155,000	152,000	163,000	152,000	149,000
	IWRC	91 %	167	−20,500,000	177,000	166,000	164,000	166,000	155,000	153,000
	PWRC	10,000			180,000	169,000	167,000	169,000	158,000	156,000
	ESWRC				173,000	162,000	160,000	162,000	151,000	149,000
	EFWRC				162,000	151,000	149,000	151,000	140,000	138,000

Table 2.2 Constants *A, B* and *C* for calculating the elasticity module of spiral round strand ropes, Feyrer and Jahne (1990)

Rope condition	New	Ten times loaded	
Load direction	Up	Up	Down
Constant A	35	149	229
Constant B			
Two strand layers	90,000	123,000	151,500
Three strand layers	89,000	121,000	149,500
Constant C	–1,700,000	–11,200,000	–26,700,000
Coefficient of determination	62 %	75 %	86 %
Standard deviation *s*	12,000	11,000	11,000

$$E_S(\sigma_z) = \frac{\sigma_z}{\frac{\sigma_z}{B_{up}} - \frac{C_{up}}{B_{up}^2} \cdot \ln\left(1 + \frac{\sigma_z}{A_{up} + C_{up}/B_{up}}\right)}. \tag{2.48}$$

This rope elasticity module is especially important for the first loading when it is installed. The constants A, B, and C are listed in Tables 2.1 and 2.2.

2.2.3.4 Rope Elasticity Module E_S Between Two Stresses

The rope elasticity module $E_S(\sigma_{1ower}; \sigma_{upper})$ between the two stresses σ_{lower} and σ_{upper} is defined by the secant between these two stresses of the stress-extension curve with a load reverse at the beginning stress, Figs. 2.9 and 2.14. The loading direction changes in most practical applications at the beginning of the considered loading. This is especially true in cases with a fluctuating load. $E_S(\sigma_{1ower},\sigma_{upper})$ is therefore the rope elasticity module normally used.

A very good approximation of this rope elasticity module can be obtained by quasi-turning the stress-extension curve (between $\sigma_z = 0$ and $\sigma_z = 800$ N/mm^2) in the "down" direction around the origin of coordinate ($\sigma_z = 0$) so far until its extension at the upper stress is the same as that of the "up" direction (between $\sigma_z = 0$ and $\sigma_z = 800$ N/mm^2)

$$\varepsilon_{up}(\sigma_{upper}) = \varepsilon_{down}(\sigma_{upper}). \tag{2.49}$$

The rope elasticity module $E_s(\sigma_{1ower}, \sigma_{upper})$ can be taken from the "down" direction stress-extension curve turned as described. The turning will be brought about by exchanging the constant B_{down} to $B_{down,upper}$ for ε_{down} (σ_{upper}). Equation (2.48) set in (2.49) gives (with this new constant for the "down" direction curve) the equation for calculating the new constant $B_{down,upper}$

$$\frac{\sigma_{\text{upper}}}{B_{\text{up}}} - \frac{C_{\text{up}}}{B_{\text{up}}^2} \cdot \ln\left(1 + \frac{\sigma_{\text{upper}}}{A_{\text{up}} + C_{\text{up}}/B_{\text{up}}}\right) = \frac{\sigma_{\text{upper}}}{B_{\text{down,upper}}} - \frac{C_{\text{down}}}{B_{\text{down,upper}}^2} \cdot \ln\left(1 + \frac{\sigma_{\text{upper}}}{A_{\text{down}} + C_{\text{down}}/B_{\text{down,upper}}}\right). \tag{2.50}$$

The constant B_{downup} has to be calculated by iteration using (2.50). The rope extension $\varepsilon_{\text{lower,upper}}$ can be calculated with (2.47), the constant $B_{\text{down,upper}}$, and the constants A_{down} and C_{down} using Tables 2.1 and 2.2. Then the rope elasticity module is

$$E_{\text{S}}(\sigma_{\text{lower}}, \sigma_{\text{upper}}) = \frac{\sigma_{\text{upper}} - \sigma_{\text{lower}}}{\varepsilon_{\text{lower,upper}}} \tag{2.51}$$

or

$$E_{\text{S}}(\sigma_{\text{lower}}, \sigma_{\text{upper}}) = \frac{\sigma_{\text{upper}} - \sigma_{\text{lower}}}{\dfrac{\sigma_{\text{upper}} - \sigma_{\text{lower}}}{B_{\text{down,upper}}} - \dfrac{C_{\text{down}}}{B_{\text{down,upper}}^2} \cdot \ln \dfrac{\sigma_{\text{upper}} + A_{\text{down}} + C_{\text{down}}/B_{\text{down,upper}}}{\sigma_{\text{lower}} + A_{\text{down}} + C_{\text{down}}/B_{\text{down,upper}}}}. \tag{2.52}$$

Calculating the rope elasticity module without the aid of a computer involves a certain amount of effort. For some chosen rope stresses σ_{lower} and σ_{upper}, the rope elasticity module $E_{\text{S}}(\sigma_{\text{lower}}, \sigma_{\text{upper}})$ is listed in tables. Table 2.3 shows the rope elasticity module for 6-strand ropes with two wire layers and for spiral round strand ropes. In case of rope oscillations with the middle stress σ_{m} and small amplitude stress σ_{a}, the elasticity module required is $E_{\text{S}}(\sigma_{\text{m}} \pm 0)$. This rope elasticity module is listed for some middle stresses in Table 2.3 as

$$E_{\text{S}}(\sigma_{\text{lower}}, \sigma_{\text{upper}}) = E_{\text{S}}(\sigma_{\text{m}}; \sigma_{\text{m}}).$$

For example, for a rope 6 × 19—IWRC with $\sigma_{\text{m}} = 200$ N/mm^2

$$E_{\text{S}}(200 \pm 0) = E_{\text{S}}(200; 200) = 117 \text{ kN/mm}^2.$$

Table 2.4 gives correction constants ΔE for 8-strand ropes and for one and three wire layers. With this, the rope elasticity module $E_{\text{S}}(\sigma_{\text{lower}}, \sigma_{\text{upper}})$ is

$$E_{\text{S}}(\sigma_{\text{lower}}, \sigma_{\text{upper}}) = E_{\text{S}}(\text{Table 2.3}) + \Delta E. \tag{2.53}$$

The standard deviation can be taken from the Tables 2.1 and 2.2.

The elasticity module between two stress levels and the rope elongation can be calculated with the help of the Excel-program SEILELA2.XLS.

Example 2.4: *Wire rope elasticity module*

Data:
wire rope IWRC + 8 × 19
rope tensile stresses between $\sigma_z = 100$ and $\sigma_z = 220$ N/mm^2.

Table 2.3 Rope elasticity module as secant between the lower and upper rope tensile stress, 6-strand ropes with two wire layers and spiral round strand ropes

Rope-condition	Rope-construct.	Rope-core	Rope elasticity module E in kN/mm^2						
			Lower tensile stress in N/mm^2						
			0						
			Upper tensile stress in N/mm^2						
			40	100	200	300	400	600	800
New	6-strands	NFC	42	49	57	62	66	71	75
	Two wire layers	SFC	36	43	51	56	60	65	69
		IWRC	53	62	71	76	80	85	88
		PWRC	70	79	88	93	97	102	105
		ESWRC	59	68	72	84	86	91	94
		EFWRC	41	50	59	64	68	73	76
	Spiral-round-	Two strand layer	57	66	72	76	78	81	82
	strand rope	Three strand layer	55	65	71	75	77	80	81
Rope-condition	Rope-construct.	Rope-core	Rope elasticity module E in kN/mm^2						
			Lower tensile stress in N/mm^2						
			0						
			Upper tensile stress in N/mm^2						
			40	100	200	300	400	600	800
Ten times loaded	6-strands	NFC	61	70	80	87	93	100	105
	Two wire layers	SFC	50	59	69	76	82	89	94
		IWRC	65	76	88	96	101	109	114
		PWRC	70	79	91	99	104	112	117
		ESWRC	61	72	84	92	97	105	110
		EFWRC	50	61	73	81	86	94	99
	Spiral-round-	Two strand layer	57	67	73	79	84	90	94
	strand rope	Three strand layer	55	65	71	77	82	88	92

(continued)

Table 2.3 (continued)

Rope-condition	Rope-construct.	Rope-core	Rope elasticity module E in kN/mm^2						
			Lower tensile stress in N/mm^2						
			40						
			Upper tensile stress in N/mm^2						
			40	100	200	300	400	600	800
Ten times loaded	6-strands	NFC	72	81	91	97	102	109	110
	Two wire layers	SFC	61	70	80	86	91	98	101
		IWRC	77	88	98	105	110	117	121
		PWRC	80	91	101	108	113	120	124
		ESWRC	73	84	94	101	106	113	117
		EFWRC	62	73	83	90	95	102	106
	Spiral-round-	Two strand layer	65	73	81	87	91	96	100
	strand rope	Three strand layer	63	71	79	85	89	94	98
Rope-condition	Rrope-construct.	Rope-core	Rope elasticity module E in kN/mm^2						
			Lower tensile stress in N/mm^2						
			100						
			Upper tensile stress in N/mm^2						
			100	200	300	400	600	800	
New	6-strand	NFC	92	101	107	111	116	119	
	Two wire layers	SFC	81	90	96	100	105	108	
		IWRC	98	107	113	118	123	127	
		PWRC	101	110	116	121	126	130	
		ESWRC	94	103	109	114	119	123	
		EFWRC	83	92	98	103	108	112	
	Spiral-round-	Two strand layer	81	89	94	98	103	106	
	strand rope	Three strand layer	79	87	92	96	101	104	

(continued)

Table 2.3 (continued)

Rope-condition	Rope-construct.	Rope-core	Rope elasticity module E in kN/mm^2						
			Lower tensile stress in N/mm^2						
			200						
			Upper tensile stress in N/mm^2						
					200	300	400	600	800
Ten times loaded	6-strand Two wire layers	NFC			111	116	119	124	126
		SFC			100	105	108	113	115
		IWRC			117	122	125	130	132
		PWRC			120	125	128	133	135
		ESWRC			113	118	121	126	128
		EFWRC			102	107	110	115	117
	Spiral-round-strand rope	Two strand layer			98	102	106	109	112
		Three strand layer			96	100	104	107	110
Rope-condition	Rope-construct.	Rope-core	Rope elasticity module E in kN/mm^2						
			Lower tensile stress in N/mm^2						
			300				400	600	800
			Upper tensile stress in N/mm^2						
			300	400	600	800	400	600	800
Ten times loaded	6-strand Two wire layers	NFC	122	125	128	130	129	136	141
		SFC	111	114	117	119	118	126	131
		IWRC	127	130	134	136	134	141	145
		PWRC	130	133	137	139	137	144	148
		ESWRC	123	126	130	132	130	137	141
		EFWRC	113	115	119	121	119	127	131
	Spiral-round-strand rope	Two strand layer	108	111	114	116	114	121	125
		Three strand layer	106	109	112	114	112	120	123

NFC natural fibre core, *SFC* synthetic fibre core, *IWRC* independent wire rope core, *PWRC* wire rope core parallel, *ESWRC* wire rope core enveloped with solid polymer, *EFWRC* wire rope core enveloped with synthetic fibres

Table 2.4 Correction constants ΔE for round strand ropes with 6- and 8-strands of one, two and three wire layers

Rope condition	Rope core	Correction constant					
		6-strands			8-strands		
		Wire layers			Wire layers		
		1	2	3	1	2	3
New	Fibre core	16	0	−1	14	−2	−3
	Steel core	15	0	−1	–2	−17	−18
Ten times loaded	Fibre core	11	0	−3	8	−3	−6
	Steel core	11	0	−2	0	−11	−13

Fibre core = NFC, SFC; steel core = IWRC, PWRC, ESWRC, EFWRC

Results:
From (2.50) and (2.52)
$E_S(\sigma_{lower}, \sigma_{upper}) = E_S\ (100; 220) = 98\ kN/mm^2$

Alternative from tables:

From Table 2.3 the rope elasticity module for a rope IWRC + 6 × 19 is $E_S(100; 200) = 107\ kN/mm^2$ and $E_S(100; 300) = 113\ kN/mm^2$ and as a middle value $E_S(100; 220) = 108\ kN/mm^2$.

From Table 2.4 the correction constant for 8-strand ropes is $\Delta E = -11\ kN/mm^2$.

This means that with (2.53), the rope elasticity module for the wire rope IWRC + 8 × 19 is $E_S\ (100; 250) = 110 - 11 = 97\ kN/mm^2$. Nearly the same as $98\ kN/mm^2$.

According to Table 2.1, the standard deviation is $s = 10\ kN/mm^2$.

2.2.4 Waves and Vibrations

2.2.4.1 Longitudinal Waves

If a long wire rope receives a shock load, a tensile force wave (strain wave) moves along the wire rope starting from the initial point of impact. The velocity of the wave is

$$c = \sqrt{\frac{E}{\rho}} \tag{2.54}$$

with E for the elasticity module and ρ for the mass density. For a single wire with, for example, $E = 196{,}000\ N/mm^2 = 196{,}000 \times 10^6\ N/m^2$ and $\rho = 7{,}800\ kg/m^3 = 7{,}800\ N\ s^2/m^4$ the velocity of the wave is

$$c = \sqrt{\frac{196{,}000 \cdot 10^6}{7{,}800}} = 5{,}010 \text{ m/s}.$$

The wave velocity is of some importance for the understanding of accidents related to wire rope installations. The tensile stress of a wave will be practically doubled when it is reflected from the termination of the rope and it is possible that the wire rope will break if the velocity v of the impact is big enough. For example, the shock load can be effected on the hanging rope by a falling weight with the striking velocity v. According to Irvine's fundamental theory (1981), the tensile rope force F produced by the shock load is

$$F = m_\mathrm{T} \cdot c \cdot v \cdot e^{(-m_\mathrm{T} \cdot c \cdot t)/\mathrm{M}}. \tag{2.55}$$

In this equation, m_T is the length-related rope mass, c the wave velocity, v the striking velocity, M the falling mass and t the time. For $t = 0$, the wire rope shock force is $F_0 = m_\mathrm{T} cv$ and this fades away in time if the tensile shock force is not great enough to break the rope. The size of the mass hitting the wire rope has no influence on the tensile shock force but only on its fading. (If the falling mass M is very large, the wire rope can of course break even if the velocity v is small. This can be the case if the weight force Mg is greater than the rope breaking force or if the falling energy is greater than the stress-extension energy of the rope.)

Irvine's theory can be used to explain the terrible accident with an aerial rope way at Cavalese on 3rd February, 1998, when an aircraft with a relatively fragile structure severed a solid track rope and the haulage rope and was still able to fly afterwards. The velocity of the aircraft was 241 m/s, the length of the tears in the aircraft wings caused by the track rope were about 1 m and those caused by the haulage rope, 0.5 m, Oplatka and Volmer (1998). They pointed out that the aircraft wings would have been totally torn off if the aircraft velocity had been lower than the limit velocity. Spontaneous wire rope breakages caused by aircraft impacts also occurred prior to Cavalese, Lombard (1998a).

The wire rope breakage caused by the impact of an aircraft hitting the wire occurs if its velocity v is big enough. According to Irvine, the minimum velocity is

$$v = c \cdot \sqrt{\varepsilon^2 + 2\varepsilon \cdot \sqrt{\varepsilon}}. \tag{2.56}$$

In this equation, ε is the breaking extension and c is once more the wave velocity. With the breaking extension of rope wires $\varepsilon = 0.007$ with a safety margin, Irvine (1981) calculated a minimum velocity $v = 150$ m/s for the aircraft. Lombard (1998a, b) calculated a minimum velocity $v = 156$ m/s with one-third of the wire elasticity module and a more realistic breaking extension $\varepsilon = 0.018$. He used his own extended theory for this calculation.

2.2.4.2 Longitudinal Oscillation of a Hanging Mass

A mass hanging on a wire rope can be made to oscillate along the axis of the rope. Without taking the damping into consideration, the angular frequency is

$$\omega_0 = \sqrt{\frac{c_S}{M}}$$

and the frequency

$$f_0 = \frac{\omega_0}{2 \cdot \pi} = \frac{1}{2 \cdot \pi} \cdot \sqrt{\frac{c_S}{M}}. \tag{2.57}$$

Here it is presupposed that the rope mass is much smaller than the hanging mass M and can be neglected. The wire rope as a spring has the spring constant

$$c_S = \frac{E_S(\sigma_{lower}, \sigma_{upper}) \cdot A}{L} \tag{2.58}$$

with the rope elasticity module $Es\ (\sigma_{lower}, \sigma_{upper})$, the metallic rope cross-section A and the rope length L. When the stress amplitude changes, the rope elasticity module will be nearly constant if the middle stress remains the same. The rope elasticity module

$$E_S(\sigma_{lower}, \sigma_{upper}) = E_S(\sigma_m \pm \sigma_a) \tag{2.58a}$$

with the amplitude σ_a and with the middle rope tensile stress

$$\sigma_m = \frac{M \cdot g}{A} \tag{2.58b}$$

can be evaluated using (2.50) and (2.52) or Tables 2.3 and 2.4.

The frequency of the hanging mass—neglecting the rope damping and other dampings—can be calculated with the help of the Excel-program SEILELA2.XLS.

In addition to the frequency, the damping of the longitudinal vibrations is of interest. Wehking et al. (1999) have made some decay tests. Figure 2.16 shows the test situation. A main mass M and a dropping mass M_A hang on a wire rope with the diameter $d = 10$ mm and the length $l = 12$ m. After cutting the thin rope between the main mass M and the dropping mass M_A the main mass swings with decreasing amplitude.

Figure 2.17 shows the typical behaviour of a decay test. Only the tests with wire ropes which were ten times loaded before will be considered here. With the

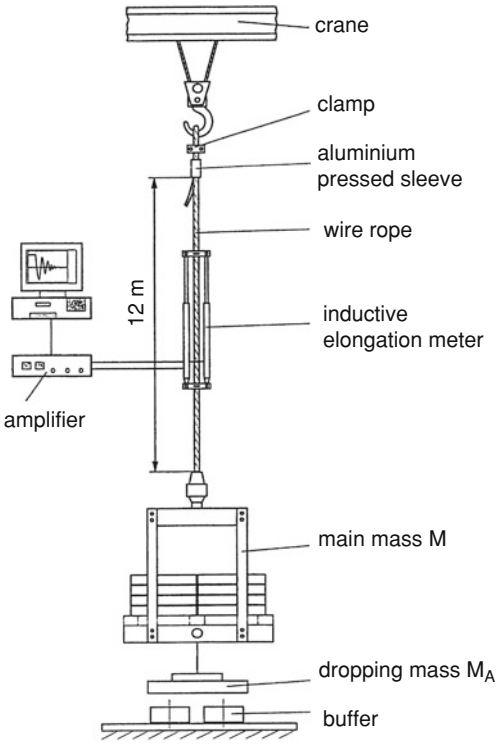

Fig. 2.16 Test situation for the measurement of rope damping, Wehking et al. (1999)

metallic cross section of the wire rope $A = 45.1$ mm^2, the middle rope tensile stresses for both of the main masses $M = 400$ and 2,000 kg are

$$\sigma_m = \frac{400 \cdot 9.81}{45.1} = 87 \text{ N/mm}^2 \quad \text{and} \quad \sigma_m = \frac{2{,}000 \cdot 9.81}{45.1} = 435 \text{ N/mm}^2.$$

Using (2.50) and (2.52), the rope elasticity module of the Warrington rope is

$$E_S(87 \pm \sigma_a) = 83{,}000 \text{ N/mm}^2 \quad \text{and} \quad E_S(435 \pm \sigma_a) = 125{,}000 \text{ N/mm}^2.$$

Or alternative, by interpolation for the 6-strand rope from Table 2.3 and ΔE from Table 2.4, the rope elasticity module E_S is approximately

$$E_S(87 \pm \sigma_a) = E_S(40;40) + (E_S(100;100) - E_S(40;40)) \cdot \frac{87 - 40}{100 - 40} + \Delta E$$

$$E_S(87 \pm \sigma_a) = 77 + (98 - 77) \cdot \frac{47}{60} - 11 = 82 \text{ kN/mm}^2$$

and

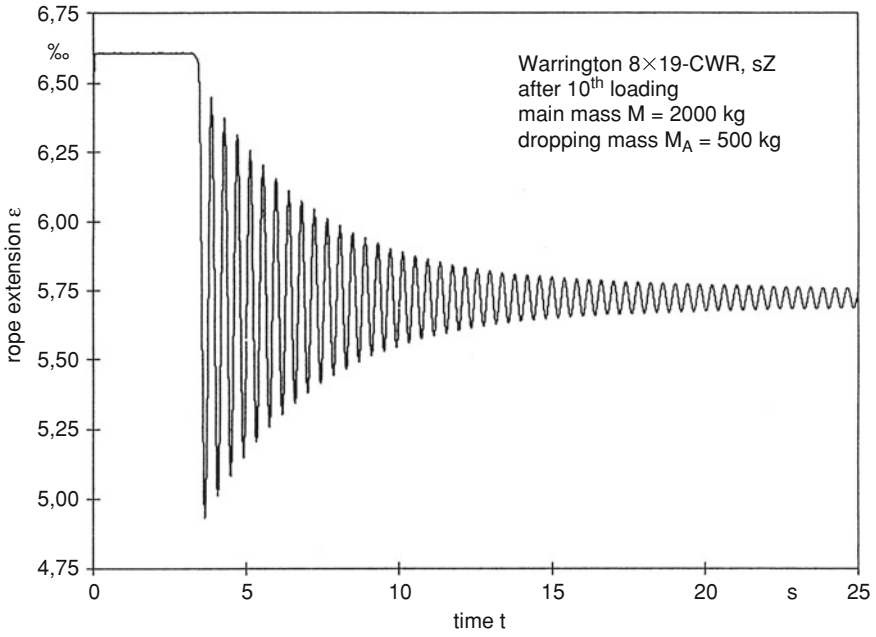

Fig. 2.17 Decay behaviour of a mass hanging on a wire rope, Wehking et al. (1999)

$$E_S(435 \pm \sigma_a) = E_S(400;400) + (E_S(600;600) - E_S(400;400)) \cdot \frac{435-400}{600-400} + \Delta E$$

$$E_S(435 \pm \sigma_a) = 134 + (141 - 134) \cdot \frac{35}{200} - 11 = 124 \ \text{kN/mm}^2.$$

For the rope elasticity modules—evaluated using (2.50) and (2.52)—the spring constants according to (2.58) are

$$c_{S87} = \frac{83{,}000 \cdot 45.1}{12{,}000} = 312 \ \text{N/mm} \rightarrow 312{,}000 \ \text{N/m and}$$

$$c_{S435} = \frac{125{,}000 \cdot 45.1}{12{,}000} = 470 \ \text{N/mm} \rightarrow 470{,}000 \ \text{N/m}.$$

Without taking the damping into consideration, according to (2.57) the frequency is then

$$f_{0;87} = 4.45 \ \text{Hz} \quad \text{and} \quad f_{0;435} = 2.44 \ \text{Hz}.$$

Under the influence of the damping, the amplitude (stress or extension) is continuously reduced and the frequency is somewhat less. With the small damping of the inner rope friction, the amplitude is

Table 2.5 Results from decay tests, Wehking et al. (1999)

Main mass, M (kg)	Middle stress, σ_z (N/mm^2)	Dropping mass, M_A (kg)	Measured frequency, f_{mes} (1/s)	Calculated frequency, f_{cal} (1/s)	Logarithm decrement, Λ (−)	Decay coefficient, δ (1/s)
400	87	134	5.03	4.45	0.125	0.629
2,000	435	134	2.48	2.44	0.046	0.115
2,000	435	500	2.41	2.44	0.089	0.215

$$x = x_0^{-\delta t} \cos \omega t. \tag{2.59}$$

In this, δ is the decay coefficient, ω the angular frequency of the damped vibration and t the time. The decay coefficient is

$$\delta = \frac{\Lambda}{T} = \Lambda \cdot f = \frac{\Lambda \cdot \omega}{2 \cdot \pi}.$$

The logarithmic decrement Λ is the natural logarithm of the ratio of two consecutive maximum amplitudes

$$\Lambda = \ln \frac{\hat{x}_i}{\hat{x}_{i+1}}.$$

The frequency of the poorly damped vibration is

$$\omega = \sqrt{\omega_0^2 - \delta^2}. \tag{2.60}$$

The results of the decay tests conducted by Wehking et al. (1999) are presented in Table 2.5. Because there is only a very small decay coefficient, the frequency is hardly reduced by the damping. The frequencies which were measured and calculated are compared in Table 2.5. For the small middle rope tensile stress 87 N/mm^2, the difference between the measured and the calculated frequency is 13 %. That is probably caused by the big deviation occurring in the measured elasticity module for small stress levels. For the big middle rope tensile stress 435 N/mm^2 there is practically no difference between the measured and the calculated frequencies.

As expected, the damping of wire ropes with longitudinal vibrations is much greater for the small mean stress than for the big one. This behaviour is caused by the inner rope friction, Andorfer (1983). The hysteresis area, enclosed by the loading and unloading loop, shows the damping energy. In Fig. 2.14, it can be clearly seen that the higher the stress level is, the smaller the enclosed area. Certainly, as far as the wire rope with fibre core in Fig. 2.14 is concerned, the damping is greater than that found for a rope with a steel core. No explanation was found for the smaller logarithm decrement Λ which was measured for the smaller dropping mass.

Example 2.5: *Frequency of a mass hanging on a wire rope*

Data:
Filler 6 × 19-IWRC-*sZ* (ten times loaded)
Mass $M = 1{,}000$ kg
Rope diameter $d = 10$ mm
Rope length $L = 50$ m

Results:
With the wire rope-cross section $A = C_2 d^2 = 45.7\ \text{mm}^2$ with $C_2 = 0.457$ accordingly Table 1.9, the rope tensile stress is

$$\sigma_m = \frac{M \cdot g}{A} = \frac{M \cdot g}{C_2 \cdot d^2} = \frac{1{,}000 \cdot 9.81}{0.457 \cdot 10^2} = 218\ \text{N/mm}^2.$$

According to (2.50) and (2.52), the wire rope elasticity module is

$$E_S = 119{,}300\ \text{N/mm}^2.$$

From that, according to (2.58), the spring constant is

$$c_S = \frac{119{,}300 \cdot 44.9}{50} = 107{,}130\ \text{N/m}$$

and the frequency according to (2.57) is

$$f_0 = \frac{1}{2 \cdot \pi} \sqrt{\frac{107{,}130}{1{,}000}} = 1.6511/\text{s}.$$

2.2.4.3 Transverse Waves

A short-time local (lateral) deflection moves as a wave along the wire rope. Czitary (1931) investigated these waves theoretically and he pointed out that the tensile force of a wire rope can be calculated by measuring the wave running time. According to Zweifel (1961) the velocity of a transverse wave is

$$\upsilon = \sqrt{\frac{g \cdot S}{q}\left[1 + \frac{EI}{S}\left(\frac{2 \cdot \pi}{\lambda}\right)^2\right]}. \tag{2.61}$$

In this S is the rope tensile force in N;

g the acceleration due to gravity in m/s^2;
q the length-related rope weight force in N/m;
E the rope elasticity module in N/m^2;
I the equatorial moment of inertia in m^4;
λ is the wave length in m.

If a wire rope is knocked with a lead hammer, transverse waves of different wave lengths will be initiated and run along the rope. As (2.61) shows, the velocity of the wave increases with the decreasing length of the wave. The velocity of a wave package with different wave lengths is therefore inhomogeneous with a scatter which increases with time. The lead hammer method is therefore unsuitable for evaluating the tensile force of a rope. Instead of this, Zweifel (1961) recommended using the kind of impulse which produces a wave length which is as large and homogeneous as possible so that the bending stiffness of the wire rope can be neglected and (2.61) can be simplified to

$$\upsilon = \sqrt{\frac{g \cdot S}{q}}.$$

With the length-related rope mass $m_r = q/g$, the wave velocity is

$$\upsilon = \sqrt{\frac{S}{m_r}}. \tag{2.62}$$

The failure for the rope tensile force calculated is smaller than 1 % if the wave length is at least $\lambda > 250$; 300 and 450d for the tensile rope stress $\sigma_z = 600$; 400 and 200 N/mm^2, Zweifel (1961). The desired wave length λ will be obtained if the impulse brought on the rope is not too sharp and $\lambda/4$ away from the end of the rope. Zweifel recommended winding a fibre rope around the wire rope and pulling on that shock-wise by hand. He supposed that the force of one hand was sufficient for a wire rope of 20 mm diameter. For thicker wire ropes, it would be necessary to have several persons pulling (increasing in number with the rope diameter squared). After pulling, the fibre rope should be slightly stressed by hand, so that the waves coming back can be sensed. For n cycles in the measured time t and for the rope length L, the length of the rope from one end to the other, the wave velocity is

$$\upsilon = \frac{2 \cdot n \cdot L}{t}. \tag{2.63}$$

According to that and (2.62), the rope tensile force in the middle of the rope field is

$$S = m_r \cdot \left(\frac{2 \cdot n \cdot L}{t}\right)^2. \tag{2.64}$$

For very large rope fields, Zweifel presented equations to calculate the rope tensile force considering the chain line.

Example 2.6: *Rope tensile force from the running time of the transverse wave*

Data:
Seale rope 6 × 19-NFC-zZ
rope diameter $d = 20$ mm
distance between rope terminations $L = 250$ m
number of cycles $n = 12$
running time t for n cycles $t = 40$ s

Results:
According to Eq. (1.5b) and Table 1.9, the length-related mass m_r of the rope is

$$m_r = \frac{1}{100} \cdot W_1 \cdot d^2 = \frac{1}{100} \cdot 0.359 \cdot 20^2 = 1.436 \text{ kg/m}$$

Then according to (2.64), the rope tensile force in the middle of the rope field is

$$S = m_r \cdot \left(\frac{2 \cdot n \cdot L}{t}\right)^2 = 1.436 \cdot \left(\frac{2 \cdot 12 \cdot 250}{40}\right)^2 = 32{,}300 \text{ N}.$$

2.2.4.4 Transverse Vibrations

Transverse vibrations are to be understood as standing waves. The equations for the velocity of the waves can be used to calculate the frequency. Because the wave length is large, the influence of the bending stiffness is very small and can be neglected. So (2.62) can be used and the running time of the wave, there and back, is

$$t_L = \frac{2 \cdot L}{\upsilon} = 2 \cdot L \sqrt{\frac{m_r}{S}}. \tag{2.65}$$

In this, L is once again the rope length (or the distance between the ends of the rope for a small curvature). The period T of a standing wave is

$$T = \frac{t_L}{i}$$

and with (2.65)

$$T = \frac{2 \cdot L}{i} \sqrt{\frac{m_r}{S}}. \tag{2.66}$$

In this i is the number of the antinodes of vibration on the rope length. The frequency is

$$f = \frac{1}{T} = \frac{i}{2 \cdot L} \sqrt{\frac{S}{m_r}}. \tag{2.67}$$

In rope fields which are not too long i.e. about 100 m, it is possible to make the rope vibrate, Zweifel (1961). Using the frequency f observed here, the rope tensile force S can be calculated according to the converted (2.67)

$$S = m_r \left(\frac{2 \cdot f \cdot L}{i} \right)^2. \tag{2.68}$$

There are strong variations of the rope tensile force in rope-ways due to braking. The movements of the ropes and their connected masses in such systems can only be calculated with large-scale methods. Such methods are presented by Czitary (1975), Engel (1977), Schlauderer (1990) and Beha (1994). For transverse vibrations, the damping depends on the rope construction, the rope tensile force and the amplitude. Raoof and Huang (1993) reported investigating into the damping of spiral ropes.

The basic frequency of transversal vibration (string) of a wire rope can be calculated with the help of the Excel-program SEILELA2.XLS.

Example 2.7: *Frequency of transverse vibration (string)*

Data from Example 2.5.

According to Table 1.9, the length-related rope mass is

$$m_r = \frac{1}{100} \cdot W_2 \cdot d^2 = \frac{1}{100} \cdot 0.4 \cdot 10^2 = 0.40 \text{ kg/m}$$

The frequency of the transverse vibration with one antinode of vibration $i = 1$ is

$$f = \frac{i}{2 \cdot L} \sqrt{\frac{S}{m_r}} = \frac{1}{2 \cdot 50} \sqrt{\frac{1{,}000 \cdot 9.81}{0.40}} = 1.5661 \text{ 1/s}.$$

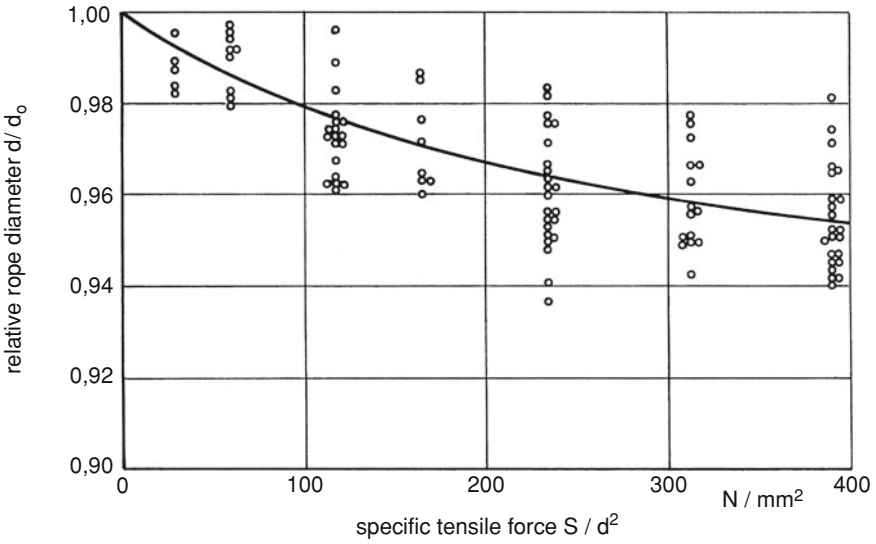

Fig. 2.18 Relative rope diameter d/d_0 of 8-strand ropes with fibre core

2.3 Reduction of the Rope Diameter Due to Rope Tensile Force

The reduction of the rope diameter due to the rope tensile force is caused by the lateral contraction of the wires, the strands and, in particular, the cores. The lateral contraction of the wires caused by its tensile stress is small. Even for a tensile stress of 670 N/mm^2 the wire contraction is only one per mil of the diameter of the wire. In comparison, the effect of the relatively low length-related compressive force of the wires and in particular of the strands on the core is much greater.

The length-related compressive force first results in resetting any loose wires and strands and then in deforming the rope in a different way. There is also some minor deformation due to the pressure between wires crossing. As far as fibre-core wire ropes are concerned, a large diameter reduction occurs and this is mainly due to the compression of the core. The diameter reduction of steel-core wire ropes, on the other hand, is normally less than that found with fibre-core wire ropes and this is mainly caused by the wires of the strands and the core becoming adjusted to one another.

Measurements were taken of the diameters of a great number of wire ropes affected by different tensile forces. Figures 2.18 and 2.19 show the diameter reduction measured as the relative rope diameter d_S/d_0 for the first loading. The diameter for the loaded wire rope is d_S and the actual diameter for the not loaded wire rope is d_0. Figure 2.18 presents the relative rope diameter of 8-strand fibre-core wire ropes and Fig. 2.19 those with steel cores. The nominal rope diameter—which is normally smaller than the actual diameter—of all these ropes is 16 mm.

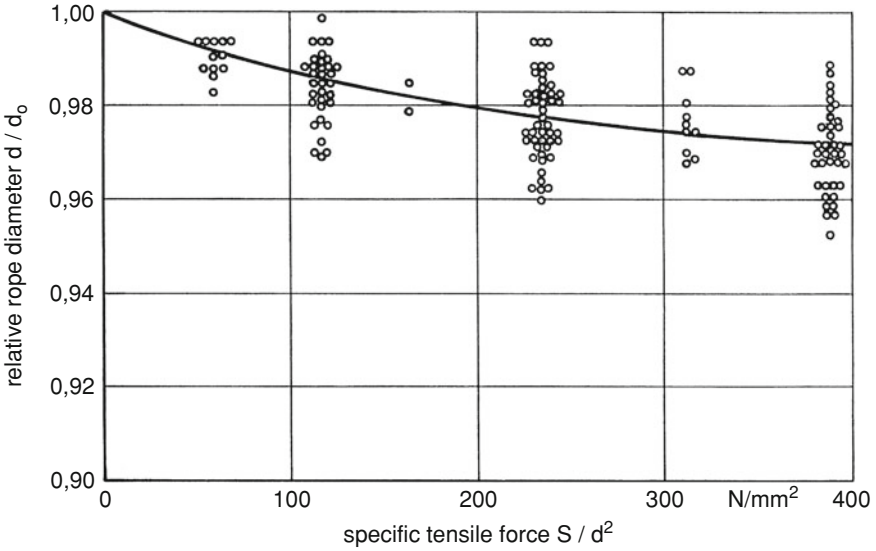

Fig. 2.19 Relative rope diameter d/d_0 of 8-strand ropes with steel core

Relative rope diameters d/d_0 deviate to a great extent. The most important influences are due to wires and strands loosening and to variations in core density. An unexpectedly small diameter reduction can result from the strands arching. Such arched strands reduce the working life of running ropes and should therefore be avoided. For the fibre-core wire ropes normally used for rope ways, the regulations therefore recommend that up to half of the wire rope breaking force the rope diameter should be at least 3.1 times the strand diameter for 6-strand ropes and 3.8 times the strand diameter for 8-strand ropes.

2.4 Torque and Torsional Stiffness

2.4.1 Rope Torque from Geometric Data

If a wire rope is loaded by a tensile force, a rope torque will occur due to the helix structure of the rope. The torque can be calculated if the geometric data of the wire rope and the rope tensile force are known. Heinrich (1942) was the first to investigate the torque of a strand by consistently taking any changes in the strand diameter and the lay length into account. Costello and Sinha (1977a, b), Costello and Miller (1979) have also arrived at this derivation. In contrast, most authors such as Dreher (1933), Hruska (1953), Unterberg (1972) and Haid (1983) made use of a practical calculation which neglected minor influences. Engel (1957, 1958) calculated the torque and the torsional stiffness as well.

By neglecting the same minor influences, it is possible to come up with a calculation method for the torque using the equations from Sect. 2.1. According to (2.11) the torque of a not twisted strand or spiral rope is (with the wire winding radius $r_W = r$)

$$M = \sum_{i=1}^{n} S_i \cdot r_i \cdot z_i \cdot \tan \alpha_i. \tag{2.69}$$

The symbols are the same as in Sect. 2.1. The lay angle α for a different lay direction is used with a different sign. In neglecting the contraction (Poisson ratio $\nu = 0$) and with the same elasticity module E for all wires, according to (2.20a) the torque is

$$M = \frac{\Delta l_S}{l_S} \cdot E \cdot \sum_{i=1}^{n} z_i \cdot r_i \cdot A_i \cdot \cos^2 \alpha_i \cdot \sin \alpha_i. \tag{2.70}$$

By neglecting the same influences, according to (2.21) the rope tensile force is

$$S = \frac{\Delta l_S}{l_S} \cdot E \cdot \sum_{i=0}^{n} z_i \cdot A_i \cdot \cos^3 \alpha_i. \tag{2.71}$$

By eliminating $E \cdot \Delta l_s / l_s$ from (2.70) and (2.71), the torque of a not twisted strand or spiral rope is

$$M = \frac{S \cdot \sum_{i=1}^{n} z_i \cdot r_i \cdot A_i \cdot \cos^2 \alpha_i \cdot \sin \alpha_i}{\sum_{i=0}^{n} z_i \cdot A_i \cdot \cos^3 \alpha_i}. \tag{2.72}$$

It is advisable to introduce a torque constant c_{1S}. With that constant, the torque for a strand or a spiral rope is

$$M = c_{1S} \cdot d_S \cdot S. \tag{2.73}$$

The torque constant c_{1S} depends only on the rope geometry. Out of (2.72) and (2.73), the torque constant for strands or spiral ropes is

$$c_{1S} = \frac{\sum_{i=1}^{n} z_i \cdot r_i \cdot A_i \cdot \cos^2 \alpha_i \cdot \sin \alpha_i}{d_S \cdot \sum_{i=0}^{n} z_i \cdot A_i \cdot \cos^3 \alpha_i}. \tag{2.74}$$

Analogous to (2.72), the torque for a stranded rope can be expressed with a torque constant c_1

$$M = c_1 \cdot d \cdot S. \tag{2.72a}$$

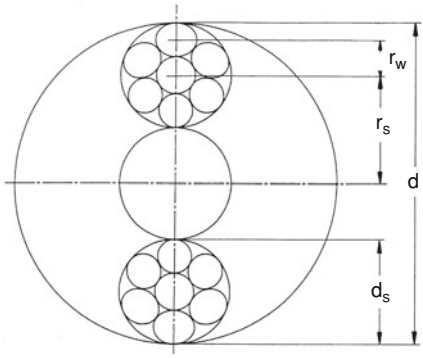

Fig. 2.20 Wire rope with one strand layer

The torque constant c_1 for a stranded rope with some round strand layers (strand lay angle β_j) with fibre or steel core is

$$c_1 = \frac{\sum_{j=1}^{n} z_j \cdot A_j \cdot r_{Sj} \cdot \cos^2 \beta_j \cdot \sin \beta_j + \sum_{j=0}^{n} z_j \cdot A_j \cdot d_{Sj} \cdot c_{1Sj} \cdot \cos^3 \beta_j}{d \cdot \sum_{j=0}^{n} z_j \cdot A_j \cdot \cos^3 \beta_j}. \quad (2.75)$$

For a one-layer round strand rope with fibre core the equation for the torque constant can be simplified enormously to

$$c_1 = \frac{r_S \cdot \tan \beta + d_S \cdot c_{1S}}{d}.$$

The symbols here are the same as in Fig. 2.20. For spiral round strand ropes with the same strands in all strand layers the torque constant is a simplification of (2.75)

$$c_1 = \frac{\sum_{j=1}^{n} z_j \cdot r_{Sj} \cdot \cos^2 \beta_j \cdot \sin \beta_j + c_{1S} \cdot d_S \cdot \sum_{j=0}^{n} z_j \cdot \cos^3 \beta_j}{d \cdot \sum_{j=0}^{n} z_j \cdot \cos^3 \beta_j}. \quad (2.76)$$

It is possible to calculate the torque of round strands and round strand ropes to a satisfactory degree of accuracy with the equations presented here provided that there is sufficient known geometric data for the rope. These methods of calculation are of particular use to rope manufacturers when designing new ropes, especially for so-called non-rotating ropes. Such ropes have to be designed in such a way that the resulting rope torque is as close to zero as possible.

Calculating the rope torque with the equations presented here is only possible for ropes which are not twisted. For twisted ropes, the torque is strongly influenced by the torsional rope stiffness.

Example 2.8: *Torque constant c of the open spiral rope in* Fig. 2.4

According to (2.74), the torque constant is

$$c_{1S} = \frac{(6 \cdot 13 - 12 \cdot 2.55 + 18 \cdot 3.8) \cdot 1.227 \cdot 0.970^2 \cdot 0.242}{8.85 \cdot [1 \cdot 1.431 + (6 + 12 + 18) \cdot 1.227 \cdot 0.970^3]}$$

$$c_{1S} = \frac{12.74}{369.45} = 0.0345.$$

2.4.2 Torque of Twisted Round Strand Ropes

2.4.2.1 Measurements

The torque of twisted and not twisted round strand ropes has been investigated by measurements. With the results of these measurements a simple calculation method will be derived with that the customer can calculate the torque for a given wire rope. This method will have the advantage that it can be used without knowing the precise geometrical data of the rope.

Torque measurements with different tensile forces and different twist angles are carried out with a series of ropes. The equipment of Feyrer and Schiffner (1986) comprises a torque meter and a rope twisting device, mounted in a tensile testing machine for carrying out the measurements. The torque meter, which measures the torque by means of strain gauges, is because of the installed membranes nearly not influenced by the tensile force. The entire equipment is shown in Fig. 2.21. Rebel and Chandler (1996) presented a measuring equipment with the opportunity to measure in addition the rope elongation and the rope diameter reduction.

In all cases the wire rope is at both ends fixed in a rope socket so that a relative motion of the wires and the strands are prevented strictly. The torques measured with different twisted wire ropes (positive sign for turn off) are shown in Figs. 2.22 and 2.23 for ordinary lay ropes 6 × 7-FC and Warrington 8 × 19-FC. As for all wire ropes with fibre core the torque increases nearly linear with the tensile force. The distance of the lines for the different twist angles is for the wire rope 6 × 7-FC bigger than for the Warrington rope 8 × 19-FC. That means the wire rope 6 × 7-FC with 42 wires is more torsion rigid than the Warrington rope with 152 wires. The Warrington rope has been measured lubricated and not lubricated with practically no different torque.

The torque for the increasing and decreasing tensile force shows nearly no hysteresis. In the following diagrams only the lines for the increasing tensile force are shown.

For wire ropes with independent made steel wire rope core IWRC the torque also increases nearly linear with the tensile force. To demonstrate this, in addition to the measured torque lines, straight lines are sketched in Fig. 2.24 for a Filler rope 8 × (19 + 6F)-IWRC-sZ.

Double parallel wire ropes (PWRC) have only a nearly linear relation between torque and tensile force for small twist angles. Figure 2.25 shows the torque of a

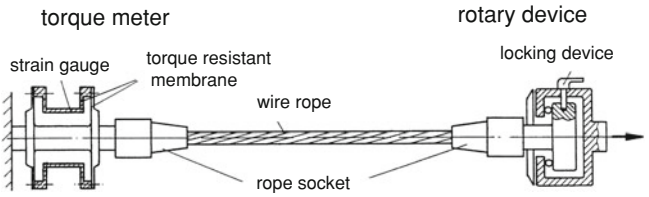

Fig. 2.21 Equipment for measuring the torque and the rotary angle, Feyrer and Schiffner (1986)

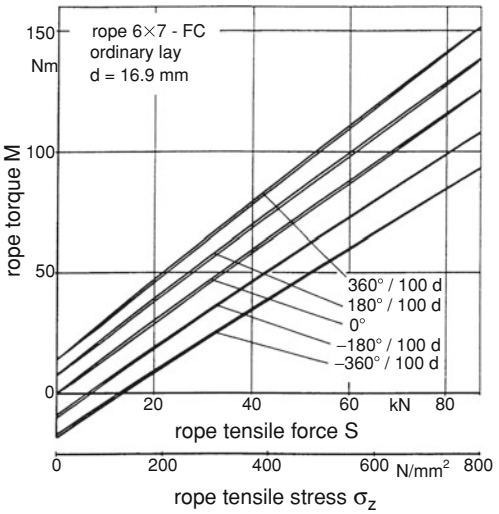

Fig. 2.22 Torque of a wire rope 6 × 7-FC-sZ, Feyrer and Schiffner (1986)

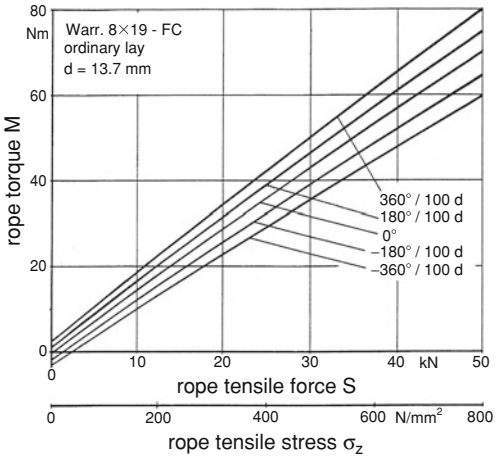

Fig. 2.23 Torque of a Warrington rope 8 × 19-FC-sZ, Feyrer and Schiffner (1986)

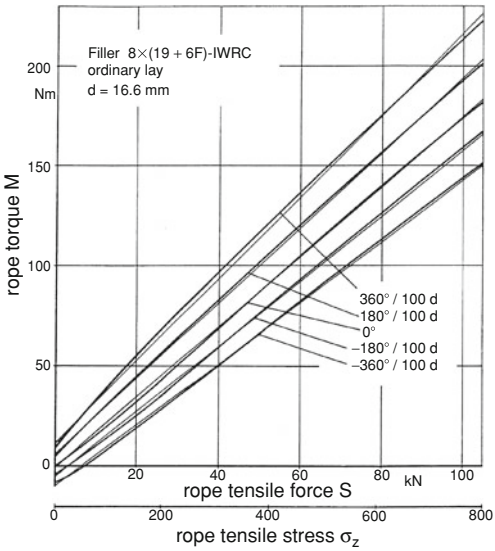

Fig. 2.24 Torque of a Filler rope 8 × (19 + 6F)-IWRC-sZ, Feyrer and Schiffner (1986)

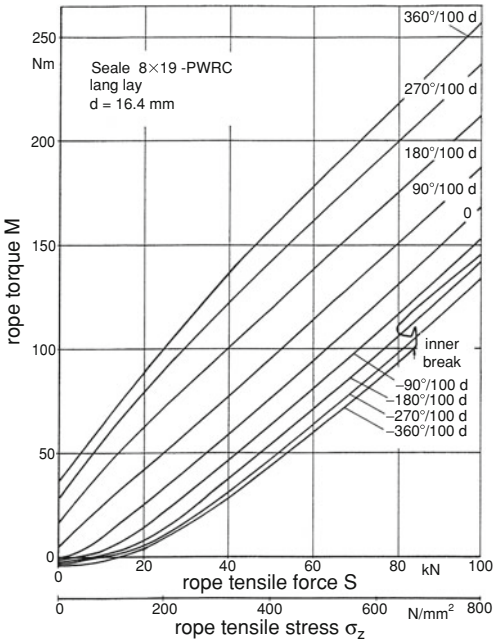

Fig. 2.25 Torque of a Seale rope 8 × 19-PWRC-zZ, Feyrer and Schiffner (1986)

Seale rope 8 × 19-PWRC-*z*Z. In the twisted state the strands and the core are loaded very differently. Therefore in the 360° untwisted wire rope on the rope length $L = 100d$, the core breaks very soon at the relative small rope tensile stress $\sigma z = 640$ N/mm^2, as to be seen in Fig. 2.25.

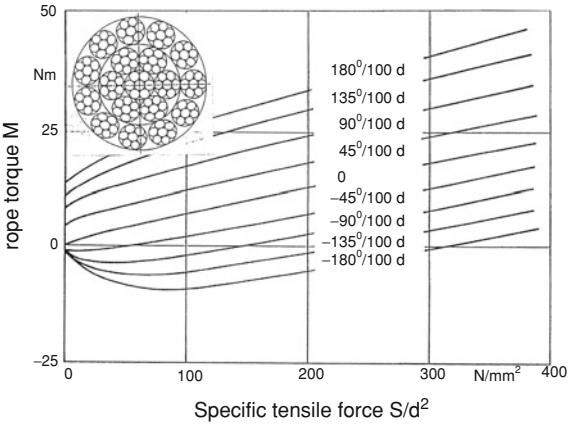

Fig. 2.26 Torque of a spiral round strand rope with two strand layers, Feyrer (1997)

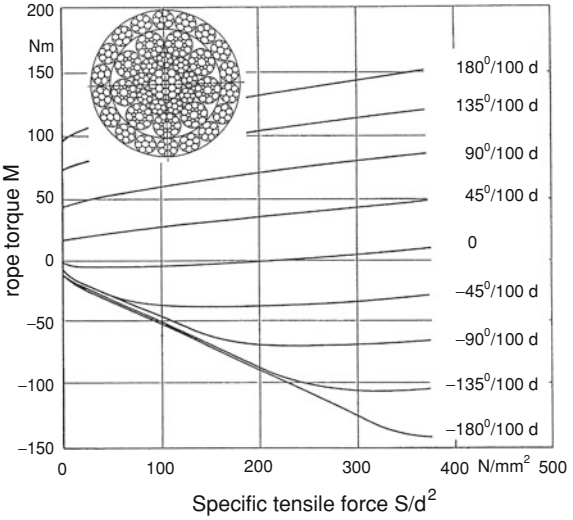

Fig. 2.27 Torque of a spiral round strand rope with three strand layers, Feyrer (1997)

In addition to the described investigation (1986) a lot of torque measurements with spiral strand ropes have been done from the Institut für Fördertechnik der Universität Stuttgart in a great part by students. This work was sponsored from AVIF and the Drahtseilvereinigung, The results of this investigation are presented by Feyrer (1997), in which the work of the students are listed.

The torque of a spiral strand rope with two strand layers is shown in Fig. 2.26 and that with three strand layers in Fig. 2.27. The torque-tensile-force lines are all buckled even for the not twisted rope. The reason for this buckling of the not twisted rope is that the different strands are not loaded from the load beginning. The relative big distance between the torque lines shows that the spiral strand ropes are twist rigid.

2.4.2.2 Calculation of the Torque for Wire Ropes

The results of the torque measurements with the round strand wire ropes with one strand layer can be very good evaluated by a regression calculation. Kollros (1974, 1976) evaluated first his torque measurements with such a regression. Based on theoretical considerations he creates an equation with two constants for the regression. Forerunner of these constants are the torque constant $\mu = M/S = c_1 d$ and the torsional stiffness $D = M/\omega$ from Engel (1957, 1958, 1966).

The torque measurements with many wire ropes by Feyrer and Schiffner (1986) show that two constants are not enough to describe the results with good precision. Therefore the regression for the results of these measurements has been made practically with the equation of Kollros but with three constants. The torque is then

$$M = c_1 \cdot d \cdot S + c_2 \cdot d^2 \cdot S \cdot \omega + c_3 \cdot G \cdot d^4 \cdot \omega. \tag{2.77}$$

Therein M is the torque;

φ	the rotary angle in rad;
d	the rope diameter;
$\omega = \varphi/L$	the twist angle;
S	the tensile force;
L	the rope length;
G	the shear module;

and, c_1 c_2, c_3, are constants.

The twist angle ω has to set positive for turning off the rope and negative for turning on the rope. The constants c and their standard deviation are listed in Table 2.6. These constants have been found by regression of Feyrer and Schiffner (1986) with their own test results, with many test results of students and with the test results of Kollros (1974) and Unterberg (1972). As limit for the use of (2.77) with the constants c, the maximum allowed twist angle $\omega_{max} = \varphi_{max}/100d$ (angle for a rope length of 100 times rope diameter) is also given in Table 2.6.

By measurements with wire ropes of diameters 55.6 and 76 mm Kraincanic and Hobbs (1997) evaluated torque constants c_1 that corresponds respecting the standard deviation with those in Table 2.6. Cantin et al. (1993) found in measurements with a 6-strand rope constants c_1 and c_2 comparable with that of Table 2.6 but the constant c_3 deviates more than 30 %. For lang's lay triangular strand ropes Rebel (1997) found that (2.77) cannot describe satisfactory the measured torques. Therefore Rebel established an equation with nine constants what he evaluated out of his measurements.

Table 2.6 Constants c_1, c_2, c_3 to the torque (2.77), Feyrer and Schiffner (1986)

Rope construction			6-strand				8-strand			
Core	Layer	Strands number of wires	c_1	c_2	$c_3 \cdot 10^3$	$\pm\varphi_{max}$ for $100d$	c_1	c_2	$c_3 \cdot 10^3$	$\pm\varphi_{max}$ for $100d$
FC	*sZ*	7	0.100	0.157	0.765	360°	0.106	0.166	0.658	360°
		19 Seale	0.109	0.207	0.400	360°	0.115	0.216	0.293	360°
		19 Filler[a],	0.102	0.212	0.376	360°	0.108	0.222	0.268	360°
		19 Warr.	0.102	0.212	0.376	360°	0.108	0.222	0.268	360°
		36 Warr.-Seale	0.105	0.212	0.376	360°	0.111	0.222	0.268	360°
FC	*zZ*	7	0.123	0.127	0.732	360°	0.129	0.137	0.624	360°
		19 Seale	0.132	0.177	0.367	360°	0.138	0.186	0.259	360°
		19 Filler[a],	0.126	0.183	0.342	360°	0.131	0.194	0.234	360°
		19 Warr.	0.126	0.183	0.342	360°	0.131	0.194	0.234	360°
		36 Warr.-Seale	0.128	0.183	0.342	360°	0.134	0.194	0.234	360°
IWRC	*sZ*	7	0.080	0.131	0.921	180°	0.086	0.141	0.813	180°
		19 Seale	0.089	0.181	0.556	180°	0.095	0.190	0.448	180°
		19 Filler[a],	0.082	0.187	0.531	180°	0.088	0.196	0.424	180°
		19 Warr.	0.082	0.187	0.531	180°	0.088	0.196	0.424	180°
		36 Warr.-Seale	0.085	0.187	0.531	180°	0.091	0.196	0.424	180°
IWRC	*zZ*	7	0.103	0.101	0.888	180°	0.109	0.112	0.779	180°
		19 Seale	0.112	0.151	0.523	180°	0.118	0.160	0.414	180°
		19 Filler[a],	0.105	0.158	0.497	180°	0.111	0.168	0.390	180°
		19 Warr.	0.105	0.158	0.497	180°	0.111	0.168	0.390	180°
		36 Warr.-Seale	0.108	0.158	0.497	180°	0.114	0.168	0.390	180°
Standard deviation			0.012	0.028	0.080		0.012	0.028	0.080	

[a] Filler 19 = Filler 19 + 6F

Example 2.9: *Wire rope torque*

Data:
Filler rope 6 × (19 + 6*F*)—NFC-sZ
rope diameter $d = 16$ mm
rope length $L = 5{,}000$ mm
shear module $G = 76{,}000$ N/mm^2
tensile force $S = 40{,}000$ N
angle of turn on $\varphi = -600°$
$\varphi = -2 \cdot \pi \cdot 600/360 = -10.47$ rad
twist angle $\omega = -10.47/5{,}000 = -0.002094$ rad/mm $= -192°/100$d

The constants out of Table 2.6 are
$c_1 = 0.102$; $c_2 = 0.212$; $c_3 = 0.376 \times 10^{-3}$

Results:
According (2.77) the rope torque is
$M = 0.102 \cdot 16 \cdot 40{,}000 - 0.212 \cdot 16^2 \cdot 40{,}000 \cdot 0.002094 - 0.376 \cdot 10^{-3} \cdot 16^4 \cdot 0.002094 \cdot 76{,}000$
$M = 65{,}800 - 4{,}540 - 3{,}920$
$M = 56{,}800$ N mm $= 56.8$ Nm.

2.4.2.3 Definition of Non-rotating Rope

The spiral strand ropes are designated for supporting loads without turning protection. Therefore they should be rotation-resistant to a great extent. This will be succeeded only approximately. Really non-rotating spiral strand ropes do not exist. But it is useful to define the limit up to this a wire rope can be declared as a non-rotating one.

A proposal for the definition of a non-rotating wire rope is:

A wire rope counts as non-rotating if the twist angle rests smaller than

$$\frac{\varphi}{L} \leq \frac{360^\circ}{1{,}000 \cdot d}$$

during the tensile loading between

$$\frac{S}{d^2} = 0 \quad \text{to} \quad \frac{S}{d^2} = 150 \ \text{N/mm}^2.$$

2.4.2.4 Spiral Round Strand Ropes

From 48 spiral round strand ropes with three strand layers (with between 14 and 20 outer strands) seven ropes are not non-rotating for the given definition. On the other hand from the 25 tested spiral round strand ropes with two strand layers (with between 10 and 12 outer strands) six ropes are still non-rotating.

The non-rotating spiral strand ropes show—if not twisted—torque-tensile-force lines with a small buckling and a mean constant $c_1 = 0.026$ with the standard deviation $s = 0.012$. For all these ropes the torque constant c_1, calculated with (2.76) on the base of geometrical data, has been very well confirmed by the torque zero is to lead back on the rope geometry not optimal chosen. Under the specific tensile force $S/d^2 = 0$–150 N/mm^2 the "non-rotating ropes" show the mean twist $\varphi/1{,}000d = -40°/1{,}000d$ in turning on direction with the standard deviation $s = 140°/1{,}000d$.

The low-rotating spiral round strand ropes with two strand layers show—if not twisted—a nearly straight torque-tensile-force line with $c_1 = 0.058$. For a small twisting up to $90°/100d$ a nearly straight torque-tensile-force line is only to expect

for specific tensile forces above $S/d^2 > 70$ N/mm^2, as can be seen in Fig. 2.26. For that the constants are

$$c_1 = 0.058$$
$$c_2 = 0.269$$
$$c_3 = 0.00853.$$

2.4.2.5 Conditions for Calculations with Rope Twist

The results of the calculations are valid on the condition that

- the wire rope is at both ends fixed in a termination so that the relative motion of wires and the strands are prevented strictly
- the twist angle $\omega < 360°/100d$ for ropes with fibre core FC
  $< 180°/100d$ for ropes with steel core IWRC

  according to the measurement limits in Feyrer and Schiffner (1986/1987)
- and in case that the angle between the chord of the rope bow and the horizontal $\beta_F < 90°$, the result of the calculation is nearly valid on the condition that the sag of the rope bow is small.

2.4.3 Rotary Angle of a Load Hanging on Two or More Wire Rope Traces

A load hanging on wire ropes will be rotated by the rope torque. The rotary angle φ of the load will be derived for two or more traces from the same wire rope. Following Unterberg (1972), who has made the first derivation, the bottom sheave of a crane will be taken as example, Fig. 2.28. Out of the energy W for lifting the bottom sheave and the load when the bottom sheave turns, he found for the reverse moment

$$M_{rev} = \frac{dW}{d\varphi} = \frac{r_1 \cdot r_2 \cdot \sin\varphi}{\sqrt{h_0^2 - 2 \cdot r_1 \cdot r_2 \cdot (1 - \cos\varphi)}} Q_{tot}. \tag{2.78}$$

Q is the force from the mass of the load and the bottom sheave. The meaning of the other symbols can be taken out of Fig. 2.28.

With the presupposition that the height h_0 is much bigger than the distances r_1 and r_2 between the wire rope traces and the load rotary axis, the reverse moment is (with the rope weight force G_{rope})

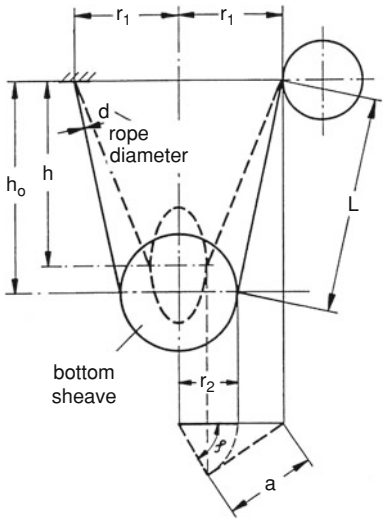

Fig. 2.28 Rotation of a bottom sheave

$$M_{rev} = \frac{r_1 \cdot r_2 \cdot \sin\varphi}{h_0} \cdot Q_{tot} = \frac{r_1 \cdot r_2 \cdot \sin\varphi}{h_0} \cdot (Q_0 + Q + G_{rope}/2) \tag{2.79}$$

with

$Q_0 + Q$ weight force of the bottom sheave and the load

G_{rope} weight force of all wire rope traces

These weight forces will be reduced by the buoyancy, if the installation is situated under water.

The torque of all the wire rope traces can be calculated with Eq. (2.77) and the constants of Table 2.6. Then for untwisted ropes ($\omega_0 = 0$) the mean torque of the bearing wire rope traces is

$$M_{rope,50} = c_1 \cdot d \cdot \left(Q_0 + Q + G_{rope}/2\right). \tag{2.80}$$

The torque, that is not exceeded in 90 % of the cases, is

$$M_{rope,90} = (c_1 + 1{,}282 s_1) \cdot d \cdot \left(Q_0 + Q + G_{rope}/2\right) \tag{2.80a}$$

with

c_1 from Table 2.6

s_1 from Table 2.6.

The bottom sheave rotated with the angle φ is in equilibriom for

$$M_{rope} = M_{rev}.$$

With that and the Eqs. (2.79) and (2.80) the mean rotary angle is

$$\varphi_{50} = \arcsin \frac{h_0 \cdot d \cdot c_1}{r_1 \cdot r_2} \tag{2.81}$$

and the rotary angle that will not be exceeded in 90 % of the ropes (for untwisted ropes, $\omega_0 = 0$) is

$$\varphi_{90} = \arcsin \frac{h_0 \cdot d \cdot (c_1 + 1{,}282 \cdot s_1)}{r_1 \cdot r_2}. \tag{2.81a}$$

In addition a pre-twisting with a twist angle $\omega_0 \neq 0$ can occur by wrong rope mounting or rope running over sheaves with side deflection. Under the influence of those pre-twisted ropes the total rotary angle is

$$\varphi_{tot} = \arcsin \left(f_{twi} \cdot \frac{h_0 \cdot d \cdot (c_1 + 1{,}282 \cdot s_1)}{r_1 \cdot r_2} \right). \tag{2.81b}$$

The twisting factor f_{twi} is the ratio between the torque M out of the Eq. (2.77) for the pre-twisted ropes ($\omega = \omega_0$) and that without pre-twisting ($\omega = 0$)

$$f_{twi} = \frac{(c_1 + 1{,}282 \cdot s_1) \cdot d \cdot S + c_2 \cdot d^2 \cdot S \cdot \omega + c_3 \cdot G \cdot d^4 \cdot \omega}{(c_1 + 1{,}282 \cdot s_1) \cdot d \cdot S} \tag{2.82}$$

with the rope tensile force

$$S = \frac{Q_0 + Q + G_{rope}/2}{z}. \tag{2.83}$$

A pre-twisting angle should be estimated according the existing circumstances. For example with two or four bearing rope traces (z = 2 or 4), a pre-twisting angle $\omega_0 = 20°/100d$ may be exist.

The presented calculation method is not only valid for two rope traces. For all number of bearing rope traces is

- r_1 is the mean distance between the upper end of all the rope traces to the load rotation axis
- r_2 is the mean distance between the lower end of all the rope traces to the load rotation axis.

An overlapping of the bearing rope traces will be prevented, if the rotary angle is smaller than 90°. The critical case is that for the load force out of the bottom sheave mass only and for the biggest possible height h_0 .

For the practical calculation of the rotary angle the Excel-program FLADREH2.xls can be used.

Example 2.10: *Rotary angle of a bottom sheave*

The distances corresponding with Fig. 2.28 are

$r_1 = 200$ mm
$r_2 = 150$ mm
$h_0 = 8{,}000$ mm

rope WS—IWRC—6 × 36—sZ—1,770 N/mm^2

$d = 16$ mm
$c_1 = 0.085$ from Table 2.6
$s_1 = 0.012$ from Table 2.6
$W = 0.409$ length mass factor, EN 12 385
$g = 9.81$ fall acceleration g in m/s^2
$z = 2$ number of bearing rope traces
$\omega_0 = 20°/100d$

Results:
The weight force of the bearing wire rope traces in N is

$$G_{rope} = W \cdot d^2 \cdot h_0 \cdot g \cdot z/100{,}000$$
$$G_{rope} = 0.409 \cdot 16^2 \cdot 8{,}000 \cdot 9.81 \cdot 2/100{,}000 = 164.3 \text{ N}$$

The wire rope tensile force is

$$S = \frac{600 + 0 + 164/2}{2} = 341 \text{ N}.$$

The twisting factor is

$$f_{twi} = \frac{1{,}128}{548} = 2.06.$$

The mean rotary angle of the bottom sheave without pre-twisting is according Eq. (2.81)

$$\varphi_{50} = \arcsin \frac{8{,}000 \cdot 16 \cdot 0.085}{200 \cdot 160} = \arcsin 03627$$
$$\varphi_{50} = 21.3°$$

and according Eq. (2.81a) in 90 % smaller

$$\varphi_{90} = \arcsin \frac{8{,}000 \cdot 16 \cdot (0.085 + 1.282 \cdot 0.012)}{200 \cdot 150} = \arcsin 0.4283$$
$$\varphi_{90} = 25.4^\circ$$

According Eq. (2.81b) the total rotary angle that the bottom sheave not exceed is

$$\varphi_{\text{rtot}} = \arcsin 2.06 \cdot 0.4283 = \arcsin 0.8823$$
$$\varphi_{\text{tot}} = 61.9^\circ.$$

An overlapping of the bearing rope traces is not to fear.

2.4.4 Rope Twist Caused by the Height-Stress

2.4.4.1 Wire Rope Supported Non-rotated at Both Ends

Because of the rope weight the tensile force in a suspending rope has on the upper end a bigger tensile force than on the lower end. The rope stress increasing with the height of the suspending rope is called height-stress. Because the rope torque along the rope length must be constant, the wire rope supported non-rotated on the upper and the lower end will twist between the both ends. The rotary angle of a vertical hanging wire rope is demonstrated in Fig. 2.29. The rope turns on in the upper field and off in the lower field.

Engel (1957) and little later Hermes and Bruuens (1957) derived at first the rotary angle caused by the height-stress, see also Gibson (1980). Engel (1959) calculated the twist angle for haul and traction ropes of rope ways. Rebel (1997) calculated with his own equation the rotation of triangular strand ropes in deep shafts. Malinovsky and Tarnavskaya (2006) derived their calculation method reminding

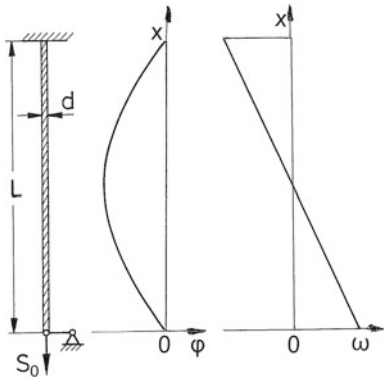

Fig. 2.29 Rotary angle φ and twist angle ω of a vertical hanging wire rope supported on both ends non-rotated

the monograph of M. F. Glushko 1966. They reported from measurements of rope lay length showing the twist and the stresses of hoist ropes in deep mine shafts.

In the following the rotary angle will be derived on the base of (2.77). That has the advantage that the constants for the different wire ropes from Table 2.6 can be used. Transforming (2.77) the twist angle is

$$\omega = \frac{\mathrm{d}\varphi}{\mathrm{d}x} = \frac{M - c_1 \cdot d \cdot S}{c_2 \cdot d^2 \cdot S + c_3 \cdot G \cdot d^4}. \tag{2.84}$$

The rope tensile force increases from the lower end with the rope length x and the angle β_F between the horizontal and the secant of the small rope bow ($S \geq m \cdot g \cdot L \cdot \cos \beta_F$ as normal in practice) approximately

$$S \approx S_0 + m \cdot g \cdot x \cdot \sin \beta_\mathrm{F}$$

with the tensile force S_0 on the lower end and the length-related rope mass m (exactly for $\beta_F = 90°$). Equation (2.84) is with that

$$\mathrm{d}\varphi = \frac{M - c_1 \cdot d \cdot (S_0 + m \cdot g \cdot x \cdot \sin \beta_\mathrm{F})}{c_2 \cdot d^2 \cdot (S_0 + m \cdot g \cdot x \cdot \sin \beta_\mathrm{F}) + c_3 \cdot G \cdot d^4} \cdot \mathrm{d}x. \tag{2.85}$$

By integrating the rotatry angle φ is

$$\varphi = \frac{c_1 \cdot x}{c_2 \cdot d} - \left(\frac{M}{c_2 \cdot d^2 \cdot m \cdot g \cdot \sin \beta_\mathrm{F}} + \frac{c_1 \cdot c_3 \cdot d \cdot G}{c_2^2 \cdot m \cdot g \cdot \sin \beta_\mathrm{F}} \right) \cdot \ln[c_2 \cdot d^2 \cdot (S_0 + m \cdot g \cdot x \cdot \sin \beta_\mathrm{F}) + c_3 \cdot G \cdot d^4] + B. \tag{2.86}$$

As preproposed the rotary angle φ is $\varphi = 0$ for $x = 0$ and $\varphi = 0$ for $x = \mathrm{L}$.

From this and (2.86) the torque M and the constant B can be derived. The torque is

$$M = -\frac{c_1 \cdot c_3 \cdot G \cdot d^3}{c_2} - \frac{c_1 \cdot d \cdot m \cdot g \cdot L \cdot \sin \beta_\mathrm{F}}{\ln\left(\frac{c_2 \cdot S_0 + c_3 \cdot G \cdot d^2}{c_2 \cdot S_0 + c_2 \cdot m \cdot g \cdot L \sin \beta_\mathrm{F} + c_3 \cdot G \cdot d^2} \right)}. \tag{2.87}$$

Then with (2.86) the rotary angle is

$$\varphi = \frac{c_1 \cdot x}{c_2 \cdot d} - \frac{c_1 \cdot L}{c_2 \cdot d} \cdot \frac{\ln\left(\frac{c_2 \cdot m \cdot g \cdot x \cdot \sin \beta_\mathrm{F}}{c_2 \cdot S_0 + c_3 \cdot G \cdot d^2} + 1 \right)}{\ln\left(\frac{c_2 \cdot m \cdot g \cdot L \cdot \sin \beta_\mathrm{F}}{c_2 \cdot S_0 + c_3 \cdot G \cdot d^2} + 1 \right)}. \tag{2.88}$$

The maximum rotary angle occurs for the rope length

$$x(\varphi_{\max}) = -\frac{c_2 \cdot S_0 + c_3 \cdot G \cdot d^2}{c_2 \cdot m \cdot g \cdot \sin\beta_F} + \frac{L}{\ln\left(\frac{c_2 \cdot m \cdot g \cdot L \cdot \sin\beta_F}{c_2 \cdot S_0 + c_3 \cdot G \cdot d^2} + 1\right)}. \tag{2.89}$$

The maximum rotary angle is given with $x = x(\varphi_{\max})$ in (2.88). The maximum twist angle $\omega_{\max}$ occurs on the lower rope end, $\chi = 0$. It will be calculated with (2.85) for $\chi = 0$ and the torque out of (2.87).

For the practical calculation of the rotary angle φ and the twist angle ω, the Excel-program SEILDRE2.XLS can be used.

2.4.4.2 Wire Rope Supported Non-rotated at Both Ends, Simplified Calculation

The torque M in the wire rope supported non-rotated at both ends can be set simplified with only a small failure

$$M = c_1 \cdot d \cdot (S_0 + m \cdot g \cdot L/2 \cdot \sin\beta_F). \tag{2.90}$$

Then with (2.85) the twist angle is

$$\omega = \frac{c_1 \cdot m \cdot g \cdot (L/2 - x) \cdot \sin\beta_F}{c_2 \cdot d \cdot (S_0 + m \cdot g \cdot x \cdot \sin\beta_F) + c_3 \cdot G \cdot d^3}. \tag{2.91}$$

With that on the upper rope end the twist angle is

$$\omega_{\text{upper}} = -\frac{c_1 \cdot m \cdot g \cdot L/2 \cdot \sin\beta_F}{c_2 \cdot d \cdot (S_0 + m \cdot g \cdot L \cdot \sin\beta_F) + c_3 \cdot G \cdot d^3} \tag{2.91a}$$

and on the lower rope end

$$\omega_{\text{lower}} = \frac{c_1 \cdot m \cdot g \cdot L/2 \cdot \sin\beta_F}{c_2 \cdot d \cdot S_0 + c_3 \cdot G \cdot d^3}. \tag{2.91b}$$

For the integration to evaluate the rotary angle φ, the denominator of (2.91) can be further simplified with $x = L/2$. The failure for that is very small if the rope weight force $mgL \sin\beta_F$ is smaller than the rope tensile force S_0. Then the twist angle is

$$\omega = \frac{c_1 \cdot m \cdot g \cdot (L/2) \cdot \sin\beta_F}{c_2 \cdot d \cdot (S_0 + m \cdot g \cdot L/2 \cdot \sin\beta_F) + c_3 \cdot G \cdot d^3} \tag{2.92}$$

and after integration the rotary angle φ is

$$\varphi = \frac{-c_1 \cdot m \cdot g \cdot \sin\beta_F \cdot (L - x) \cdot x/2}{c_2 \cdot d \cdot (S_0 + m \cdot g \cdot \sin\beta_F \cdot L/2) + c_3 \cdot G \cdot d^3}. \tag{2.93}$$

The maximum rotary angle (for $x = L/2$) is

$$\varphi_{max} = \frac{1}{8} \cdot \frac{-c_1 \cdot m \cdot g \cdot \sin\beta_F \cdot L^2}{c_2 \cdot d \cdot (S_0 + m \cdot g \cdot \sin\beta_F \cdot L/2) + c_3 \cdot G \cdot d^3}. \tag{2.94}$$

Example 2.11 *Wire rope supported non-rotated at both ends*

Data:
Warr. 8 × 19-NFC-sZ,
rope diameter $d = 16$ mm or $d = 0.016$ m
rope length related mass $m = 0.89$ kg/m
shear module $G = 76{,}000$ N/mm^2 or $G = 76 \times 10^9$ N/m^2
rope length $L = 500$ m
lower tensile load $S_0 = 10{,}000$ N
angle $\beta_F = 90°$
constants (Table 2.6) $c_1 = 0.108$; $c_2 = 0.222$; $c_3 = 0.000268$

Results:
According to (2.87) the torque is

$$M = -40.58 + 61.56 = 20.98 \text{ Nm}.$$

According (2.89) the maximum angle occurs at the rope length

$$x(\varphi_{max}) = 4080.8 - 3835.8 = 245 \text{ m}$$

The maximum rotary angle—(2.88)—is

$$\varphi_{max} = -232.8 \text{ rad}.$$

The maximum number of rope turns is then

$$n_{max} = \frac{\varphi_{max}}{2 \cdot \pi} = -37.$$

According to (2.85) and (2.87), the maximum twist angle is on the lower rope end ($x = 0$)

$$\omega_{lower} = \omega(\chi = 0) = 1.94 \text{ rad/m} = 111°/\text{m} = 178°/100\text{d}.$$

The twist angle on the upper rope end is

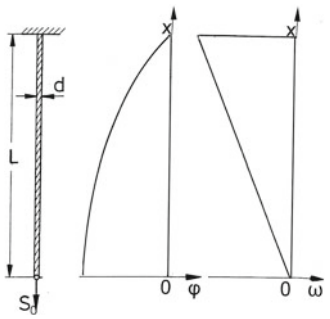

Fig. 2.30 Rotary angle φ and twist angle ω of a vertical hanging wire rope without rotation protection at the lower end

$$\omega_{upper} = \omega(\chi = \mathrm{L}) = -1.79\ \mathrm{rad/m} = -103^\circ/\mathrm{m} = -164^\circ/100d.$$

The calculated twist angles are smaller than the allowed limit 360°/100*d* (Table 2.6).

Results simplified calculation:

With the simplificated calculation the maximum rotary angle is

$$\varphi_{\max} = -232.6\,\mathrm{rad}$$

and the twist angles are

$$\omega_{lower} = \omega(\chi = 0) = 1.98\ \mathrm{rad/m} \quad \text{and} \quad \omega_{upper} = \omega(\chi = \mathrm{L}) = -1.75\ \mathrm{rad/m}.$$

2.4.4.3 Suspended Wire Rope Without Rotation Protection at the Lower End

At the lower end the wire rope has no rotation protection. However this rope end is like the upper rope end fixed in a termination so that the relative motion of wires and the strands are prevented [this is the condition for the validity of the constants c of the Table 2.6 and all the equations based on Eq. (2.77)]. The rotary angle φ and twist angle ω of a vertical hanging wire rope without rotation protection at lower end is demonstrated in Fig. 2.30.

With the torque M = 0 the twist angle is (again for $S_0 \geq m \cdot g \cdot L \cdot \cos\beta_F$) according to (2.85)

$$\omega = \frac{-c_1 \cdot d \cdot (S_0 + m \cdot g \cdot x \cdot \sin\beta_\mathrm{F})}{c_2 \cdot d \cdot (S_0 + m \cdot g \cdot x \cdot \sin\beta_\mathrm{F}) + c_3 \cdot G \cdot d^4}. \tag{2.85a}$$

$$\varphi = -\frac{c_1 \cdot (L-x)}{c_2 \cdot d} - \frac{c_1 \cdot c_3 \cdot d \cdot G}{c_2^2 \cdot m \cdot g \cdot \sin\beta_F} \times \ln \frac{c_2 \cdot d^2 (m \cdot g \cdot x \cdot \sin\beta_F + S_0) + c_3 \cdot G \cdot d^4}{c_2 \cdot d^2 (m \cdot g \cdot L \cdot \sin\beta_F + S_0) + c_3 \cdot G \cdot d^4}. \tag{2.86a}$$

The maximum rotary angle φ_{max} occurs at the lower end of the rope, that means for $x = 0$. The most interesting maximum twist angle ω_{max} occurs at the upper rope end, for $x = L$.

According to (2.85), the maximum twist angle is

$$\omega_{max} = \frac{-c_1 \cdot d \cdot (S_0 + m \cdot g \cdot L \cdot \sin\beta_F)}{c_2 \cdot d^2 \cdot (S_0 + m \cdot g \cdot L \cdot \sin\beta_F) + c_3 \cdot G \cdot d^4}. \tag{2.85b}$$

For the practical calculation of the rotary angle φ and the twist angle ω, the Excel-program FREEDRE2.XLS can be used.

Example 2.12: *Suspended wire rope without rotation protection at the lower end*

Data:
The same data will be used as in Example 2.11, but the tensile force at the lower rope end is $S_0 = 0$.

Results:
According to (2.93), the maximum rotary angle at the lower rope end is

$$\varphi_{max} = -\ 15{,}202 - 81{,}795\ \cdot\ \ln 0.8433 = -15{,}292 + 13{,}943$$
$$\varphi_{max} = -1{,}259 \text{ rad}.$$

With that, the number of rope turns at the lower end is

$$n_{max} = \frac{\varphi_{max}}{2\pi} = \frac{-1{,}259}{2\pi} = -200.4.$$

According to (2.94), the maximum twist angle (rotary angle per length unit at the upper rope end) is

$$\omega_{max} = -4.766 \text{ rad/m} \ \rightarrow \omega_{max} = -273^\circ\,\wedge/\text{m} \ \rightarrow \omega_{max} = -437^\circ/100d$$

The numbers are given with four or more digits to make it easier to follow the calculation. But, of course, the results are only valid in a scattering following the standard deviation of the constants c from Table 2.6. Above that, the maximum twist angle 437°/100d exceeds the limit 360°/100d for the validity of the constants. But for the rope considered here according to Fig. 2.23, there is practically no change of the constants c to be expected.

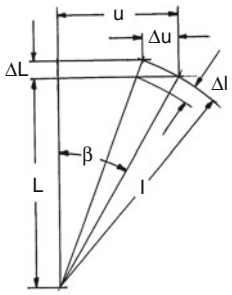

Fig. 2.31 Change of rope length by twisting the rope

2.4.5 Change of the Rope Length by Twisting the Rope

By twisting a wire rope, the rope length and the lay length will be increased in the "on" rotary direction and decreased in the "off" rotary direction. For this problem, Hankus (1997) remembered the equations of Glushko (1996). He measured and calculated the rotary angles of wire ropes in mining shafts, Hankus (1993, 1997).

In the following, the change of rope lengths will be calculated using geometric data for wire ropes with one strand layer and a fibre core. It can be presupposed that the strand length l and the strand winding radius r will remain constant. On the base of Fig. 2.31 the change of the rope length is given by the equation

$$L + \Delta L_{\mathrm{D}} = \sqrt{l^2 - (u - \Delta u)^2}. \tag{2.95}$$

In this L is the rope length and ΔL_{D} is the rope elongation when the rope is twisting.

Δu is the change of the circle bow length for the strand helix. With the strand winding radius $r_{\mathrm{S}} = r = \text{const.}$ and the rotary angle φ, the circle bow and the change of the circle bow length are

$$u = r \cdot \varphi \quad \text{and} \quad \Delta u = r \cdot \Delta\varphi.$$

Then, from (2.95), the rope elongation by twisting the rope is

$$\Delta L_{\mathrm{D}} = \sqrt{l^2 - r^2 \cdot (\varphi - \Delta\varphi)^2} - L. \tag{2.96}$$

With the strand lay angle β it is

$$l = L/\cos\beta, \quad r \cdot \varphi = L \cdot \tan\beta \quad \text{and} \quad \Delta\varphi/L = -\omega.$$

Using that, the rope elongation (+) or shortening (−) is

$$\Delta L_{\mathrm{D}} = \sqrt{\frac{L^2}{\cos^2 \beta} - L^2 \cdot \tan^2 \beta - 2 \cdot r \cdot L^2 \cdot \omega \cdot \tan \beta - r^2 \cdot \omega^2 \cdot L^2} - L.$$

Divided by L, the rope extension by twisting the rope is

$$\varepsilon_{\mathrm{D}} = \frac{\Delta L_{\mathrm{D}}}{L} = \sqrt{1 - 2 \cdot r \cdot \omega \cdot \tan \beta - r^2 \cdot \omega^2} - 1. \tag{2.97}$$

For a constant rope twisting over the rope length L, the change of the rope length is

$$\Delta L_{\mathrm{D}} = \varepsilon_{\mathrm{D}} \cdot L$$

and if the twisting over the rope length is not constant, the change of the rope length is

$$\Delta L_{\mathrm{D}} = \int_{x=0}^{L} \varepsilon_{\mathrm{D}} \cdot \mathrm{d}x = \int_{x=0}^{L} \left(\sqrt{1 - 2 \cdot r \cdot \omega \cdot \tan \beta - r^2 \cdot \omega^2} - 1 \right) \cdot \mathrm{d}x \tag{2.97a}$$

and with ω from (3.85) the change of the rope length is

$$\Delta L_{\mathrm{D}} = \int_{0}^{L} \left(\sqrt{1 - \frac{(M - c_1 \cdot d(S_0 + m \cdot g \cdot x)) \cdot 2 \cdot r \cdot \tan \beta}{c_2 \cdot d^2 \cdot (S_0 + m \cdot g \cdot x) + c_3 \cdot G \cdot d^4} - r^2 \cdot \left(\frac{M - c_1 \cdot d \cdot (S_0 + m \cdot g \cdot x)}{c_2 \cdot d^2 \cdot (S_0 + m \cdot g \cdot x) + c_3 \cdot G \cdot d^4} \right)^2} - 1 \right) \mathrm{d}x \tag{2.98}$$

The equation has to be calculated numerically.

The lay angle β' of the twisted wire rope is

$$\tan \beta' = \frac{u - \Delta u}{L + \Delta L_{\mathrm{D}}} = \frac{L \cdot \tan \beta - L \cdot r \cdot \omega}{L + \Delta L_{\mathrm{D}}}.$$

With $L + \Delta L_D = L \cdot (1 + \varepsilon_D)$, the lay angle of the twisted wire rope is then

$$\beta' = \arctan \frac{\tan \beta - r \cdot \omega}{1 + \varepsilon_{\mathrm{D}}}. \tag{2.99}$$

and with the elastic rope extension ε_{E} the lay angle is

$$\beta'' = \arctan \frac{\tan \beta - r \cdot \omega}{1 + \varepsilon_{\mathrm{D}} + \varepsilon_{\mathrm{E}}}. \tag{2.99a}$$

The lay length of the twisted wire rope is

$$h'_S = h_S \frac{\tan\beta}{\tan\beta'}. \tag{2.100}$$

Example 2.13: *Change of length of a twisted wire rope*

To demonstrate the rope length calculations, Examples 2.9, 2.11 and 2.12 will be continued. The lay angle is $\beta = 20°$.

Example 2.13a: *Constant twist angle over the entire rope length, continuation of Example 2.9*

According to (2.97), the rope elongation by twisting the rope is

$$\Delta L_D = \left(\sqrt{1 + 2 \cdot 5.4 \cdot 0.002094 \cdot 0.364 - 5.4^2 \cdot 0.002094^2} - 1\right) \cdot 5{,}000$$

$$\Delta L_D = \left(\sqrt{1.008103} - 1\right) \cdot 5{,}000 = 20.2 \text{ mm}$$

With the metallic rope cross-section $A = 100.5$ mm^2 and the rope elasticity module $E_S = 93{,}000$ N/mm^2 from Table 2.3 for the pre-loaded rope between $\sigma_z = 0$ and 400 N/mm^2, the elastic rope elongation is

$$\Delta L_E = \frac{S \cdot L}{A \cdot E_S} = \frac{40{,}000 \cdot 5{,}000}{100.5 \cdot 93{,}000} = 21.4 \text{ mm}.$$

The overall elongation is

$$\Delta L = \Delta L_D + \Delta L_E = 20.2 + 21.4 = 41.6 \text{ mm}.$$

The small neglected part of the elongation ΔL_T from twisting the strands, see Example 2.14a.

Example 2.13b: *Wire rope supported non-rotated at both ends, continuation of Example 2.11*

Integrating (2.98) leads to a small reduction of the rope length for the twisted wire rope

$$\Delta L_D = -0.01138 \approx -0.011 \text{ m}$$

From the length $x = 245$ m, the lower rope section turns off and the upper rope section turns on with the rotary angle φ_{max}. The rope elongation from twisting on the larger upper rope section $L_u = 255$ m is 0.494 m shorter than the shortening by 0.505 m of the relatively small lower rope section $L_l = 245$. The difference is therefore $\Delta L_D = -0.011$ m.

The elastic rope elongation is

$$\Delta L_{\mathrm{E}} = \varepsilon_{\mathrm{E}} \cdot L = \frac{\sigma_z}{E_{\mathrm{S}}} \cdot L = \frac{S_0 + m \cdot g \cdot L/2}{A \cdot E_{\mathrm{S}}} \cdot L.$$

$$\Delta L_{\mathrm{E}} = \frac{10{,}000 + 2{,}180}{87.5 \times 71{,}000} \cdot 500 = 0.979 \text{ m}.$$

The shortening by twisting of the rope supported non-rotated at both ends is much less than the elastic rope elongation. In comparable cases, this rope shortening can always be neglected.

According to (2.99) and with extension $\varepsilon_{\mathrm{D}}(x = 500) = 0.00378$ according to (2.97a), the lay angle of the twisted rope is on the upper end

$$\beta'(x = 500) = \arctan \frac{\tan \beta - r \cdot \omega}{1 + \varepsilon_{\mathrm{D}}} = \arctan \frac{0.364 - 0.0059 \cdot 1.789}{1 + 0.00378} = 19.40^\circ$$

and with the elastic rope extension $\varepsilon_{\mathrm{E}}(x = 500) = 0.00231$ the lay angle is

$$\beta''(x = 500) = \arctan \frac{\tan \beta - r \cdot \omega}{1 + \varepsilon_{\mathrm{D}} + \varepsilon_{\mathrm{E}}} = 19.35^\circ.$$

Example 2.13c: *Suspended wire rope without rotation protection at the lower end, continuation of Example 2.12*

For the twisted wire rope, the integration of (2.98) leads to the rope elongation

$$\Delta L_{\mathrm{D}} = 2.62 \text{ m}.$$

The elastic rope elongation is

$$\Delta L_{\mathrm{E}} = \varepsilon_{\mathrm{E}} \cdot L = \frac{\sigma_{z\mathrm{m}}}{E_{\mathrm{S}}} \cdot L = \frac{m \cdot g \cdot L/2}{A \cdot E_{\mathrm{S}}} \cdot L.$$

$$\Delta L_{\mathrm{E}} = \frac{2180}{87.5 \times 59{,}000} \cdot 500 = 0.000422 \cdot 500 = 0.211 \text{ m}.$$

According to (2.99), the lay angle of the twisted rope on the upper end is

$$\beta'(x = 500) = \arctan \frac{\tan \beta - r \cdot \omega}{1 + \varepsilon_{\mathrm{D}}} - \arctan \frac{0.364 - 0.0059 \cdot 4.765}{1 + 0.00979} = 18.40^\circ$$

and, together with the elastic rope extension on the upper rope end $\varepsilon_{\mathrm{E}}(500) = 0.000844$, the lay angle is

$$\beta''(x = 500) = \arctan \frac{\tan \beta - r \cdot \omega}{1 + \varepsilon_{\mathrm{D}} + \varepsilon_{\mathrm{E}}} = \arctan \frac{0.354 - 0.0059 \cdot 4.765}{1 + 0.00979 + 0.000844} = 18.38^\circ$$

On the upper end, the lay length of the twisted and elastic elongated rope is

$$h''_S(x = 500) = \frac{\tan\beta}{\tan\beta''} \cdot h_S = \frac{0.364}{0.332} \cdot 0.1019 = 1.095 \cdot 0.1019 = 0.1116 \text{ m}.$$

The big increase of the lay length on the upper rope end can lead to a lasting change of the rope structure. When a wire rope is let down, the lower rope end should always be protected against turning. This rule has to be followed for wire ropes with steel cores even if there are only small differences in height.

2.4.6 Wire Stresses Caused by Twisting the Rope

When twisting the wire rope, the wires will be stressed by torsion. Furthermore the wires of the different wire layers and the strands of the different strand layers will be elongated or shortened differently. However, these different elongations will be prevented because the cross-sections of the strands and of the rope must remain plane. Therefore a common elongation or shortening of the twisted strands or ropes is forced by inducing longitudinal stresses in the wires and the strands.

The influence of the rope twisting on the rope stresses is so great that parts of the rope can be broken far below the normal wire rope breaking force. For example, in Fig. 2.25 the effect of the breakage of the rope core can be seen. For an untwist angle $\omega = -360^{\circ}/100d$ of the rope, the rope core has been broken at about 40 % of the normal rope breaking force. In the diagram the core breakage is shown by an abrupt increase of the rope torque.

The derivation of the stress calculation is done again on the condition that the wire ropes are of perfect geometry, that all wires are without self-contained stresses and that each wire of the rope will be unstressed before and stressed from the very beginning of the rope loading.

The sign definition:

rotary and twist angle is	positive for turn off
	negative for turn on (loosen)
longitudinal stress is	positive for tensile stress
	negative for compressive stress

2.4.6.1 Torsional Stress

When a round strand wire rope is twisted by rope twist angle ω (+ for turn off), the strand twist angle of the strand layer j is

$$\omega_j \pm \omega \cdot \cos \beta_j$$

(+ for lang lay rope) and the twist angle ω_{ij} of the wire i in the strand j of the round strand rope is

$$\omega_{ij} = \omega \cdot \cos \alpha_{ij} \cdot \cos \beta_j.$$

The torsional stress for a wire with the diameter δ_{ij} and the shear module G is

$$\tau_{ij} = \omega_{ij} \cdot G \cdot \frac{\delta_{ij}}{2}. \tag{2.38b}$$

2.4.6.2 Unimpeded Change of Lengths

The unimpeded change of lengths of the different wire and strand helixes means that the wires and strands can move against each other and a cross-section of the strands and the rope will not remain plane. For a spiral rope twisted with the rope twist angle ω, the unimpeded change in the length of a wire helix from the wire layer i in the direction of the spiral rope axis (or a strand axis) is according to (2.97) for the winding radius r_i (presupposed as constant) and the lay angle a_i of a wire i

$$\frac{\Delta l_i}{l} = \sqrt{1 - 2 \cdot r_i \cdot \omega \cdot \tan \alpha_i - r_i^2 \cdot \omega^2} - 1. \tag{2.97b}$$

In a twisted stranded wire rope with fibre core and one strand layer $j = 1$, the unimpeded change of a wire helix of the wire layer i,1 in the direction of the strand axis of the strand layer 1 is

$$\frac{\Delta l_{i,1}}{l_1} = \sqrt{1 - 2 \cdot r_{i,1} \cdot \omega_1 \cdot \tan \alpha_{i,1} - r_{i,1}^2 \cdot \omega_1^2} - 1. \tag{2.97c}$$

In this equation the strand twist angle is
for lang lay ropes $\omega_1 = \omega \cdot \cos \beta_1$ and
for ordinary lay ropes $\omega_1 = -\omega \cdot \cos \beta_1$.
$r_{i,1}$ is the winding radius of a wire i in the strand 1 and
$a_{i,1}$ is the lay angle of a wire i in the strand 1.

In a wire rope with steel core or in a multi-strand layer rope, the unimpeded length change of a strand helix of the strand layer j in the direction of the rope axis is

$$\frac{\Delta L_j}{L} = \sqrt{1 - 2 \cdot r_j \cdot \omega \cdot \tan \beta_j - r_j^2 \cdot \omega^2} - 1. \tag{2.97d}$$

r_j is winding radius of a strand j and
β_j is lay angle of a strand j.

The length changes of the wire helix and the strand helix can be calculated independently from each other.

2.4.6.3 Longitudinal Stress

With practically all rope terminations the relative motion of the wires and strands in straight ropes are prevented and the cross-sections remain plane when the rope is twisted. By preventing the relative motions, longitudinal forces are induced by extensions ε of the wires and strands. The sum of the components in the rope axis direction of all these forces is

$$\sum S_{i,j} = 0. \tag{2.97e}$$

The stress in a wire i of a wire rope with fibre core and only one strand layer will be looked at a great detail as an example. The unimpeded wire elongation $\Delta l_{i,1}$ is transformed to the common strand elongation Δl_1 as a real elongation. Then the component in the strand axis direction from the necessary longitudinal force of the wire i is with the same elasticity module E for all wires

$$S_{i,1} = \frac{\Delta l_1}{l_1} \cdot A_{i,1} \cdot E - \frac{\Delta l_{i,1}}{l_1} \cdot A_{i,1} \cdot E. \tag{2.97f}$$

With the abbreviation

$$\mathrm{A}_{i,1} = \mathrm{z}_{i,1} \cdot \cos_{i,1} \cdot \delta_{i,1}^2 \cdot \pi/4$$

and

$$\mathrm{A}_1 = \sum \mathrm{A}_{i,1}$$

is according to (2.97e)

$$0 = \sum_{i=0}^{n_\mathrm{w}} \frac{\Delta l_{i,1}}{l_1} \cdot A_{i,1} - \frac{\Delta l_1}{l_1} \cdot A_1.$$

From that the common extension of the strand is

$$\varepsilon_T = \frac{\Delta l_1}{l_1} = \frac{1}{A_1} \cdot \sum_{i=0}^{n_w} \frac{\Delta l_{i,1}}{l_1} \cdot A_{i,1}. \tag{2.97g}$$

Introduced in (2.97f) the component of the longitudinal force of the wire i in the strand axis direction—induced by the rope twisting—is

$$S_{i,1} = \frac{A_{i,1}}{A_1} \cdot \sum_{i=0}^{n_w} \frac{\Delta l_{i,1}}{l_1} \cdot A_{i,1} \cdot E - \frac{\Delta l_{i,1}}{l_1} \cdot A_{i,1} \cdot E.$$

and the enforced extension of the wire i in strand axis direction is

$$\varepsilon_i = \frac{1}{A_1} \cdot \sum_{i=0}^{n_w} \frac{\Delta l_{i,1}}{l_1} \cdot A_{i,1} - \frac{\Delta l_{i,1}}{l_1}.$$

With this equation and the relation for the parallel lay strands

$$\tan \alpha_i = \frac{r_i}{r_n} \cdot \tan \alpha_n = \frac{r_i}{r_n} \cdot \tan \alpha$$

the enforced extension of the wire i in the strand axis direction is

$$\varepsilon_i = \sum_{i=0}^{n_w} \left(\frac{A_{i,1}}{A1} \cdot \left(\sqrt{1 - 2 \cdot r_{i,1} \cdot \omega_1 \cdot \frac{r_{i,1}}{r_{n,1}} \cdot \tan \alpha - r_{i,1}^2 \cdot \omega_1^2} - 1 \right) \right) - \sqrt{1 - 2 \cdot r_{i,1} \cdot \omega_1 \cdot \frac{r_{i,1}}{r_{n,1}} \cdot \tan \alpha - r_{i,1}^2 \cdot \omega_1^2} + 1. \tag{2.97h}$$

The longitudinal stress of a wire i according to (2.20)—neglecting the strand contraction and left out the index 1 as there is only one strand layer—is

$$\sigma_{\text{long},i} = \varepsilon_i \cdot E.$$

In addition to that the tensile stress from an outer rope tensile force is according to (2.31)

$$\sigma_{\text{t},i} = \frac{S}{A \cdot \cos \alpha_i \cdot \cos \beta}.$$

The both stresses can be added to a resulting tensile stress

$$\sigma_{\text{res},i} = \sigma_{\text{long},i} + \sigma_{\text{t},i}.$$

The calculation is only valid and the rope structure remains intact, if the resulting longitudinal stresses of all wires are tensile (positive).

For the practical calculation of the stresses the Excel-program STRESS2.XLS can be used.

Example 2.14a *Wire stresses caused by twisting the rope*
Constant twist angle over the entire rope length, continuation of Example 2.9

Data:

rope construction	Filler FC
number of strands	6
lay direction	sZ
rope diameter	d = 16 mm
tensile force	S = 40 kN
twist angle	$\omega = -192°/100d$

The lay angle the outer wires and the strands are

$$\alpha_{n,1} = 15^\circ \quad \text{and} \quad \beta_1 = 20^\circ$$

Results:

Wire layer	0	1	2(F)	3
Torsional stress τ	78	76	31	69
Longitudinal stress from rope twist σ_{rot}	−148	−89	22	65
Longitudinal stress from the rope force σ_S	492	485	473	468
Resulting longitudinal wire stress σ_{res}	344	396	495	533

Because all resulting longitudinal wire stresses are positive—that means tensile—the rope structure remains intact.

By untwisting the ordinary lay rope, the strands are twisted off. The longitudinal stresses of the wires from the rope tensile force will be reduced for the centre wire and the wires of the first wire layer by $\sigma_{0,1}$ respectively $\sigma_{1,1}$ and increased for the filler wires and the outer wires by $\sigma_{2,1}$ respectively $\sigma_{3,1}$.

The change of the rope length from twisting off the strands is according to Eq. (2.97f)

$$\Delta L_T = \varepsilon_T \cdot L = -0.00077 \cdot 5{,}000 = -3.85 \text{ mm}.$$

2.4.6.4 Stresses in Wire Ropes Supported Non-rotated at Both Ends

For the wire rope supported non-rotated at both ends, (2.38b) is again valid for the torsional stress and (2.97f) or similar equations for the longitudinal stresses. The twist angles ω to be set in these equations have been derived in Sect. 2.4.4.

In the present case, the twist angle from the simplified (2.91) is precise enough. The maximum stresses on both of the rope ends can then be calculated with the twist angles from (2.91a) and (2.91b).

By analysing the equations, it will be found that the stresses are independent from the rope diameter and depend only on:

- The constants involved (Tables 1.8, 1.9 and 2.6) the rope construction being considered
- The wire rope length L and
- The specific tensile force S_0/d^2 on the lower rope end.

Example 2.14b *Wire stresses caused by twisting the rope*
Wire ropes supported non-rotated at both ends, continuation of Example 2.11.

The data of Example 2.11 is again valid. Further data of the Warrington rope being considered has been taken from Tables 1.8, 1.9 and 2.6. The rope lay angles are

$$\alpha = a_{3,1} = 15^\circ \quad \text{and} \quad \beta = \beta_1 = 20^\circ.$$

Data:

rope construction	Warrington FC
number of strands	8
lay direction	sZ
rope diameter	d = 16 mm
rope length	L = 500 m
tensile force, lower rope end	S = 10 kN
twist angle, lower rope end	ω = 178°/100d
tensile force, upper rope end	S = 14,35 kN
twist angle, upper rope end	ω = −164°/100d

Results: for the lower rope end

Wire layer	0	1	2	3
Torsional stress τ	−51	−60	−61	−46
Longitudinal stress from rope twist σ_{rot}	101	55	−38	−60
Longitudinal stress from the rope force σ_S	137	135	132	131
Resulting longitudinal wire stress σ_{res}	238	191	94	71

Results: for the upper rope end

Wire layer	0	1	2	3
Torsional stress τ	57	55	56	42
Longitudinal stress from rope twist σ_{rot}	−94	−52	35	56
Longitudinal stress from the rope force σ_S	197	194	189	188
Resulting longitudinal wire stress σ_{res}	103	143	224	244

For all wires and especially for the outer wires, the resulting tensile stresses from the rope rotation and from the rope tensile force are positive. Therefore the outside wires will not be loose and inner wires do not break out. The rope structure remains intact.

2.4.6.5 Steel Core

If instead of a rope with fibre core a rope with steel core were to be used, then the longitudinal and the torsional stresses in the wires would be a little smaller than those in the wire rope with fibre core. However, a tensile strand stress has to be added to these tensile stresses and a large tensile stress range will occur in the steel core and the strands.

At the upper rope end the steel core can—depending on the core construction—even be loaded by the whole rope tensile force with totally unloaded strands. And at the lower rope end a large compressive stress of the core exists because normally the core cannot escape laterally.

2.4.7 Rope Endurance Under Twist

2.4.7.1 Twist Angle Constant: Tensile Force Fluctuating

With small changed termination devices very normal tension–tension machines can be used for these wire rope testings, Ernst (2012).

Ernst and Wehking (2012), Ernst (2012) evaluated the endurance of two wire ropes under constant twist and pulsating tensile force. The constant twist during the tests differs between −360°/100d and 360°/100d. The two ropes from that the test pieces have been taken are

- Spiral round wire rope 1 × 19, 12 mm
- Seale 8 × 19-IWRC-sZ, 12 mm.

The rope pieces have been fixed at both ends in resin sockets. The tension–tension tests end with the rope break or with 2 million load cycles if no rope break occurs.

Figure 2.32 shows the result of the tension–tension tests with pieces of the spiral wire rope 1 × 19. In that Figure the diameter related force range is $2S_a/d^2 = 250\ N/mm^2$. Under the influence of the rope twisting the rope endurance is strongly reduced in all the tests. For a twist angle −180°/100d as an example, the remaining endurance has a percentage between 22 and 62 % of the untwisted rope piece. The endurance loss is greater the greater the twist angle is.

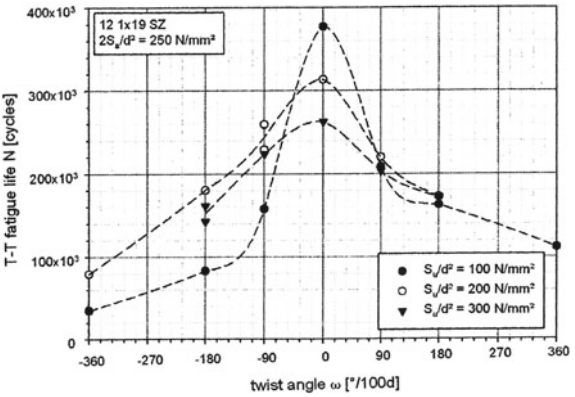

Fig. 2.32 T-T fatigue test results of a spiral strand 1 × 19 at load range $2S_a/d^2 = 250$ N/mm^2, Ernst (2012)

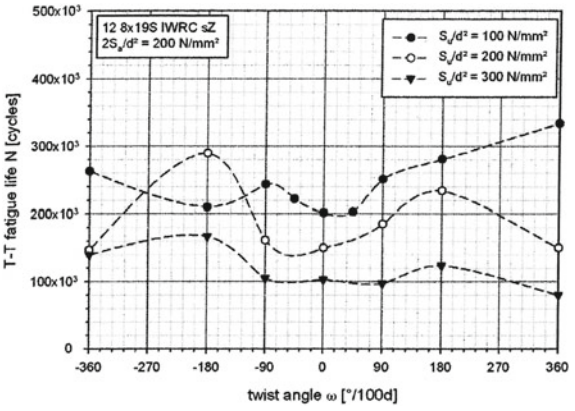

Fig. 2.33 T-T fatigue test results of a Seale rope 8 × 19 at load range $2S_a/d^2 = 200$ N/mm^2, Ernst (2012)

With twisted samples from the Seale rope 8 × 19 Ernst (2012) have made several tension–tension tests. The endurance of the twisted samples is mostly bigger than the untwisted samples in opposite to those from the spiral rope 1 × 19. However the endurance does not simply increase with the twist angle. The endurance relation between the twisted and untwisted samples differs from 0.61 to 3.03. The mean endurance relation is for the twisted Seale rope 1.23. In Fig. 2.33 the endurance is shown for the tests with the load range $2S_a/d^2 = 200$ N/mm^2 and different lower tensile loads S_u/d^2. In analising the test results Ernst and Wehking (2012), Ernst (2012) have made different regression calculations. From such a regression the constants for the endurance of the tested Seale rope not twisted is listed in Table 2.9.

2.4.7.2 Fluctuating Tensile Force: Fluctuating Twist

The first people to test how the endurance of wire ropes is affected by fluctuating twist and tension were Oplatka and Roth (1996). In their test machine which they designed themselves, the wire rope is stressed by a fluctuating tensile force and a

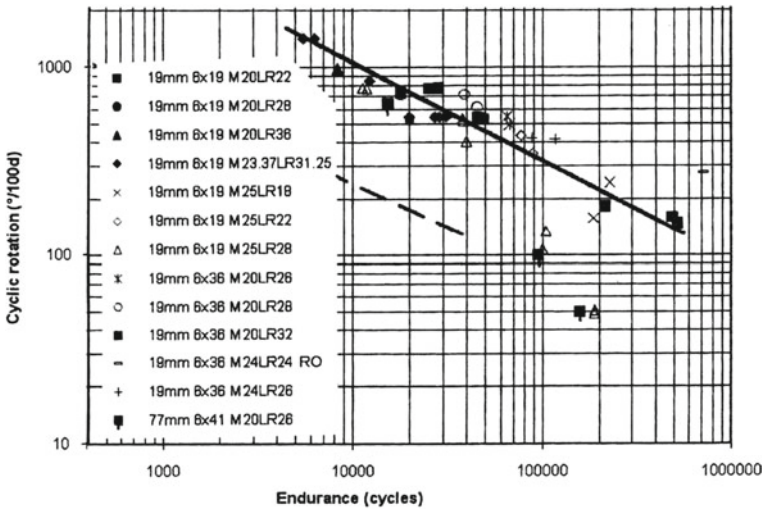

Fig. 2.34 Tension-torsion fatigue endurance of stranded wire ropes as a function of cyclic rotation, Ridge (2010)

fluctuating twist. The twist angle range is—for a constant middle tensile force S_m—approximately proportional to the tensile force range $2S_a$. They have carried out fatigue tests with a stress level where a high rope endurance has to be expected if there would be no fluctuating twist. Together with the fluctuating twist the numbers of load cycles are only about $N = 50{,}000$ for ropes with cast sockets as terminations. With Oplatka's clamp-sockets which allow slight movements of the wires and thus reduce the longitudinal stresses from the rope twist, they get more than ten times the number of load cycles for relatively short ropes.

Chaplin (2002) started his investigations in this field by defining the demand for a special testing machine which would enable rope endurance to be evaluated when the rope is stressed by constant or fluctuating twist in combination with constant or fluctuating tensile stress. Now Chaplin (2005) has reported that the new testing machine functions. He has presented first results in a diagram with the axis not scaled, because the results—belonging to a sponsor—are still confidential.

Ridge (2010) reported from extensive wire rope tension-torsion tests—that means tests with wire ropes under fluctuating tensile force and fluctuating twist angle. In that tests the tensile force and the twist angle varies in phase. The three tested wire ropes are

Seale 6 × 19—IWRC—1,770—bright—d = 19 mm
Warr.Seale 6 × 36—IWRC—1,770—zinc—d = 19 mm
Warr.Seale 6 × 41—IWRC—1,770—zinc—d = 77 mm.

The result of the tension-torsion tests is shown in Fig. 2.34. The tests have been done with fluctuating twist angles between 0 and 1,400°/100d. In the legend, M is mean load, LR is load range (both expressed as a % of the rope's measured UBL),

RO is run out. Then M20 LR22 means as example a mean load of 20 % and a load range of 22 % of the measured rope breaking force.

Figure 2.34 shows a trend line that represents the numbers of load cycles that have been get under

- load range 18–36 % UBL ($2S_a d^2 = 125–250$ N/mm^2)
- twist angle (amplitude of the cyclic rotation) $\omega = 140°/100d$ to $1{,}400°/100d$.

In this field the number of load cycles of the wire rope—stressed by different fluctuating tensile forces—depends to the main part on the fluctuating twist angle. As example the number of load cycles is N = 10,000 for $\omega = 1{,}000°/100d$ and N = 100,000 for $\omega = 300°/100d$.

For smaller cyclic rotation, the rope endurance is dominated by the fluctuating tensile force. In case of no or very small twist, the number of load cycles to breakage can be calculated with the equations of Sect. 2.8 for 6-strand Warr.-Seale—IWRC—sZ. For the untwisted 77 mm wire rope, the calculated mean number of load cycles is N = 220,000 with the given $2Sa/d^2 = 180$ N/mm^2 and $S_u/d^2 = 48.5$ N/mm^2 as can be seen in Fig. 2.34 for the same endurance region.

2.4.7.3 Stationary Wire Ropes

A wire rope supported non-rotated at the upper and the lower ends rotates with a rotary angle φ as can be seen in Fig. 2.29. The twist angle on the upper and the lower rope ends are expressed accurately enough by the simplified Eqs. (2.91a) and (2.91b). The fluctuating twist angle depends on the sum of the constant force from the rope mass and the fluctuating force S_0. In most cases these fluctuating twist angles and the fluctuating stresses from that are relative small.

2.4.7.4 Running Ropes

Fluctuating twist angles occur in running ropes of elevators, mine hoistings and rope ways. Between the guided car and the drum or traction sheave, the wire rope is twisted as a hanging stationary rope. When the car mounts, the twist angles—caused by the rope weight—in the remaining rope length will be continually reduced. In addition to the variable twist angle, there is also a constant twist angle ω_{con}—constant over the rope length—which usually arises from the installation itself and its loading history. A third twist angle ω_{side} can be produced, when the wire rope is wound in the groove of the sheave or drum. This occurs especially if the wire rope moves under side deflection sliding and rolling over the groove flank in the groove, Neumann (1987) and Schönherr (2005).

The maximum fluctuating twist angle and therefore the maximum fluctuating stress occurs in the rope piece above the car or the counter weight. The twist angles in that rope piece can be calculated under the supposition that no twist angle exists from installing the rope and its loading history and that no further twist angle is introduced

by winding the wire rope in the sheave or drum groove with side deflection or other influences. For the lowest car position, the twist angle is given by (2.91b) and for the highest car position the twist angle is about zero. After passing a traction sheave, that piece of rope is twisted in the opposite direction according (2.91a) and this causes a great range of stresses, as in the Oplatka and Roth (1996) tests described.

The real twist angles should be investigated under different influences by computer simulation and measuring in installations. Furthermore a method should be found by which the influence of fluctuating torsion and longitudinal stresses from rope twisting can be introduced in the endurance calculation of wire ropes.

For installations not covering too great a height difference, wire ropes with fibre core can be used as they have been up to now. Because of the great fluctuating stresses especially in the steel core which even result in the total loosening of the strands at the upper end of the rope, wire ropes with steel core in normal construction with relative large torque should only be used to cover relatively small differences in height. For installations with a very height difference rotation-resistant ropes should be used.

However wire ropes with special steel core can be used for longer differences of height, for that they are qualified by good experience or by calculated relative small stresses.

2.5 Wire Rope Breaking Force

2.5.1 Measured Breaking Force

The breaking force F_m of the wire ropes has of course to be evaluated by measuring it. In the pieces of rope to be tested, it should be ensured that there are no visible loose strands or wires. To compensate for any unavoidable minor loosening, the rope length between the terminations should be at least longer than 30 times the diameter of the rope. For the standard tension test, metal sockets are used as terminations. If the wire rope breaks in or near a termination, the measured breaking force of the wire rope may not be really obtained and the test should be repeated.

The tension test can of course be done with every kind of rope termination. But the breaking force so determined is not the breaking force of the wire rope. It is normally smaller. However, the tension test with resin sockets is an exception. In most cases the breaking force with these resin sockets is a little higher than with metal sockets and can therefore be taken too as the measured breaking force. But normally the measured breaking force will be evaluated by the standard tension test with metal sockets.

2.5.2 Minimum Breaking Force

For standardised wire ropes, the measured breaking force F_m is mostly greater than the minimum breaking force F_{min} given in the norm. From tests with 49 round strand ropes, about half with fibre and half with steel cores, the mean ratio of the measured breaking force (metal sockets) to the standardised minimum breaking force is

$$\left(\frac{F_m}{F_{min}}\right)_m = 1.156$$

with the standard deviation $s = 0.054$.

In accordance with that, Chaplin and Potts (1991) found that the measured breaking force is 5–20 % bigger than the minimum breaking force. The reason for this difference is that the measured strength is normally greater than the nominal strength and that the minimum breaking force in the norm is carefully chosen.

2.5.3 Wire Rope Breaking Force with Different Terminations

The wire rope breaking force is valid for wire ropes terminated with either resin or metal sockets. For wire ropes with other terminations, the wire rope breaking force (more or less reduced) can be estimated with the breaking force factor f_F. The breaking force factor is the ratio of the rope breaking force with a certain termination F_{mT} and the measured rope breaking force terminated with metal sockets F_m.

The required minimum breaking force of the wire rope with the terminations T is then

$$F_{minT} = f_F F_{min} \geq v \cdot S.$$

The breaking force factor is listed in Table 2.7.

Table 2.7 Breaking force factor f_F for rope terminations related to metal sockets

Rope termination	Breaking force factor f_F
Splice eye	0.50–0.80
Cylindric aluminum ferrule eye	0.85–1.00
Flemic eye with steel clamp	0.90–1.00
Press bolt	0.90–1.00
Wedge socket (rope lock)	0.80–0.95
U-bolt clamp DIN 1142	0.85–0.95

2.6 Wire Ropes Under Fluctuating Tension

2.6.1 Conditions of Tension–Tension Tests

A wire rope can only be loaded in connection with rope terminations. The wire rope and the terminations form one unit and the results from tension–tension tests refer only to this unit. In order to determine the actual characteristics of the wire ropes themselves fairly accurately, it is therefore necessary to use terminations which exert only minimal influence. In any case, it is difficult to avoid the effect of the terminations completely. Even a wire rope breakage occurring in the free length of the rope is no certain indication that there is no influence from the termination.

Of all known terminations, resin sockets exert the least influence on the endurance of wire ropes. Just how small this influence is can be seen by the small deviation in the numbers of load cycles reached in repeated tension–tension tests with specimens of the same rope, see the following Figs. 2.39 and 2.40. Results gained using metal sockets have much greater deviation with smaller numbers of load cycles.

The tension–tension tests for determining rope characteristics as described here, in particular those used to determine rope endurance, are conducted using resin sockets. Normally the ropes are lubricated. The rope ends, which were degreased before fitting the resin sockets, were lubricated again on the outside of the sockets after fitting.

The temperature needs to be kept low during tension–tension fatigue tests to ensure that the lubrication remains fairly effective. A top limit can be set at about 50 °C or for a lubricant with very high viscosity at the most 60 °C. The temperature increases greatly with the diameter of the rope. A certain limit for the frequency of testing in relation to the rope diameter cannot be given because the maximal possible frequency also depends on the extension hysteresis occurring during the load cycles. As Fig. 2.14 (Sect. 2.2.3) shows, the hysteresis effect increases the greater the stress range is and the smaller the lower stress. Ventilation can help to reduce the temperature.

The tension–tension fatigue tests normally end with rope breakage. Strand breakage or rope deformations count as rope breakage too if they result in the tests being discontinued. The results of rare tests where rope breakage occurs near the terminations (about two times rope diameter) are to be disregarded as untrue for the rope itself. Of 49 tests, three resulted in breakage occurring at a distance up to two rope diameters and two others at a distance up to 2.5 rope diameters. Four of these five reached a number of load cycles higher than the mean number.

Tension–tension fatigue tests with wire ropes are much rarer than bending tests. Where the results of tension–tension fatigue tests have been published, it is often not possible to evaluate them in common with other tests. As Chaplin and Potts (1991) pointed out, one problem is that there are no precise specifications laid down for the wire ropes to be tested or for the test conditions. One other problem at

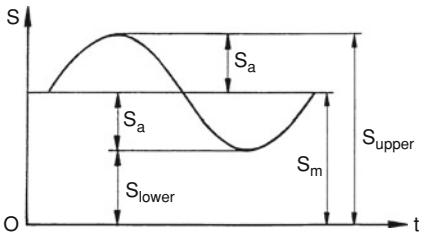

Fig. 2.35 Fluctuating tensile force

that time was that there was no convincing regression formula. To overcome the first problem OIPEEC (1991) passed OIPEEC-Recommendation No. 7 laying down that the specifications for wire ropes and test conditions should at least be described. The solution for the other problem will be described in the next chapter.

2.6.2 Evaluating Methods

2.6.2.1 Goodman Line

Wire rope endurance under fluctuating tension depends on the amplitude force S_a and the middle force S_m or the lower force S_{lower}. These forces are defined for a sinus course in Fig. 2.35. For the evaluation of a group of wire ropes with varying rope diameters, all these forces have to be replaced by the wire rope stresses or by the specific forces S/d^2.

The first proposals to evaluate the results of tension–tension fatigue tests with wire ropes came from Yeung and Walton (1985) and at the same time from Matsukawa and others (1985). For spiral ropes, they proposed to combine the force range $2S_a$ and the middle force S_m to produce an equivalent force S_q on the basis of the Goodman line. According to their proposal, the equivalent force is

$$S_q = \frac{F}{F + S_a - S_m} \cdot 2 \cdot S_a \quad \text{or} \quad S_q = \frac{F}{F - S_{lower}} \cdot 2 \cdot S_a \tag{2.101}$$

F is the wire rope breaking force, for this Yeung and Walton, and Matsukawa and others differ in their definitions. The lower force is $S_{lower} = S_m - S_a$.

The use of the equivalent force seems very attractive, because this means that the number of variables is reduced. The endurance of a wire rope can be described with the single variable S_q by the very simple equation for the number of the load cycles

$$N = a \cdot S_q^b.$$

This equation has been used to evaluate the results of different tension–tension fatigue tests and it discloses a profound difficulty. For the same equivalent force, the number of load cycles is much smaller with a small lower force than with large

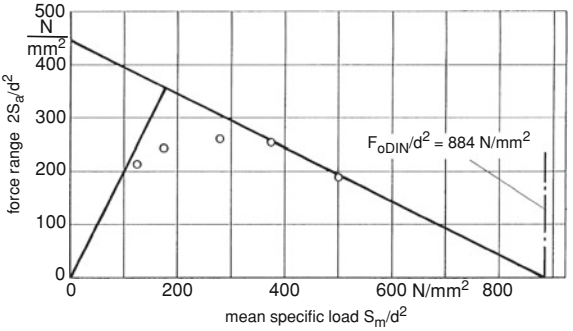

Fig. 2.36 Haigh diagram for wire rope C, resin socket, number of load cycles $N = 100{,}000$

lower force. Therefore, an evaluation using this equation can only be done separately for different lower force segments. This means that this method is unsatisfactory.

Haigh diagrams have been designed for a bigger number of test results. As an example, the best one—that is, the diagram where the test results follow the Goodman line at least in part—is shown in Fig. 2.36. In this figure, the force range $2S_a/d^2$ has been drawn for the number of load cycles $N = 100{,}000$ of the wire rope *C*, in Table 2.10. Because the number of load cycles cannot be gained using direct testing, the drawn force ranges $2S_a$ in Fig. 2.36 are evaluated by interpolation. For smaller middle forces, the force range is drawn using points. For larger middle forces, the force range follows the Goodman line which is also drawn in Fig. 2.36. A limit line starting from the origin of coordinates has been introduced for the lower force $S_{lower} = 0$, because the wire rope cannot transfer a compressive force.

The force range $2S_a$ is small for small middle forces S_m. It increases at first and then reduces with the growing middle force S_m along the Goodman line. Where this reduction begins, the upper force $S_{upper} = S_m + S_a$ (of the oscillating force) reaches 75 % of the calculated breaking force of the rope.

Therefore the force range $2S_a$ resulting from the tests with a stranded wire rope is not represented at all by a Goodman line in the region of practical usage.

The reduced force range $2S_a$ for small middle forces is caused by the additional stresses arising from the bigger fluctuating contraction of the wire rope in this force region, see Sect. 2.1. The wire rope is not a piece of material for which the Goodman line is valid. The additional stresses distinguish the wire rope as a machine element rather than as a piece of material.

2.6.2.2 Endurance Formula

Numerous tension–tension fatigue tests have been carried out on three resin-socketed round strand wire ropes A, B and C (as listed in Table 2.10) by systematically varying the forces in order to determine a better method for evaluating the test results. After a number of trials, the best regression equation for the

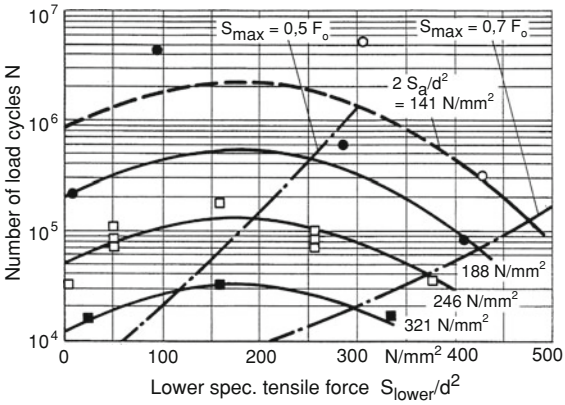

Fig. 2.37 Number of load cycles N for wire rope C, Warr. 8 × 19-IWRC-*zZ*, resin socket, Feyrer (1995)

number of load cycles N up to the wire rope breakage has been found to be, Feyrer (1995)

$$\lg N = a_0 + a_1 \cdot \lg \frac{2 \cdot S_a \cdot d_e^2}{d^2 \cdot S_e} + a_2 \cdot \frac{S_{lower} \cdot d_e^2}{d^2 \cdot S_e} + a_3 \cdot \left(\frac{S_{lower} \cdot d_e^2}{d^2 S_e} \right)^2 + a_4 \cdot \lg \frac{d}{d_e}. \tag{2.102}$$

To make them dimensionless, $S_e = 1$ N and $d_e = 1$ mm are introduced into the equation. The other symbols are known already. For using this equation for practical purposes, the forces are divided by the rope diameter square as so-called specific forces. The rope diameter d is the nominal rope diameter as used for the regression calculation. This has the advantage that the deviation of the rope diameter is included in the standard deviation for the calculated number of load cycles.

In Table 2.9, the coefficient of determination B and the standard deviation lg s for the three stranded ropes A, B and C—calculated with this regression—are listed as well as the constants a_i. The great coefficients of determination $B = 0.916$–0.941 show that the test results are well expressed with this equation. Wehking and Klöpfer (1999) found that (2.102) was equally valid both for spiral wire ropes and for Warrington–Seale ropes. For the regression calculation, the numbers of load cycles $N > 10^6$, or in other cases $N > 1.75 \times 10^6$, are not taken into account as they are considered to be outside the sphere of finite life strength.

In Fig. 2.37, the lines for the calculated number of load cycles N with (2.102) as well as the test results for the wire rope C are drawn as an example. It is to be seen that the lines and the test results up to $N = 10^6$ are close together. The number of load cycles N increases at first with increasing lower tensile force S_{lower}. As additional information, Fig. 2.37 also includes lines of the upper force with 50 % (surely the maximum allowed upper force in all cases) and 70 % of the calculated rope breaking force.

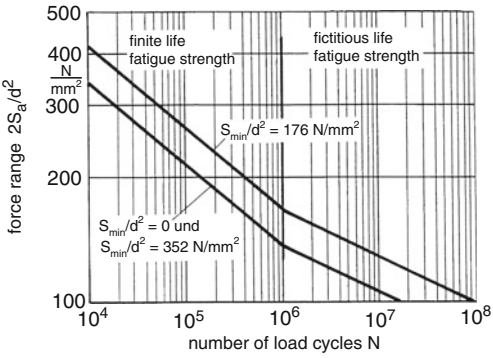

Fig. 2.38 Woehler diagram, wire rope C, Warr. 8 × 19-IWRC-*zZ*, resin socket

The mean number of load cycles $\overline{N}$ is calculated with (2.102) and the constants. The number of load cycles where with a certainty of 95 % the highest quantile γ % (for example, 10 or 1 %) of the wire ropes are broken can be calculated with

$$\lg N_\gamma = \lg \overline{N} - k_{T\gamma} \cdot \lg s. \tag{2.103}$$

The standard deviation lg s is determined with the regression calculation. The constant $k_{T\gamma}$ has to be calculated as a mean value for the region of the wire rope forces being considered, Stange (1971).

In contrast to the rope bending fatigue tests, all the known tension fatigue tests have been carried out up to wire rope breakage mostly without detecting any outside wire breaks or other discard criteria. Magnetic inspection to detect inner wire breaks during the fatigue tests has not been used up to now, Feyrer and Wehking (2006). For practical purposes in connection with safety requirements, for the time being it seems reasonable to evaluate the number of load cycles N_1 as that which—with a certainty of 95 %—not more than 1 % of the wire ropes under consideration are broken. It can be expected that up to this limit possible rope defects will be detected and show that the rope has to be discarded. For wire ropes without safety requirements, the number of load cycles N_{10} may be used as having—with a certainty of 95 %—not more than 10 % of the ropes broken.

2.6.2.3 Woehler Diagram

With the help of (2.102) a Woehler diagram can be drawn for the sphere of finite life strength. The test results let us see that the sphere of finite life fatigue strength ends for not much more than $N = 1{,}000{,}000$. There are only a small number of test results available above this number of load cycles and from these results it is not possible to derive the relation between the acting forces and the number of load cycles. Supposing a more or less constant fatigue strength does not exist, a fictitious continuation of the fatigue strength line according to Haibach (1989) can be drawn as a conservative form, Sonsino (2005). To be on the safe side the fictitious

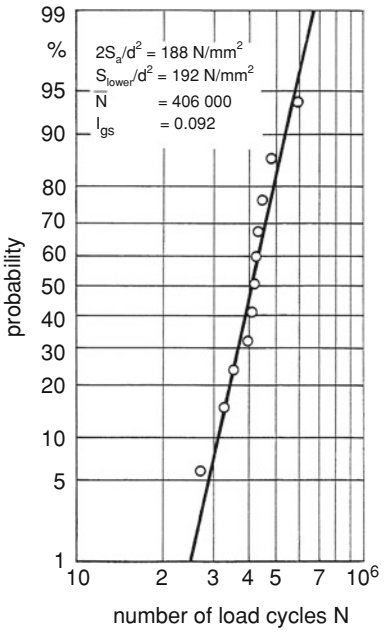

Fig. 2.39 Number of load cycles N, wire rope A, Warr. 8 × 19-SFC-*sZ*, resin socket

continuation may start at the limiting load cycles $N_D = 2{,}000{,}000$. The number of load cycles for this fictitious continuation is

$$N = N_D \cdot \left(\frac{2S_a/d^2}{2 \cdot S_{aD}/d^2} \right)^{2 \cdot a_1 + 1}. \tag{2.104}$$

In this equation, $2 \cdot S_{aD}/d^2$ is the force range at the number of load cycles $N_D = 2{,}000{,}000$. The Woehler diagram in Fig. 2.38 is still drawn for wire rope C in two lines for $N_D = 1{,}000{,}000$ (as found from Fig. 2.37) with the help of (2.102) and (2.104). The first line has the value $S_{lower}/d^2 = 0$ for the lower specific force and at the same time for $S_{lower}/d^2 = 352$ N/mm^2. The second line with the maximum possible mean number of load cycles has the value $S_{lower}/d^2 = 176$ N/mm^2 for the lower specific force. A Woehler line can be calculated and drawn between these lines for other lower specific forces.

2.6.2.4 Distribution of the Number of Load Cycles

As can be seen from the form of (2.102), the described regression is based on the logarithm normal distribution. This is justified because it was found, for example, that the logarithm normal distribution provided a very good degree of conformity for the number of load cycles of the specimens from wire ropes A and C which

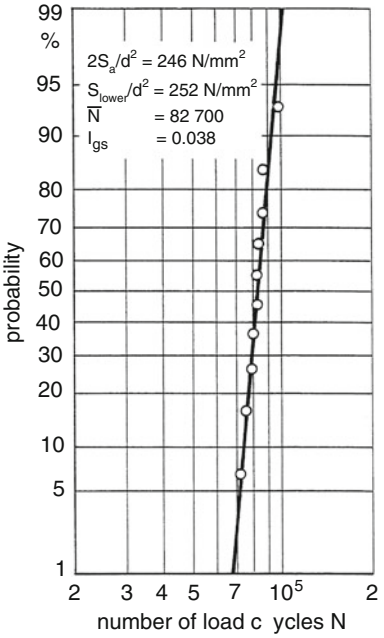

Fig. 2.40 Number of load cycles N, wire rope C, Warr. 8 × 19-IWRC-*zZ*, resin socket

were each tested under nominally identical conditions as shown in Figs. 2.39 and 2.40, Feyrer (1995).

Raoof and Hobbs (1994) found on the contrary that it was preferable to use the Gumbel distribution for the number of load cycles in the tension fatigue tests on stranded ropes tested repeatedly under the same conditions.

Unfortunately, the numbers of load cycles they counted are in the region of $N = 355{,}000$–$1{,}636{,}000$ which is where finite life fatigue strength ends. Also, with its difficult relation to the regression, the Gumbel distribution does not describe their test results better than the logarithm normal distribution would have done.

Castillo et al. (1990) proposed using the Weibull distribution with three parameters to describe the number of load cycles for repeated tension tests with the same conditions. This distribution has the disadvantage that many more tests would be needed to evaluate the three parameters and, above all, these parameters cannot be combined simply with a regression calculation.

2.6.3 Results of Tension Fatigue Test-Series

2.6.3.1 Spiral Wire Ropes with Resin Sockets

Wehking and Klöpfer (2000) in Stuttgart, and Casey (1993) and Paton et al. (2001) in East Kilbride, Glasgow have completed extensive tension fatigue investigations

Table 2.8 Constants for the number of load cycles of open spiral wire ropes for (2.102), resin sockets

Reference	Wire rope	Nominal rope diameter d	Nominal strength R_0	Test frequency	Free rope length	Number of tests	Constants						Standard deviation lg s	$\overline{N}$ for $d = 30$ mm, $S_u/d^2 = 60$, $2S_u/d^2 = 300$ N/mm^2
		mm	N/mm^2	Hz	L/d	n	a_0	a_1	a_2	a_3	a_4	a_5		
Wehking and Klöpfer (2000) and Klöpfer (2002)	Open spiral ropes $1 \times 37z$ n, lubricated	4	1,370			12								
		4	1,770			4								
		5	1,370	1.5		12								
		10	1,770	bis	40	11	15.90	−3.862	0.0009	−0.0000030	−0.779	–	0.227	168,000
		16	1,770	8.0[b]		19								
		16	1,770			11								
		24	1,770			16								
Cassey (1993) and Paton et al. (2001)[a]	Open spiral $1 \times 292zn$	40	1,570	≥0.3	100	4								
	1×135	66.6				4								
	1×147	70				2	20.587	−5.420	−0.00019	−0.000024	−1.040	–	0.107	337,000
	1×127	73				2								
	1×292 zn	127	1,570		55	4								
Wehking and Klöpfer (2000), Casey (1993) and Paton et al. (2001)	Open spiral ropes 1×37 to 1×292	4–127	1,370–1,770		40 100	101	15.401	−3.910	0.00118	−0.0000037	−0.793	0.399	0.214	For $z = 37$ 169,000 For $z = 199$ 331,000

[a] Lower specific tensile force $S_u/d^2 = 84$ N/mm^2

[b] Partly with ventilator for cooling

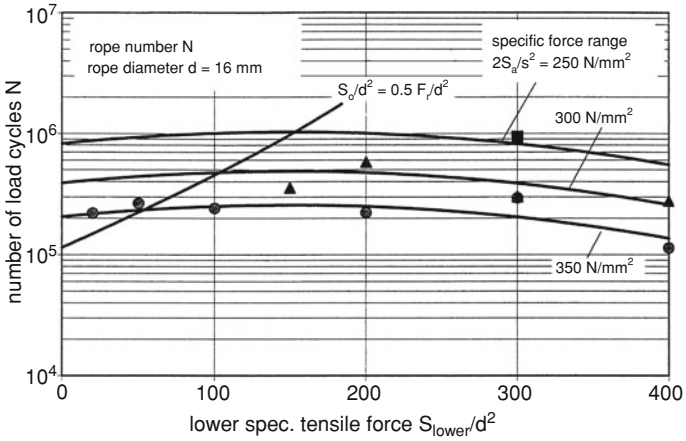

Fig. 2.41 Number of load cycles of an open spiral rope 1 × 37, Wehking and Klöpfer (2000)

with open spiral ropes. In all cases the wire ropes were fastened in resin sockets. The results of these tests have been evaluated by regression with (2.102). The constants and the rope and test data are listed in Table 2.8.

Wehking and Klöpfer (2000) and Klöpfer (2002) tested open spiral ropes with round wires 1 + 6 + 12 + 18 (short 1 × 37) with different diameters. The free length between the sockets was uniformly $L = 40d$. The wire ropes had zinc coated wires and were lubricated. The numbers of load cycles up to $N = 1.75 \times 10^6$ are included in the regression calculation. For every wire rope, the coefficient of determination is high but the standard deviation varies between lg $s = 0.094$ and 0.236. The constants a_i in Table 2.8 determined by Wehking and Klöpfer (2000) was corrected slightly by Klöpfer (2002) by neglecting the results with rope breakages near the terminations. This then reduces the standard deviation to lg $s = 0.227$.

The maximum number of load cycles has been reached for the mean lower specific force $S_{lower}/d^2 = 140$ N/mm^2 with a relatively large deviation. The numbers of load cycles for a spiral rope with the diameter $d = 16$ mm are presented in Fig. 2.41 as an example. The line for the upper force as a half rope breaking force has been included in the figure to show the maximum usable region. It can be seen in Fig. 2.41 that the endurance curves are relatively flat. In accordance to that Alani and Raoof (1997) found that under fluctuating tensile forces the endurance of spiral ropes has been nearly independent from the lower respectively the middle stress.

Two of the seven wire ropes tested had the unusual wire lay direction SSZ. In comparison with the normal lay direction ZSZ, the wire lay direction SSZ has lower endurance.

Casey (1993), and Paton et al. (2001), National Engineering Laboratory (NEL) East Kilbride, Glasgow, have done numerous tension–tension fatigue tests with

open spiral ropes having larger diameters. The wire ropes have different numbers of wires. The wire ropes with the diameters $d = 40$ mm and 127 mm have the biggest number of wires with the construction $1 + 7 + 7/7 + 14 + 19 + 25 + 31 + 42 + 48 + 49 = 292$, Casey (1993).

The constants a_i and other results of the regression calculation for these spiral ropes are listed in Table 2.8. The results of Casey, and Paton and others are used for the regression again up to the number of load cycles $N \leq 1.75 \times 10^6$. The lower specific force is at maximum $S_{\text{lower}}/d^2 = 84$ N/mm^2. Therefore, with the constants a_i of these wire ropes, (2.102) is only valid up to this lower specific force.

A common regression calculation has been carried out using the results of Wehking and Klöpfer, Casey, and Paton and others. Because of the very different numbers of wires z, the regression equation has been—compared with Feyrer (2003)—complemented here by the number of wires z.

$$\lg N = a_0 + a_1 \cdot \lg \frac{2 \cdot S_a \cdot d_e^2}{d^2 \cdot S_e} + a_2 \cdot \frac{S_{\text{lower}} \cdot d_e^2}{d^2 \cdot S_e} + a_3 \cdot \left(\frac{S_{\text{lower}} \cdot d_e^2}{d^2 \cdot S_e} \right)^2 + a_4 \cdot \lg \frac{d}{d_e} + a_5 \cdot \lg z. \tag{2.102a}$$

The constants a_i from the common regression are also listed in Table 2.8. According to the ropes used, the mean number of load cycles is given with these constants and (2.102a) for open spiral ropes with the diameter $d = 4$–127 mm and with the number of wires $z = 37$–292. The standard deviation is $\lg s = 0.214$. Using the constants $k_{T10} = 1.69$ respectively $k_{T1} = 2.93$, with a certainty of 95 % at the most 10 % respectively 1 % of the wire ropes are broken at the number of load cycles

$$N_{10} = 0.435 \cdot \overline{N} \quad \text{respectively} \quad N_1 = 0.236 \cdot \overline{N}.$$

For open spiral ropes, the relation between the wire rope stress and the specific force is about

$$\sigma_z = 1.70 \cdot \frac{S}{d^2}.$$

With an increasing rope diameter, the endurance decreases. On the other hand the endurance increases with the number of wires. Thereby the influence of the rope diameter predominates. In the range tested, the number of load cycles decreases with the rope diameter exponent $a_4 = -0.793$ and increases with the number of wires exponent $a_5 = 0.399$. All the spiral ropes tested were zinc coated and lubricated. It is not possible to evaluate the influence of the nominal strength on the rope endurance from the existing database. The constants in Table 2.8 are therefore valid for wire ropes with a nominal strength between 1,370 and 1,770 N/mm^2.

In the last column in Table 2.8, the mean numbers of load cycles are registered, calculated with (2.102a) for a rope diameter $d = 30$ mm. The difference between the numbers of load cycles from regressions of both diameter ranges tested with the mean numbers of wires $z = 37$ respectively 199 and those of the common regression is very small. Therefore, the common regression is legitimated.

2.6.3.2 Spiral Wire Ropes with Metal Sockets

Hugo Müller has carried out tension–tension fatigue tests (unpublished) with a locked coil spiral rope with metal sockets. The rope with a diameter $d = 28$ mm has round wires $1 + 6 + 12 + 18$ and 19Z-wires outside. His results ($a_0 = 12.528$; $a_1 = -2.960$) showed about 55 % of the endurance found for a comparable open spiral rope terminated with resin sockets. Yeung and Walton (1985) have done numerous tension–tension fatigue tests with spiral ropes. They did not use constant forces but a light force collective. This means that the results cannot be compared with those using constant forces.

2.6.3.3 Round Strand Wire Ropes with Resin Sockets

Tension–tension fatigue tests have been carried out with various round strand wire ropes using resin sockets as terminations. The wire ropes tested are listed in Table 2.9. The results of the tests have been used in regression calculations based on (2.102). The constants thus determined are also included in Table 2.9.

A very large number of tension–tension fatigue tests have been carried out using Warrington–Seale 6-strand ropes in ordinary lay with steel core. Wehking and Klöpfer (2000) tested ropes with diameters $d = 8$–36 mm and Casey (1993) ropes with diameters $d = 38$–127 mm. For the ropes with smaller diameters of up to 40 mm, the strands had 36 wires, the wire rope with a diameter of 70 mm had 41 wires and the 127 mm wire rope had 49 wires.

Of the Warrington-Seale ropes tested by Wehking and Klöpfer, seven ropes were zinc coated and five bright. The wire ropes Casey tested were all zinc coated. All the wire ropes were lubricated. From the existing database, it is not possible to evaluate whether either the zinc coating or the nominal strength influence the endurance of the rope. Therefore the constants for the Warrington-Seale ropes in Table 2.9 are valid for ropes, whether zinc coated or bright, with a nominal strength between 1,570 and 1,960 N/mm^2.

The results of the regression calculations based on the data from the tests on the Warrington-Seale ropes are also listed in Table 2.9. The common regression calculation done on the basis of the data from Wehking and Klöpfer and Casey is very well-founded as the numbers of load cycles for both test series calculated with their constants come very close to that for a rope diameter 38 mm. As the ropes tested varied greatly in quality, the coefficient of determination is only $B = 0.68$ and the standard deviation is $\lg s = 0.266$. Then, using the constants $k_{T10} = 1.575$

Table 2.9 Constants for the number of load cycles of stranded wire ropes for Eq. (2.102), Resin sockets

Reference	Wire rope	Nominal diameter d mm	Nominal strength R_0 N/mm^2	Test frequency Hz	Free rope length L/d	Number of tests n	Constants a_0	a_1	a_2	a_3	a_4	Standard deviation lg s	$\bar{N}$ for $d = 16$ mm, $S_u/d^2 = 20$, $2S_a/d^2 = 200$ N/mm^2
Wehking and Klöpfer (1999) Klöpfer (2002)	Warr.-Seale 6 × 36 IWRC-sZ lubricated bright or zinc	8	1,770	1.5 bis 8.0	40	21	17.49	−4.268	0.00374	−0.000014	−1.547	0.273	751,000
		8	1,770	–[b]		23							
		10	1,770			4							
		10	1,960			18							
		10	1,770			19							
		10	1,770			11							
		16	1,770			14							
		16	1,770			16							
		24	1,770			17							
		24	1,960			24							
		30	1,770			18							
		36	1,770			8							
Casey (1993)	WS-IWRC[b] 6 × 36-sZ 6 × 36-sZ 6 × 41-sZ 6 × 49-sZ zn, lubricated	38	1,570	≥0.3	100	4	16.161	−4.180	0.0235	−0.000249	−0.926	0.116	–
		40			100	13							
		70			50	10							
		127			55	8							
Wehking and Klöpfer (1999), Casey (1993)	WS-IWRC 6 × 36-sZ to 6 × 49-sZ bright or zinc lubricated	8–127	1,570–1,960		40–100	217	16.302	−3.939	0.00326	−0.000012	−1.180	0.266	755,000
Casey (1993)	Spiral[b]-multistrand op. (1 + 5 + 11 + 17 + 23) × 7 = 57 × 7 zn, lubricated	40	1570	≥0.3	100	6	17.669	−4.736	−0.00110	−0.000016	0.849	0.072	–
		127			55	4							
Feyrer (1995)	A: War 8 × 19 FC-sZ B: War 8 × 19 IRWC-sZ C: War- 8 × 19 IWRC-zZ lubricated	16	1570	3.3	87	22	19.66	−6.201	0.00382	−0.0000185	–	0.132	289,000
		16	1960	–[b]		19	14.40	-4.078	-0.00246	-0.0000066	–	0.148	116,000
		16	1960			16	16.74	−5.033	0.00493	−0.0000140	-	0.131	179,000
Ridge (1993)	Filler 6 × 19[a] IWRC-sZ-lubricated	13	1770	3.0	50	9	25.108	−8.565	0.00288	0.000041	–	0.141	
Ernst (2012)	Seale IWRC 8 × 19-sZ-lubricated	12	1960	1.3	140	13	13.524	−3.760	0.00445	−0.0000117	–	0.127	91,000

[a] Lower specific tensile force $S_u/d^2 = 20$ N/mm^2

[b] Partly with ventilator for cooling

respectively $k_{T1} = 2.76$, with a certainty of 95 % at the most 10 % respectively 1 % of the wire ropes are broken at the number of load cycles

$$N_{10} = 0.38 \cdot \overline{N} \quad \text{respectively} \quad N_1 = 0.184 \cdot \overline{N}.$$

For the Warrington–Seale ropes with 6-strands and steel core IWRC, the relation between the wire rope stress and the specific force is

$$\sigma_z = 2.195 \cdot \frac{S}{d^2}.$$

Of the wire ropes with steel core, the 6-strand Warrington–Seale ropes reach a much higher number of load cycles than both of the 8-strand Warrington ropes compared in the last column of Table 2.9. Even for the same specific forces, the 8-strand Warrington rope with fibre core has shown a higher endurance than both of those with steel cores. For the same wire rope stress, Reemsnyder (1972) also found that wire ropes with fibre cores had an advantage as far as endurance is concerned.

2.6.3.4 Round Strand Wire Ropes with Metal Sockets

The results of tension–tension fatigue tests on wire ropes with metal sockets are listed in the Table 2.10. These results are presented because wire ropes with metal sockets are frequently used and because it is very informative to see the endurance results with metal sockets under different conditions. Most of the results come from Müller (1962, 1963, 1966 as well as other unpublished results). For all his tests, the lower specific force was about $S_{lower}/d^2 = 20$ N/mm^2. He found that the parallel lay wire ropes always have much higher endurance than cross lay ropes although the cross lay ropes with the same wire lay angle in all wire layers have the advantage of having theoretically the same tension in the different wire layers. The reason for the smaller endurance of the cross lay ropes may just be due to the pressure between the crossing wires.

There is not much variation in the number of load cycles of the cross lay ropes FNC + 6 × 19, 6 × 37 and 6 × 61 whereby the higher number of wires tends to show an advantage. The simple wire rope FNC + 6 × 7 has a slightly higher endurance. Here again, the reason may be that there are no crossing wires. This may overcome the disadvantage of the thicker wires. In all cases, he found that the lubrication gave higher endurance. This result comes from the smaller second tensile stress, see Sect. 2.1.4.

Table 2.10 Constants a_i for the number of load cycles of stranded wire ropes for (2.102), metal sockets

Reference	Wire ropes	Nominal diameter d	Nominal strength R_o	Test frequenzy	Free rope length	Number of tests	Constants					Standard deviation	$\overline{N}$ for $d = 16$ mm, $S_u/d^2 = 20$, $2S_a/d^2 = 200$ N/mm^2
		mm	N/mm^2	Hz	L/d	n	a_0	a_1	a_2	a_3	a_4	lg s	
Müller (1962, 1963, 1966)	Cross lay ropes 6 × 19—NSC—sZ	2.5	2,160	4.7	320	1/1	Lubricated						
		3.2	1,570	4.7	280	5/3							
		5.0	1,770	4.2	190	4/5	14.03	−3.461	–	–	−1.021	0.393	68,200
		8.5	1,570	4.2	110	6/7	Unlubricated						
		16	1,570	3.0	65	7/6	12.82	−3.215	–	–	−0.718	0.385	35,800
		28	1,570	3.0[b]	27	6/6[c]							
Müller (1962, 1963, 1966)	Cross lay ropes 6 × 19—NFC—zZ	2.5	2,160	4.7	320	1/1	Unlubricated						
		3.2	1,570	4.7	280	3/3							
		5.0	1,770	4.2	190	5/5	12.74	−3.205	–	–	−0.535	0.178	52,700
		8.5	1,570	4.2	110	5/6	Unlubricated						
		16	1,570	3.0	40	4/6	13.08	−3.245	–	–	−0.821	0.341	42,200
		28	1,570	3.0[b]	27	7/6[c]							
Müller (1962, 1963, 1966)	Filler[a] 6 × 19—NSC—zZ	16	1,570	3.0	50	2/2	Lubricated						
							18.740	−5.729	–	–	–	–	381,000
						2/2[c]	Unlubricated						
							15.324	−4.470	–	–	–	–	109,000
Müller (1962, 1963, 1966)	Seale[a] 6 × 19—NSC—sZ lubricated	16	1,570	3.0	50	5	16.055	−4.680	–	–	–	0.021	193,000
Müller (1962, 1963, 1966)	Filler[a] 8 × 19—NSC—sZ lubricated	16	1,570	3.0	50	5	16.891	−5.476	–	–	–	0.055	136,000

(continued)

Table 2.10 (continued)

Reference	Wire ropes	Nominal diameter d	Nominal strength R_o	Test frequenzy	Free rope length	Number of tests	Constants					Standard deviation	$\overline{N}$ for $d = 16$ mm, $S_u/d^2 = 20$, $2S_a/d^2 = 200$ N/mm^2
		mm	N/mm^2	Hz	L/d	n	a_0	a_1	a_2	a_3	a_4	lg s	
Müller (1962, 1963, 1966)	Warrington[a] 8 × 19—NFC—sZ lubricated	16	1,570	3.0	50	6	18.025	−5.109		–	–	0.194	266,000
Suh and Chang (2000)	Warrington 6 × 19—IWRC—sZ lubricated	12.5	1,570		70 140 210	8 6 4	10.555	−2.137	0.000459	−0.0000015	–	0.137	
Müller (1962, 1963, 1966)	Cross lay ropes lubricated[a]												
	6 × 7—NFC—sZ	16	1,570	3.0	50	5	12.219	−3.175	–	–	–	0.035	81,900
	6 × 19—NFC—sZ	16	1,570		50	10	12.760	−3.474	–	–	–	0.143	58,400
	6 × 37—NFC—sZ	16	1,570		50	7	12.457	−3.327	–	–	–	0.080	63,400
	6 × 61—NFC—sZ	16	1,570		50	7	12.537	−3.356	–	–	–	0.112	65,200

[a] Lower specific tensile force $S_u/d = 20$ N/mm^2
[b] Partly with ventilator for cooling
[c] Lubricated/unlubricated

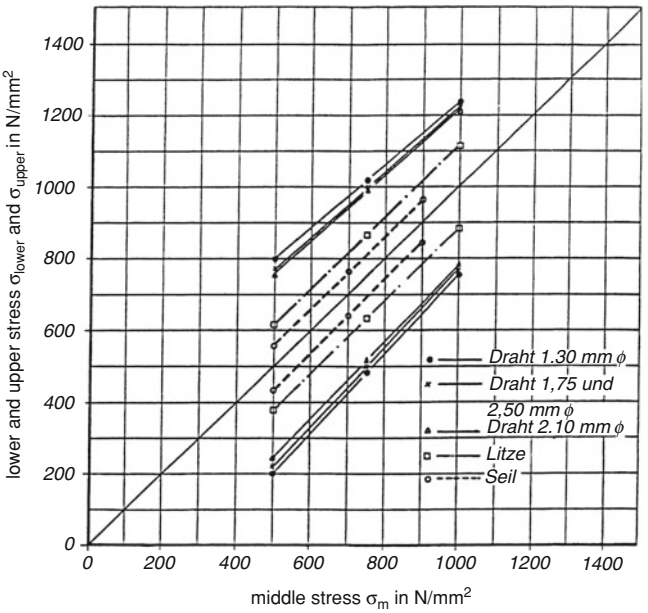

Fig. 2.42 Smith diagram for a Warrington-Seale rope 6 × 36-FC-sZ in comparison with the strands and wires, Setzer (1978)

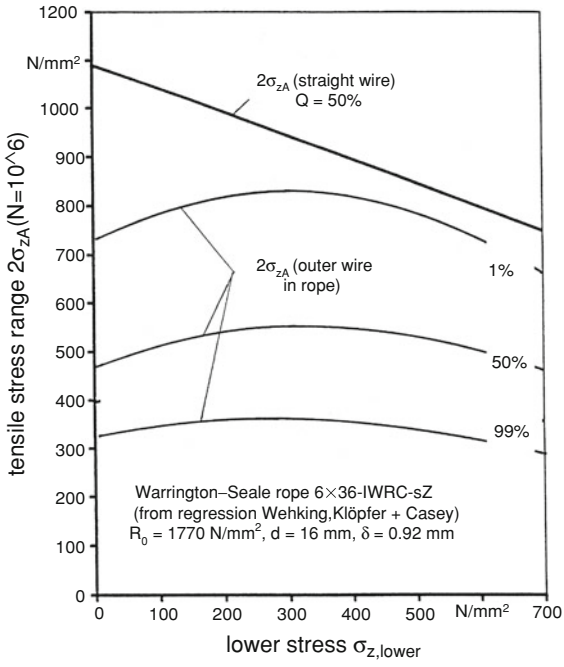

Fig. 2.43 Stress range in outside wires of a Warrington-Seale rope in comparison to straight wires of the same diameter at the number of load cycles $N = 10^6$

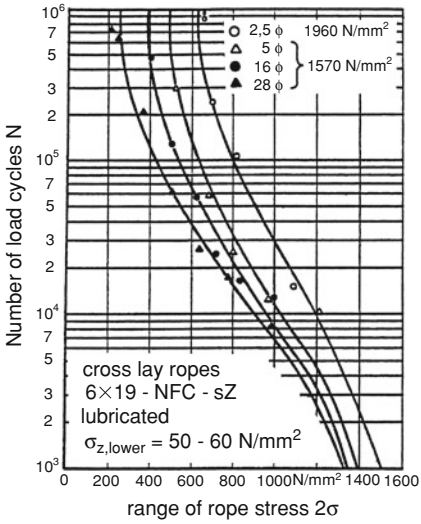

Fig. 2.44 Number of rope cycles N for cross lay ropes 6 × 19-FNC—*sZ* with different diameters, Müller (1966)

2.6.4 Further Results of Tension Fatigue Tests

2.6.4.1 Number of Load Cycles for Wire and Wire Rope

Setzer (1976) did tension fatigue tests with a Warrington–Seale rope and compared them to the strands and wires of this rope before being manufactured into a rope. He presented the result of these tests as a Smith diagram shown here in Fig. 2.42. The diagram is based on a number of load cycles $N = 2 \times 10^6$. For the middle stress $\sigma_m = 500$ N/mm^2 Setzer found a stress range $2\sigma_a = 550$–600 N/mm^2 for the wires and only $2\sigma_a = 140$ N/mm^2 for the wire rope.

A further comparison of the stress range for the wires and the wire rope is shown on the basis of the data of Table 2.9 for the Warrington-Seale ropes. Figure 2.43 shows the stress range in the outside wires for a rope with the diameter $d = 16$ mm where the wire rope breaks at the number of load cycles $N = 10^6$, with a probability of 1, 10 or 50 %. In order to take the additional stresses into consideration, the stress range for the wire rope (better for the outside wires of the rope) has been drawn 20 % above the global wire rope stress $\sigma_z = S/A_m$ calculated using (2.102). In comparison, the strength range for straight wires with the same diameter as the outside rope wires is drawn in Fig. 2.43. This strength range has been calculated with (1.3) and (1.3b) for a breakage probability of 50 %.

Even for a high quality wire rope (failure probability 1 %), the stress range for the breakage at the number of load cycles $N = 10^6$ is clearly smaller than the mean stress range of the straight wires. The remaining difference can be declared by the unsystematic increased stresses of individual wires or strands due to the loosening of the others, Evans and others (2001). Furthermore, the pressure between the wires has not been included in the stress calculation.

2.6.4.2 Size Effect Wire Rope Diameter

Müller (1966) was the first to investigate the effect of the size of the rope diameter on cross lay wire ropes 6 × 19—FNC—*sZ*. Figure 2.44 shows his results. The mean ratio of the number of load cycles N_1/N_2 of two wire ropes with the diameters d_1 and d_2 is

$$\frac{N_1}{N_2} = \left(\frac{d_1}{d_2}\right)^{a_4}. \tag{2.105}$$

For the lubricated cross lay ropes, Müller found exponents $a_4 = -1.021$ and 0.535. For different test series the constants a_4 are listed in the Tables 2.8, 2.9 and 2.10. For the whole diameter sphere of the open spiral ropes 4–127 mm, the constant is $a_4 = -0.793$. For the diameter sphere 8–127 mm of the Warrington-Seale ropes, the constant is $a_4 = -1.180$. The influence of the rope diameter is higher in the case of tension–tension fatigue than in the case of bending fatigue with the exponent −0.63.

There is no explanation for this difference between the exponents for tension and bending. It could have been expected that the size of the diameter had a greater influence on bending due to the stress gradient effect. In any case, the results emphasize Unterberg's statement (1967) that a stress gradient effect does not exist for rope wires.

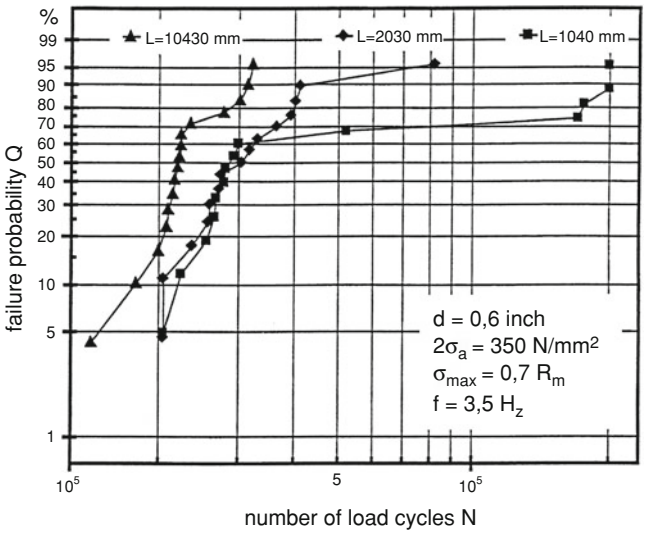

Fig. 2.45 Number of load cycles for a strand 1 × 7 for different lengths *L*, Esslinger (1992)

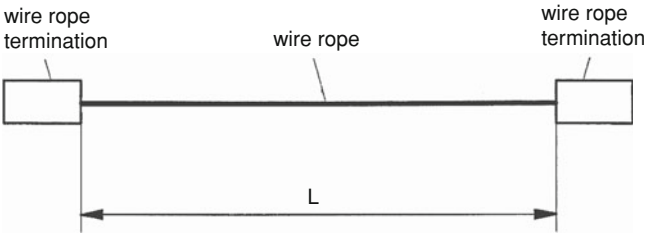

Fig. 2.46 Test sample, wire rope with termination

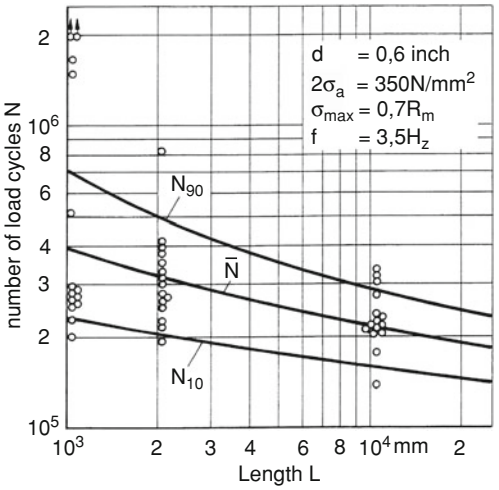

Fig. 2.47 Number of load cycles of a strand 1 × 7 for different lengths using Esslinger's results in Fig. 2.45

2.6.4.3 Size Effect Wire Rope Length

Suh and Chang (2000) carried out tension–tension fatigue tests on a Warrington rope with rope lengths of 10, 20 and 30 lay lengths. To their surprise, they found that the number of load cycles increased slightly with the length of the rope. They want to do further tests to help to understand this unexpected result. It is to be supposed that the reason for the greater endurance of the longer rope pieces lies in the fact that the loosening of the rope structure, especially in the neighbourhood of the sockets, could be compensated better in longer pieces of rope.

Esslinger (1992) carried out tension–tension fatigue tests with a simple strand 1 × 7 with 0.6 in. and rope lengths $L = 1{,}040$, 2,030 and 19,430 mm. Figure 2.45 shows his results. Contrary to the findings of Suh and Chang, he discovered that, as expected, the mean number of cycles decreases with the rope length. For the simple strand Esslinger tested there can only be minimal possible loosening of the rope structure.

Therefore, the loosening of the structure and the sockets can be considered as not affecting the influence of the length on the strand endurance.

The number of load cycles can be calculated with the methods of the reliability theory. Without any explanation, Gabriel (1979) first presented this method in a diagram for wire ropes of different lengths. The survival probability of the rope with the length L as a serial grouping of the pieces with the length L_0 is (while neglecting the influence of the sockets)

$$P = P_0^{L/L_0}. \tag{2.106}$$

Figure 2.46 shows the rope with sockets and defines the rope lengths. Once more, the logarithm normal distribution has been used to evaluate Esslinger's results. In Fig. 2.47 the numbers of load cycles found by Esslinger are introduced from Fig. 2.45 and in addition the lines calculated are drawn for the mean number of load cycles $\overline{N}$ and for the number of load cycles N_{10} and N_{90}, at which point, at the most 10 % respectively 90 % of the ropes will be broken. The numbers of load cycles N for the rope length $L_0 = 2{,}030$ mm have been taken as the basis for the calculation because there is only one extreme number of load cycles. For that distribution, the mean number of load cycles is $\overline{N}_0 = 318{,}000$ and the standard deviation is $\lg s = 0.148$. The test results and the calculated lines harmonise quite well.

From the results of (2.106), an equation can be derived for the load cycles ratio of the rope lengths L and L_0 [(2.107)]. With this, the endurance (2.102) can be corrected for different rope lengths. Equation (2.102) and their constants in Tables 2.8, 2.9 and 2.10 are related on a mean rope length of about $L_0 = 60$d of the test rope lengths 40d, 55d and 100d. Based on this rope length, the numbers of load cycles—respectively—the rope length factor, Feyrer (2011), is

$$\mathrm{f_L} = \frac{\mathrm{N_L}}{\mathrm{N_{60}}} = \frac{1.54}{2.54 - \left(\dfrac{\mathrm{l/d} - 2.5}{57.5}\right)^{-0.14}}. \tag{2.107}$$

The results of (2.106) and (2.107) depend on the standard deviation of the number of load cycles. The standard deviation, known until now for two Warrington ropes with a the length 87d is $\lg s = 0.038$ (Fig. 2.40, $\overline{N} = 82700$) and $\lg s = 0.092$ (Fig. 2.39, $\overline{N} = 406{,}000$) and for the strand 1×7 with a length 133d, is $\lg s = 0.148$ (Fig. 2.45, $\overline{N} = 318{,}000$). The standard deviation is non-uniform and probably increases as for materials normally found with the number of load cycles.

As for the rope bending, a mean standard deviation is set at $\lg s = 0.047$ for the rope length $L/d = 60$. The standard deviation for fluctuating tension is probably greater. On the other hand, the rope endurance will possibly at first not decrease with the rope length as shown in the findings of Suh and Chang (2000). With this standard deviation, the decrease of the number of load cycles with the

rope length has been at least partly taken into consideration. In (2.107), the constant $\alpha_{6\gamma}$ for this together with the constants from Tables 2.8 and 2.9 are listed in Table 2.11.

2.6.4.4 Palmgren-Miner Rule (Damage Accumulation Hypothesis)

For roller bearings loaded by a series of load cycles with different loads, Palmgren (1924) stated the hypothesis that the sum of ratios n_i/N_i (called damage sum) will be 1. That means

$$\sum_{i=1}^{m} \frac{n_i}{N_i} = 1. \tag{2.108}$$

In this, n_i is the number of load cycles under the load i (load defined by i) and N_i is the endurance under the load i. Miner (1945) found that this rule is also valid for other elements and special kinds of loads.

According to (2.108a) the endurance Z of an element under a series of different loads i will be

$$Z = \frac{1}{\sum_{i=1}^{m} \frac{w_i}{N_i}}. \tag{2.108a}$$

Here $w_i = n_i/Z$ is the portion of the number of load cycles n_i under the load i.

However, this rule is only a hypothesis and it must be checked to see whether it can be used for wire ropes under fluctuating tension. From the results of tension–tension tests in four series of block loads, Chaplin (1988) found damage sums between 0.897 and 1.109, and Rossetti and Maradei (1992) found damage sums between 1.24 and 1.28. From similar tests with Warrington–Seale ropes, Casey (1993) got damage sums between 0.6022 and 1.2584.

All these results show that the Palmgren-Miner rule can be used for wire ropes under fluctuating tension.

2.6.4.5 Discard Criteria

The amplitude stresses for the inner wires are normally greater than in the outer wires, Sects. 2.12–2.14. Therefore, outside wire breaks cannot be detected in most cases during tension–tension tests, Wehking and Klöpfer (2000). That means, the point at which the wire rope requires replacement is not defined by the number of outer wire breaks. Wehking and Klöpfer therefore recommend inspecting wire ropes under fluctuating tension by means of a magnet inductive test. Because a

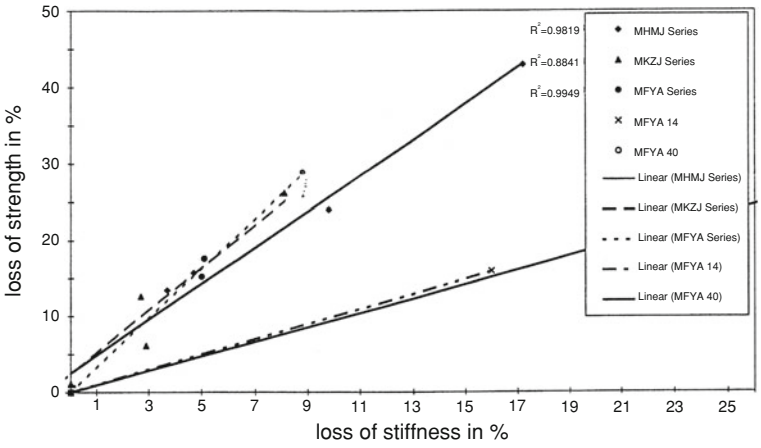

Fig. 2.48 Relation between loss of strength and loss of stiffness, Paton et al. (2001)

relation between rope endurance and the number of (inner) wire breaks is still unknown, the wire rope should be designed for the number of load cycles where at most 1 % of the rope wires on a rope length 30 d are broken.

Paton et al. (2001) tested the residual rope breaking force after having different numbers of load cycles. They found a relation between the loss of rope breaking force and the loss of length stiffness $S/\Delta L$. In Fig. 2.48 this relation is shown for 6-strand Warrington-Seale ropes with steel cores of 40 and 70 mm diameters. They recommend using a discarding criterion of a loss of 10 % of the wire rope breaking force measured.

2.6.5 Calculation of the Number of Load Cycles

2.6.5.1 Resin Sockets

With the test results and the related equations, the number of load cycles prior to rope breakage can be calculated for open spiral ropes of nominal strength 1, 370–1, 770 N/mm^2, zinc coated and for Warrington–Seale ropes 6 × 36 to 6 × 49-IWRC-sZ of the nominal strength 1, 570–1, 960 N/mm^2, bright or zinc coated, lubricated. For these, the regression (2.102) respectively (2.102a), (2.103) for the varying quantile γ and (2.107) for the influence of the rope length will be combined. To give a better overview, the unit factors $S_e = 1$ N and $d_e = 1$ mm (to make the ratios dimensionless) will be removed. Then, for a rope with the length L, the number of load cycles—where with a certainty of 95 % at most a quantile γ of the wire ropes has been broken—is

$$\lg N_\gamma = a_0 + a_1 \cdot \lg \frac{2S_a}{d^2} + a_2 \cdot \frac{S_{\text{lower}}}{d^2} + a_3 \cdot \left(\frac{S_{\text{lower}}}{d^2}\right)^2 + a_4 \cdot \lg d + a_5 \cdot \lg z + \lg \mathrm{f_L} - k_{T\gamma} \cdot \lg s.$$

This equation is also valid for the Warrington–Seale ropes if here the constant a_5 is set $a_5 = 0$. For the failure quantiles of 50, 10 and 1 %, the constant parts can be summarised to

$$a_{0\gamma} = a_0 - k_{T\gamma} \cdot \lg s. \tag{2.109}$$

With this constant $a_{0\gamma}$ the number of load cycles N_γ—where with a certainty of 95 % at most a quantile γ of wire ropes has been broken—is

$$\lg N_\gamma = a_{0\gamma} + a_1 \cdot \lg \frac{2S_\mathrm{a}}{d^2} + a_2 \cdot \frac{S_{\text{lower}}}{d^2} + a_3 \cdot \left(\frac{S_{\text{lower}}}{d^2}\right)^2 + a_4 \cdot \lg d + a_5 \cdot \lg z + \lg \mathrm{f_L}. \tag{2.110}$$

In Table 2.11, the constants a_i for (2.110) are listed Casey (1993), Paton et al. (2001), Klöpfer (2002) Feyrer and Wehking (2006). The constants a_1–a_5 have been taken from Table 2.8 for the open spiral ropes and from Table 2.9 for the Warrington–Seale ropes. The constant $a_{0\gamma}$—listed in Table 2.11—has been calculated with (2.109) for the different quantiles $\mathrm{f_L}$ is given in Eq. (2.107).

Equation (2.110) and the constants of Table 2.11 are valid up to the limiting number of load cycles $\mathrm{N_D}$. With the reduced gradient of Haibach (1989), the number of load cycles above $N_\mathrm{D} = 2 \times 10^6$ is (as explained under Woehler Diagram)

$$N_k = N_\mathrm{D} \left(\frac{2S_\mathrm{a}/d^2}{2S_\mathrm{aD}/d^2}\right)^{2a_1+1}. \tag{2.104}$$

S_aD is the amplitude of the tensile force for which the limiting number of load cycles $N_\mathrm{D} = 2 \times 10^6$ has to be expected. This limiting amplitude of tensile force can be calculated with the following equation (inverted from Eq. (2.110)).

Table 2.11 Constants for calculating the number of load cycles, (2.110)

Wire ropes	γ (%)	$a_{0\gamma}$	a_1	a_2	a_3	a_4	a_5
Open spiral ropes	50	15.401					
	10	15.039	−3.910	0.00118	−0.0000037	−0.793	0.399
	1	14.774					
Warr-Seale ropes	50	16.302					
IWRC—sZ	10	15.883	−3.939	0.00326	−0.000012	−1.180	0
	1	15.568					

$$\lg \frac{2S_{a\gamma}}{d^2} = \frac{\lg N_\gamma}{a_1} - \frac{1}{a_1} \cdot \left(a_{0\gamma} + a_2 \cdot \frac{S_{\text{lower}}}{d^2} + a_3 \cdot \left(\frac{S_{\text{lower}}}{d^2} \right)^2 + a_4 \cdot \lg d + a_5 \cdot \lg z + \lg f_L \right). \tag{2.111}$$

with $N_j = N_D = 2 \cdot 10^6$.

With (2.110), the number of load cycles will be calculated, directly valid up to 2×10^6 for all quantiles γ. Numbers of load cycles above that should be corrected with (2.104). By using the limiting number of load cycles 2×10^6 for all quantiles, the standard deviation will be—as in reality—strongly extended in the region above the limiting number of load cycles.

For the practical calculation of the numbers of load cycles the Excel-program SWINGSP2.XLS can be used.

Example 2.15: *Number of load cycles*

Data:
Warrington-Seale rope 6 × 36—IWRC—*sZ*
Wire rope diameter $d = 20$ mm, nominal strength $R_0 = 1,770$ N/mm^2, lubricated
Rope length $L = 120$ m, terminated with resin sockets
The fluctuating tensile forces are
Lower tensile force $S_{\text{lower}} = 30$ kN, $S_{\text{lower}}/d^2 = 75$ N/mm^2
Upper tensile force $S_{\text{upper}} = 80$ kN

The range of the specific force is

$$2S_a/d^2 = \frac{S_{\text{upper}} - S_{\text{lower}}}{d^2} = 125 \text{ N/mm}^2.$$

Results:
Using (2.110) and the constants from Table 2.11, the numbers of load cycles are

$$N_{50} = 3{,}690{,}000 \qquad N_{10} = 1{,}410{,}000 \qquad N_1 = 680{,}000$$

From these numbers only

$$N_1 = 680{,}000 \quad \text{and} \quad N_{10} = 1{,}410{,}000$$

are directly valid. The mean number of loading cycles—greater than 2×10^6—has to be corrected. For that, using (2.111), the limit range of the specific tensile force is

$$2S_{aD50}/d^2 = 146 \text{ N/mm}^2.$$

Then, with (2.104) the mean number of load cycles is

$$N_{50k} = 5{,}820{,}000.$$

Example 2.16: *Number of load cycles Z, load collective*

Data:
The data from Example 2.15 are valid again. The lower force remains constant $S_{lower} = 30$ kN. The load collective for the force range is given by

Part of the number of cycles	w_i	0.2	0.3	0.5
Relative force range	q_i	1	0.8	0.6

Results:
The three specific force ranges $q_i * 2Sa/d^2 = q_i * 125$ are

$$125 \quad 100 \quad 75$$

and according to Eq. (2.110) the numbers of load cycles N_1 are

$$680{,}000 \quad 1{,}640{,}000 \quad 5{,}090{,}000$$

The last number of load cycles—greater than 2×10^6—has to be corrected. For that, using the Eq. (2.111), the limit range of the specific tensile force is

$$2S_{aD1}/d^2 = 97.5\,\text{N/mm}^2.$$

Then, according to Eq. (2.104) the corrected number of load cycles is

$$N_{1K} = 10{,}200{,}000.$$

The common number of load cycles Z_1, at which with a certainty of 95 % at most 1 % of the wire ropes are broken, is according to Eq. (2.106)

$$Z_1 = \frac{1}{\frac{0.2}{680{,}000} + \frac{0.3}{1{,}640{,}000} + \frac{0.5}{10{,}200{,}000}} = 1{,}900{,}000.$$

Table 2.12 Endurance factor $f_T = N_V/N_w$, for rope with terminations related to resin sockets

Rope termination	Number of ropes z	Number of tests n_V/n_w	Logarithm of the endurance factor lg f_T	Standard deviation lg s_{fT}	Endurance factor f_T
Metal socket[a,d]					
Cross-NFC-6 × 37		2/2	−0.544	0.367	0.286
Warr-SFC-8 × 19		12/19			
Warr-IWRC-8 × 19		5/26			
Splice eye[b]					
Warr-SFC-8 × 19	1	2/19	−1.008	0.161	0.098
Cylindric aluminum ferrule eye termination[c,d,e,f,g,h]					
Cross-NFC-6 × 37	1	1/2	−0.463	0.368	0.345
Warr-NFC-8 × 19	1	15/19			
Warr-IWRC-8 × 19	1	5/26			
WS-IWRC-6 × 36	2	8/26			
Flemic eye with steel clamp[d,i]					
Cross-NFC-6 × 37	1	9/2	−0.428	0.314	0.373
Warr-SFC-8 × 19	1	9/19			
Press bolt[j]					
Spiral 37 × 1	1	7	−0.700	0.263	0.20
Wegde socket (rope lock)[d,k]					
Warr-SFC-8 × 19	1	36/19	$= -1.347 + 0.0071\,\alpha + 0.145\,l_K/d^n$	0.306	α = 14° 28° 14° 28° l_K/d = 4 4 6 6 f_T = 0.216 0.271 0.420 0.529
Warr-IWRC-8 × 19	1	46/26			
U-bolt clamp DIN 1142[d,l,m]					
Warr-SFC-8 × 19	1	5/19	−0.871	0.152	0.108

[a] Müller (1971), [b] Müller (1976), [c] Müller (1966), [d] Feyrer (1995), [e] Feyrer et al. (1987), [f] Hemminger (1989), [g] Wehking et al. (2000), [h] Klöpfer (2002), [i] Schneidersmann (1980), [j] Vogel (2005), [k] Feyrer (1984), [l] Ulrich (1973), [m] Müller (1975), [n] for clamping angle $\alpha = 14°$ to 30° and clamping length l_K/d = 3,5 bis 6

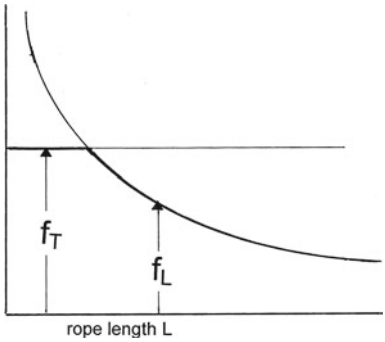

Fig. 2.49 Application of the termination factor f_T or the rope length factor f_L

2.6.5.2 Rope Terminations

The number of load cycles will be reduced if rope terminations other than resin sockets are used. For ropes with these terminations, the number of load cycles is normally

$$N_{\gamma Term} = f_T \cdot N_{\gamma,60} \quad \text{for} \quad f_T lt f_L \tag{2.109a}$$

with the endurance factor f_T for the termination taken from Table 2.12 (still from a very small database) and with the number of load cycles $N_{\gamma,60}$ for ropes with resin sockets and the rope length L = 60d.

However for very long ropes it may be that the wire rope does not fail in the termination region but on the free rope length. In that case—when the endurance factor f_T is bigger than the endurance factor f_L for the rope length—the number of load cycles is

$$N_{\gamma Term} = f_T \cdot N_{\gamma,60} \quad \text{for} \quad f_T > f. \tag{2.109b}$$

From the both endurance factors f_T and f_L the smaller one has to be used, Fig. 2.49.

2.7 Dimensioning Stay Wire Ropes

Stay wire ropes have to be dimensioned in such a way that they can stand up to extreme forces which only occur rarely, be sufficiently durable in case of fluctuating forces and have safe discard criteria. These safety limits are characterised by:

- Extreme forces
- Fluctuating forces
- Discard criteria

Stationary wire ropes have to meet all these requirements independent of each other.

2.7.1 Extreme Forces

To prevent a wire rope breaking due to an extreme force which occurs only rarely, technical regulations normally require that the minimum breaking force F_{min} is several times higher than the nominal rope tensile force S

$$F_{\min} \geq v \cdot S. \tag{2.112}$$

The so-called safety factor v takes the increase of the tensile force due to possible overloading into consideration as well as the weakening of the wire rope breaking force due to fatigue occurring over time in the case of fluctuating forces or by corrosion. Paton et al. (2001) found a reasonable weakening of the wire rope breaking force occurs long before the rope breaks under the fluctuating tensile force. One of their results shows that the breaking force for the spiral ropes tested is reduced by 15 % at between about 20 and 70 % of their endurance. The 15 % loss of breaking force occurs late if the endurance is low ($N \approx 50{,}000$) and earlier if it is high ($N \approx 5 \times 10^6$).

In technical regulations, experts have defined the reference values for the safety factors based on their own experience combined with theoretical considerations. Of course, for each individual technical field, the safety factor varies according to whatever extreme forces may occur there. For example the safety factor for stay ropes for cranes is about $v = 3.2$. For steel constructions and bridges, the safety factor is smaller being about $v = 2.2$ as the greater part of the forces comes from their own constant weight.

The wire rope breaking force is valid for wire ropes terminated with either resin or metal sockets. For wire ropes with other terminations, the wire rope breaking force (more or less reduced) can be calculated with the breaking force factor f_F from Table 2.7.

The required minimum breaking force of the wire rope with the terminations T is then

$$F_{\min T} = f_F \cdot F_{\min} \geq v \cdot S. \tag{2.113}$$

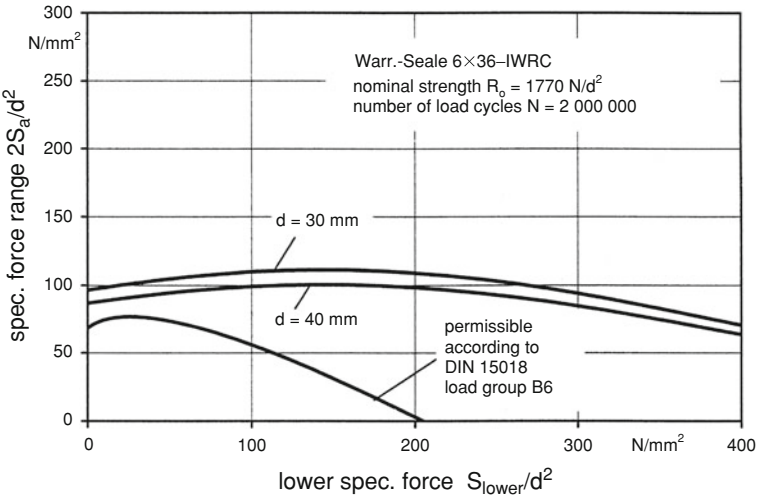

Fig. 2.50 Allowed range of specific force of Warrington-Seale ropes after DIN 15018 and from tests, Wehking and Klöpfer (2000)

2.7.2 Fluctuating Forces

2.7.2.1 Technical Rules–Test Results

In the existing technical regulations, the larger the lower stress is, the smaller the stress range that is allowed. This restriction of the stress range for large lower stresses cannot be explained at all by the test results. On the contrary, the test results show that for a certain number of load cycles the stress range tends to increase with the lower stress up to the allowed maximum stress. As an example, Fig. 2.50 from Wehking and Klöpfer (2000) shows the range of the specific rope force allowed after DIN 15018 compared with the test results. The comparison was made for Warrington–Seale ropes 6 × 36-IWRC-sZ with rope diameters 30 and 40 mm. The specific force range allowed in the DIN loading group B6 for a strong load collective is compared with test results where the ropes are loaded with the full force range for all load cycles (full load cycles) and where only 10 % of the ropes break before 2×10^6 load cycles have been reached.

In future technical regulations, the range of the specific force found for the lower force 0 can simply be allowed for all lower forces, or, taking the influence of the lower forces into consideration, the allowed range of specific forces (stress) can be calculated for a given lower specific force and for a given number of load cycles. That is possible at this time for open spiral ropes zinc coated and lubricated and for ordinary lay Warrington–Seale ropes, bright or zinc coated and lubricated.

Table 2.13 Range of diameter related force 2 S_a/d^2 of open spiral ropes for certain numbers of load cycles N_1, at which with a certainty of 95 % at most 1 % of the ropes are broken

Rope diameter d (mm)	Number of wires z	Range of diameter related force $2S_{a1}/d^2$ in N/mm^2 for load cycles N_1						
		N_1 = 20,000	50,000	125,000	320,000	800,000	2,000,000	10,000,000
10	37	402	318	251	198	156	124	98
12.5	37	385	304	241	189	150	118	94
16	61	386	305	241	190	150	119	94
20	61	369	292	231	182	144	114	90
25	85	366	290	229	180	142	113	89
32	85	349	276	218	172	136	107	85
40	100	340	269	213	167	132	105	83
50	125	333	264	209	164	130	103	81
63	160	327	259	205	161	127	101	80
80	200	320	253	200	157	124	98	78
100	250	313	248	196	154	122	97	76
125	292	305	241	191	150	119	94	74

Lower tensile force $S_{lower} = 0$; rope length $L = 100$ m; terminations: resin socket
Rope tensiele stress $\sigma_z = 1.70\ S/d^2$

2.7.2.2 Force Range

As has been repeatedly pointed out, the range of specific force should be calculated in such a way that with a certainty of 95 % at most 1 % of the ropes is broken for a required endurance. If the required number of load cycles (full load cycles) is smaller than 2×10^6, the allowed specific force range can be calculated directly with (2.111) and the constants in Table 2.11.

If the required number of load cycles is bigger than 2×10^6, first the specific force range $2S_{aD\gamma}/d^2$ has to be calculated with (2.111) for $N_\gamma = 2 \times 10^6$. Then for the required number of load cycles bigger than 2×10^6, according to the inverted (2.104) the range of the specific force is

$$2S_{a\gamma}/d^2 = 2S_{aD\gamma}/d^2 \cdot \left(\frac{N_\gamma}{N_D}\right)^{1/(2a_1+1)}. \tag{2.114}$$

For both (2.111) and (2.114) the constants have to be taken from Table 2.11.

A survey of the range of specific forces $2S_{a1}/d^2$ is presented in Table 2.13, with which open spiral ropes with resin sockets can reach a given number of load cycles N_1. These numbers N_1 mean the number of full load cycles at which with a certainty of 95 % at most 1 % of the wire ropes are broken. The lower specific force is $S_{lower}/d^2 = 0$. With increasing rope diameters d, an increased number of wires z in the wire rope have been inserted as is usual in practice. The rope length is $L = 100$ m.

As Table 2.13 shows, the allowed range of specific force is strongly reduced with an increasing rope diameter. For the smallest rope diameter $d = 10$ mm and

the smallest required number of load cycles $N_1 = 20{,}000$, the force range is restricted by the maximum allowed specific force. This maximum allowed specific force for spiral ropes in steel constructions is about $S_{max}/d^2 = 400$ N/mm^2. For open spiral ropes (in contrast to Warrington–Seale ropes) the influence of the lower force is relatively low.

Example 2.17: *Allowed specific force range*

Data:

Required number of load cycles $N_1 = 5{,}000{,}000$ at which with a certainty of 95 % at most 1 % of the wire ropes are broken.
Spiral rope 1 × 61, lubricated
$d = 20$ mm, strength $R_0 = 1{,}770$ N/mm^2
Rope length $L = 120$ m, $L/d = 6{,}000$
Lower rope force $S_{lower} = 30$kN, $S_{lower}/d^2 = 75$ N/mm^2
Resin sockets

Results:

According to (2.111), the specific force range for the limiting number of load cycles $N_{D1} = 2 \times 10^6$ is

$$\lg \frac{2S_{aD1}}{d^2} = \frac{\lg 2{,}000{,}000}{-3.910} - \frac{1}{-3.910} \cdot \left(14.774 + 0.00118 \times 75 - 0.0000037 \times 75^2 - 0.793 \times \lg 20 + 0.399 \times \lg 61 + \lg 0.763\right)$$

$2S_{aD1}/d^2 = 118$ N/mm^2.

For the required number of load cycles $N_1 = 5{,}000{,}000$, the specific force range according to (2.114) is

$$2S_{a1}/d^2 = 118 \left(\frac{5{,}000{,}000}{2{,}000{,}000}\right)^{1/(-2\times 3.910+1)}$$

$$2S_{a1}/d^2 = 103.2 \text{ N/mm}^2$$

and the force range and the stress range are

$$2S_{a1} = 41.3 \text{ kN} \quad \text{and} \quad 2\sigma_{a1} = 175 \text{ N/mm}^2.$$

2.7.2.3 Rope Termination

The calculation of the allowed range of specific force for wire ropes under fluctuating forces described here is based on test results relating to wire ropes terminating in resin sockets. For ropes with other terminations, the allowed range of specific forces can be calculated in the same way. In this case the constant a_G has to be estimated with (2.109a) or (2.109b).

2.7.3 Discard Criteria

Wire ropes always have a limited working life. Prior to rope breakage, the rope has to be discarded and replaced. It is necessary to have safety inspections to ascertain the state of the wire rope, i.e. the state at which the wire rope should be discarded.

The discarding state of stay wire ropes will be indicated by damage near the terminations as well as wire breaks or corrosion on the free rope length. The inner wires of ropes with tensile loads are always stressed to a greater degree than the outer wires. This means that in wire ropes suffering under fluctuating tension, it is the wires in the inner rope in particular which break. Therefore the wire rope has to be inspected by magnetic methods Feyrer and Wehking (2006).

In any case, wire breaks in or close to the sockets are promoted by transverse vibrations of the ropes, Hobbs and Smith (1983), Oplatka and Roth (1991, 1993), Brevet and Siegert (1996), Siegert et al. (1997), Gourmelon (2002) and Siegert and Brevet (2005). Gabriel and Nürnberger (1992) pointed out that in the most cases, the stay wires rope has to be discarded because of damage near the terminations or corrosion but not because of wire breaks on the free length.

The transversal vibration of stay ropes should be minimised by dampers, Gourmelon (2002). However these vibrations that induce wire breaks in the sockets cannot totally avoided. As Oplatka and Roth (2000) stated, there is no method found that can show in field-test the condition of the rope even in resin sockets with sufficient accuracy. Therefore the transversal vibration should be kept away from the sockets. The wire rope should be hold by a fastening in front of the socket on that the transversal vibration ends. This fastening should be removable so that the wire rope can be inspected in this region with magnetic methods.

References

Alani, M., Raoof, M.: Effect of mean axial load on axial fatigue life of spiral strands. Int. J. Fatigue **19**(1), 1–11 (1997)

Andorfer, K.: Die Zugkraftverteilung in schwingend beanspruchten geraden drahtseilen. Universität Graz, Diss Techn (1983)

Becker, K.: On the fatigue strength of wire ropes. OIPEEC Round Table, Luxembourg, Chaps. 1–3 (1977)

Beha, R.: Bewegungsverhalten und Kraftwirkungen des Zugseiles und der Fahrzeuge von Zweiseilbahnen zur Berechnung der Dynamik des Gesamtsystems. Diss. Universität Stuttgart. Kurzfassung ISR (1995) 1, S11–15 (1994)

Benndorf, H.: Beiträge zur Theorie der Drahtseile. Zeitschr. d. öster- reichischen Ingenieur- u. Architektenvereins **56**(30), S433–S437 (1904) (u. 31, S449–453)

Berg, F.: Der Spannungszustand einfach geschlungener Drahtseile. Diss. TH Hannover 1907 und Dinglers Polytech. J. **88**(19), S289–S292 (1907) (u. 20, S307–311)

Bock, E.: Die Bruchgefahr der Drahtseile. Diss. TH Hannover (1909)

Brevet, P., Siegert, D.: Fretting fatigue of seven wire strands axially loaded in free bending fatigue tests. OIPEEC Bull. **71** (1996)

Buchholz, G., Eichmüller, H.: Tätigkeitsbericht 1986–1988. Staatl. Mate-rialprüfungsamt Nordrhein-Westfalen, Dortmund 1988, S58–S62

Cantin, M., Cubat, D., Nguyen Xuan, T.: Experimental analysis and modelisation of the stiffness in torsion of wire ropes. OIPEEC Round Table, pp. II.67–II.77, Delft, Sept 1993

Casey, N.F.: The fatigue endurance of wire ropes for mooring offshore structures, pp. I.21–I.49. OIPEEC Round Table, Delft, Sept 1993

Casey, N.F., Waters, D.M.: Condition monitoring for fatigue test assessment and life prediction of six-strand rope, pp. 7.1–7.20. OIPEEC Round Table, Zürich, Sept 1989

Castillo, E., Fernadez-Canteli, A.: Statistical models for fatigue analysis of long elements. Introductory Lectures of the IABSE-Workshop "Length Effect on the Fatigue of Wires and Strands", Madrid, Sept 1992

Castillo, E., Fernandez-Canteli, A., Ruiz-Tolosa, J.R., Sarabia, J.M.: Statistical models for analysis of Fatigue life of long elements. Trans. ASCE J. Eng. Mech. **116**(5), 1036–1049 (1990) (paper 24618)

Chaplin, C.R.: Tension-tension fatigue in mooring offshore structures. OIPEEC Bull. **56**, 9–22 (1988)

Chaplin, C.R.: Problems of torque and rotation in wire ropes. First International Stuttgart Rope Day, Institut für Fördertechnik und Logistik, Universität Stuttgart, 21 Feb 2002

Chaplin, C.R.: Deepwater moorings: challenges, solutions and torsion. Second International Stuttgart Rope Day, Institut für Fördertechnik und Logistik, Universität Stuttgart, 17–18 Feb 2005

Chaplin, C.R., Potts, A.E.: Wire Rope Offshore—A Critical Review of Wire Rope Endurance Research Affecting Offshore Application. HSE Publication, London (1991)

Costello, G.A.: Theory of Wire Rope, 2nd edn. Springer, New York (1997). ISBN 0-387-98202-7

Costello, G.A., Miller, R.E.: Lay effect of wire rope. J. Eng. Mech. Div. ASCE **105**(EM5), 597–608 (1979)

Costello, G.A., Sinha, S.K.: Torsional stiffness of twisted wire cables. J. Eng. Mech. Div. ASCE **103**(EM5), 766–770 (1977a)

Costello, G.A., Sinha, S.K.: Static behaviour of wire rope. J. Eng. Mech. Div. ASCE **103**(EM5), 1011–1022 (1977b)

Czitary, E.: Spannkraftermittlung in Seilen durch Schwingungs-messung. Wasserwirtschaft **15**(16), S246–S249 (1931)

Czitary, E.: Seilschwebebahnen. Springer, Wien (1952)

Czitary, E.: Über das Schwingungsverhalten des Trag- und Zugseiles von Seilschwebebahnen. ISR Int. Seilbahn-Rundschau, Seilbahnbuch 1975, S27–S34

Donandt, H.: Zur Dauerfestigkeit von Seildraht und Drahtseil. Archiv für (1950) das Eisenhuottenwesen **21**(9/10), S283–S292 (1950)

Dreher, F.: Ein Beitrag zur Theorie der Drehung und Spannungsver-teilung bei zugbelasteten Litzen und Seilen. Diss. TH, Karlsruhe (1933)

Engel, E.: Ein Beitrag zur Berechnung der Verdrehungen von Draht-seilen und deren Bedeutung bei Seilbahnen. Diss. TH, Wien (1957)

Engel, E.: Das Drehbestreben der Seile und ihre Drehsteifigkeit. Österreichische Ingenieur-Zeitschrift **1**(1), S33–S39 (1958)

Engel, E.: Verdrehungserscheinungen an Seilen bei Seilbahnen. Österreichische Ingenieur-Zeitschrift **2**(6), S215–S220 (1959)
Engel, E.: Der Seildrall. Int. Berg- und Seilbahn-Rundschau **9**(2), S33–S35 (1966)
Engel, E.: Nichtlineare Seilschwingungen bei Seilbahnen. ISR Int. Seilbahn-Rundschau **3**, S39–S40 (1977)
Ernst, B.: Zum Einfluss von Verdrehungen auf die Eigenschaften von zugschwellbelasteter Drahtseile. Dr.-Ing. Diss. Universität Stuttgart (2012)
Ernst, B., Wehking, K.-H.: The influence of twist on tension-tension fatigue of wire ropes, part II. OIPEEC-Bull. **102**, 5–32 (2012a)
Esslinger, V.: Fatigue testing of wires and strands. Introductory. Lectures of the IABSE-Workshop "Length Effect on the Fatigue of Wires and Strands", Madrid, Sept 1992
Evans, J.J., Chaplin, C.R.: The effect of wire breaks and overload on wire strain differences in six strand wire ropes under tensile fatigue, pp. 45–57. OIPEEC Round Table, Reading, Sept 1997
Evans, J.J., Ridge, I.M.L., Chaplin, C.R.: Wire strain variations in normal and overloaded ropes in tension-tension fatigue and their effect on endurance. J. Strain Anal **36**(2), 219–230 (2001)
Feyrer, K.: Effect of bending length on endurance of wire ropes. Wire World Int **23**, 115–119 (1981)
Feyrer, K.: Das Tragverhalten von Seilklemmen und Seilschlössern. DRAHT **35**(5), S239–S245 (1984)
Feyrer, K., Jahne, K.: Seilelastizitätsmodul von Rundlitzenseilen. DRAHT **41**(4), S498–S504 (1990)
Feyrer, K., Schiffner, G.: Torque and torsional stiffness of wire ropes. WIRE **36**(8), 318–320 (1986) (and **37** (1), 23–27, 1987)
Feyrer, K.: Klemmwinkel und Klemmwinkelvon Seilschlössern. Schriftenreihe der Bundesanstalt für Arbeitsschutz Fb 622. Bremerhaven: Wirtschaftsver-lag NW 1991 Clamping angle and clamping length of rope wedge…. HSE Translation No 14265 l, Nov 1991, Health and Safety Executive. Harpur Hill
Feyrer, K.: Reference values for the evaluation of wire rope tests. OIPEEC Bull, **63** and Wire Ind, **55**, 593–594 (1992)
Feyrer, K.: Endurance formula for wire ropes under fluctuating tension, pp. 2.1–2.10, OIPEEC Technical Meeting, Stuttgart, Sept 1995
Feyrer, K.: Torsion of multilayer round strand ropes. WIRE **3**, 45–47 (1997). Deutsch: DRAHT **48**(2), S34–S36 (1997)
Feyrer, K.: Endurance of wire ropes under fluctuating tension. OIPEEC Bull. **85**, 19–26 (2003)
Feyrer, K., Wehking, K.H.: Lebensdauer von Drahtseilen unter schwellen-der Zugkraft—Wissensstand und Ausblick. Bauingenieur **81**, 533–537 (2006)
Feyrer, K.: The service lives of running wire ropes under the influences of size effect. Lift-Report **31**(1), S20–S26 (2011)
Fuchs, D., Spas, W.: A method of calculating the hoisting cycles of a rope as a function of stress to the point of discarding, pp. I.91–I.102. OIPEEC Round Table, Delft, Sept 1993
Fuchs, D., Spas, W., Dürrer, F.: Elastische Dehnung von Förder-seilen während des Betriebs. DRAHT **47**(4/5), S281–S287 (1996)
Gabriel, K.: Anwendungen von statistischen Methoden und Wahr-scheinlichkeitsbetrachtungen auf das Verhalten von Bündeln und Seilen aus vielen langen Drähten. Vorbericht zum 2. Int. Symposium des Son-derforschungsbereiches **64** (1979)
Gabriel, K.: Fatigue resistance of locked coil ropes, pp. Ill.27–Ill.39. OIPEEC Round Table, Delft, Sept 1993
Gabriel, K., Nürnberger, U.: Failure mechanims in fatigue. Introductory Lectures of the IABSE-Workshop "Length Effect on the Fatigue of Wires and Strands", Madrid, Sept 1992
Gibson, P.T.: Wire rope behaviour in tension and bending. In: Proceedings of the First Annual Wire Rope Symposion, pp. 3–31. Engineering Extension Service, Washington State University, Colorado (1980)
Glushko, M.F.: Steel lifting ropes. Kiev Technica, p. 327 (1996)

Gourmelon, J.P.: Fatigue of staying cables, organisation and results of the research programme. OIPEEC Bull. **84** (2002)
Gräbner, P., Thomasch, A.: Zur Dimensionierung drehungsarmer Seile. Hebezeuge und Fördermittel **23**(6), S166–S169 (1983)
Haibach, E.: Betriebsfestigkeit. Düsseldorf VDI Verlag GmbH (1989). ISBN 3–18–400828–2
Haid, K.-D.: Determination of forces in strand wires. WIRE **33**, 1 (1983)
Hankus, J.: Loangsverformungen von Förderseilen. Glückauf-Forschungshefte **37**(2), S19–S21 (1976)
Hankus, J.: Regressionsmodelle der Längsverformungen und des Elastizitätsmoduls von Foorderseilen. Glückauf-Forschungshefte **39**(6), S252–S256 (1978)
Hankus, J.: The actual breaking force of steel wire ropes. OIPEEC Bull. **45**, 101–112 (1983)
Hankus, J.: Mechanische Eigenschaften von Drahtseilen. Drahtwelt **75**(4), S9–S17 (1989)
Hankus, J.: Non-typical process of the progressive weakening of a mining hoisting rope, pp. II21–II34. OIPEEC Round Table, Delft, Sept 1993
Hankus, J.: Consideration of mine hoisting rope cantraction. OIPEEC Bull. **73**, 9–19 (1997)
Heinrich, G.: Zur Statik des Drahtseiles. Wasserwirtschaft und Technik **4**(30), S267–S271 (1937)
Heinrich, G.: Über die Verdrehung der zugbelasteten Litzen. Der Stahl- bau (Beilage zu Bautechnik) **15**(12/13), S41–S45
Hemminger, R.: Drahrtseile mit Aluminium-Preßverbindungen und Kauschen. DRAHT **40**(10), S781–S785 (1989)
Hermes, J.M., Bruens, F.P.: The twist variations in a non-spin rope of a hoist installation. Geologie and Minjnbouw **19**, 467–476
Hobbs, R.E., Ghavami, K.: The fatigue of structural wire strands. Int. J. Fatigue **4**, 69–72 (1982)
Hobbs, R.E., Smith, B.W.: Fatigue performance of socketed terminations of structural strands. Proc. Inst. Civ. Eng. Part **2**(75), 35–48 (1983)
Hruska, F.H.: Calculation of stresses in wire ropes. Wire Wire Prod **26**, 798 (1951)
Hruska, F. H.: Radial forces in wire ropes. Wire Wire Prod. **27**(1), 44 (1952)
Hruska, F.H.: Tangential forces in wire ropes. Wire Wire Prod **28**(5), 455–460 (1953)
Hudler, S.: Der Elastizitätsmodul des Drahtseiles. Wasserwirtschaft und Technik **28**(30), S271–S279 (1937)
Irvine, H.M.: Cable structures, pp. 119–129. The Massachusetts Institute of Technology (1981). ISBN 0-262–09023–6
Jehmlich, G.: Anwendung und Überwachung von Drahtseilen. VEB Verlag Technik, Berlin (1985)
Jiang, W.G., Yao, M.S., Walton, J.M.: Modelling of rope strand under axial and torsional loads by finite element method, pp. 17–35. In: OIPEEC Round Table Conference, Reading, Sept 1997
Klöpfer, A.: Untersuchung zur Lebensdauer von zugschwell-beanspruchten Drahtseilen. Diss. Universität Stuttgart, Stuttgar (2002)
Kollros, W.: Der Zusammanhang zwischen Torsionsmoment, Zugkraft und Verdrillung in Seilen. Int. Berg- und Seilbahn-Rundschau **18**(2) (1974), S 49–S58 and DRAHT **26**(10), S475–S480 (1975)
Kollros, W.: Relationship between torque, tensile force and twist in wire ropes. WIRE **26**(1), 19–24 (1976)
Kraincanic, I., Hobbs, R.E.: Torque induced by axial load in a 76 mm wire rope. Comparison of experimental results and theoretical prediction, pp. 173–185. OIPEEC Round Table, Reading, Sept 1997
Leider, M.G.: Krümmung und Biegespannungen von Drähten in gebogenen Drahtseilen. Draht **28**(1), S1–S8 (1977)
Lombard, J.: Aeroplane versus rope—what happened? OIPEEC Bull. **76**, 25–29 (1998). Deutsch ISR **5** S8–S9 (1998a)
Lombard, J.: Defornation of a rope during impact from an aeroplane. OIPEEC Bull. **76**, 31–50 (1998b)
Malinovsky, V.A., Tarnavskaya, N.A.: Adapted hoist ropes. OIPEEC-Bull. **91**, 29–44 (2006)

Martin, P.A., Berger, J.R.: On mechanical waves along aluminium conductor steel reinforced (ACSR) power lines. J. Appl. Mech. **69**, 740–748 (2002)
Matsukawa, A., Kamei, M., Fukui, Y., Saski, Y.: Fatigue resistance analysis of parallel wire strand cables based on statistical theory of extreme. Stahlbau **54**(11), S326–S335 (1985)
Miner, M.A.: Cumulative damage in fatigue. J. Appl. Mech. Trans. ASNE **67**, 159–164 (1945)
Müller, H.: The properties of wire rope under alternating stresses. Wire World **3**(5), 249–258 (1961)
Müller, H.: Beziehungen zwischen Seilbeanspruchung und Seil-konstruktion. Vortrag Drahtseilvereinigung **23** (1962)
Müller, H.: Fragen der Seilauswahl und der Seilbemessung an Turmdrehkranen. Technische Überwachung **4**(2), S62–S66 (1962)
Müller, H.: Drahtseile im Kranbau. VDI-Bericht Nr. 98und dhf **12**(11), S714–S716 und **12**, S766–773 (1966)
Müller, H.: Untersuchung an Seilvergußmetallen. Goldschmidt informiert **3**(16), S23–S38 (1971)
Müller, H.: Untersuchungen an Drahtseilklemmen. DRAHT **26**(8), S371–S378 (1975)
Müller, H.: Untersuchungen an Augensleiβen.von Drahtseilen. DRAHT **27**(6), S264–S269
NEL-Report: The fatigue of 40 mm diameter six strand wire rope in a sea-water environment. National Engineering Labratory (NEL) Report No. ENER/14 for the UK Department of Energy, March 1984
Neumann, P.: Untersuchungen zum Einfluß tribologicher Beanspruchung auf die Seilschädigung. Diss. TH, Aachen (1987)
OIPEEC Recommendation No 7: Tension-tension fatigue test. OIPEEC Bull. **61**, 50 (1991)
Oplatka, G., Roth, M.: Bending Fatigue of Locked Coil Ropes in the Neighbourhood of Cast Sockets. OIPEEC Technical Meeting, Nantes (1991)
Oplatka, G., Roth, M.: Bending fatigue of locked coil ropes in the neighbourhood of cast sockets. Part 2. Influence of lubrication. OIPEEC Technical Meeting, Delft, Sept 1993
Oplatka, G., Roth, M.: Endurance of steel wire ropes under fluctuating tension and twist. OIPEEC Bull. **71**, 13–22 (1996)
Oplatka, G., Roth, M.: Non-destructive testing of resin cast sockets - possibilities and limits. OIPEEC Bull. **79** (2000)
Oplatka, G., Volmer, M.: Wieso bricht des Seil und nicht der Flügel? ISR Int. Seilbahn-Rundschau **4**, S13–S14 (1998)
Palmgren, A.: Die Lebensdauer von Kugellagern. Z.VDI **68**, S339–S341 (1924)
Paton, A.G., Casey, N.F., Fairbairn, J., Banks, W.M.: Advances in the fatigue assessment of wire ropes. Ocean Eng. **28**, 491–518 (2001)
Raoof, M., Hobbs, R.E.: Analysis of axial fatigue data wire ropes. Int. J. Fatigue **16**(7), 494–501 (1994)
Raoof, M., Huang, Y.P.: Lateral vibrations of steel cables including structural damping. Proc. Inst. Civ. Eng. Struct. Build **99**, 123–133 (1993)
Reemsnyder, H.S.: The mechanical behaviour and fatigue resistance of steel wire, strand and rope. Homer Research Laboratories, Bethehem Steel Corporation, Bethlehem PA, June 1972
Rebel, G.: The torsional behaviour of triangular strand ropes for drum winders. OIPEEC Bull. **74**, 29–55 (1997)
Rebel, G., Chandler, H.D.: A machine for the tension-tension testing of steel wire ropes. OIPEEC Bull. **71**, 55–73 (1996)
Ridge, I.: Bending-tension fatigue of wire rope. OIPEEC Bull. Nr. **66**, 31–50 (1993)
Ridge, I.M.L.: Tension-torsion fatigue behaviour of wire ropes in offshore moorings. OIPEEC-Bull. **100**, pp. 17–41 (2010)
Rossetti Rossetti, U., Maradei, F.: Check on the validity of the Miner's hypothesis for tension-tension fatigue. OIPEEC Boll. **64**, 23–28 (1992)
Schiffner, G.: Spannungen in laufenden Drahtseilen. Diss. Universität Stuttgart (1986)
Schlauderer, A.: Untersuchungen zur Zug- und Biegebean-spruchung be-weglicher Anschluss-leitungen von Leitungswagen- Stromversorgungsanlagen. Fortschritt-Berichte VDI, Reihe 13 Nr 35. Düsseldorf VDI Verlag (1990)
Schmidt, K.: Die sekundare Zugbeanspruchung der Drahtseile aus der Biegung. Diss. TH Karrlsruhe (1965)

Schneidersmann, E.O., Kraft, G., Domita, E.: Festigkeitsverhalten von Seilendverbindungen. Stahl Eisen **100**(14), S770–S775 (1980)
Schönherr Schönherr, S.: Einfluss der seitlichen Seilablenkung auf die Lebens-dauer von Drahtseilen beim Lauf über Seilscheiben. Diss. Universität Stuttgart (2005)
Setzer, M.: Feststellung der an die Dauerfestigkeit von Drähten, Litzen und Seilen für Fördereinrichtungen zu stellenden Anforderungen. Forschungs- bericht der Seilprüfstelle Bochum, Nov 1976
Siegert, D., Brevet, P.: Fatigue of stay cables inside end fittings: high frequencies of wind induced vibrations. OIPEEC Bull. **89** (2005)
Siegert, D., Brevet, P., Royer, J.: Failure mechanisms in spiral strands under cyclic flexural loading close to terminations, pp. 111–119. OIPEEC Round Table, Reading, Sept 1997
Sonsino, C.M.: Dauerfestigkeit—Eine Fiktion. Konstruktion **4**, S87–S92 (2005)
Stange, K.: Angewandte Statistik. 2. Teil, Mehrdimensionale Probleme. Springer, Berlin (1971)
Suh, J.-I., Chang, S.P.: Experimental study on fatigue behavior of wire ropes. Int. J. Fatigue **22**, 339–347 (2000)
Ulrich, E.: Untersuchungen über die Tragfähigkeit von Seileinbänden und Seilendverbindungen mit Doppelbackenklemmen. Diss. Aachen (1973)
Unterberg, H.-W.: Die Dauerfestigjeit von Seildráhten bei Biegung und Zug. Diss. TH Karlsruhe (1967)
Unterberg, H.-W.: Das Verdrillen der Seilstränge bei Kranen mit groβen Hak-enwegen. Fördern und Heben **29**(2), S90–S92 (1972)
Utting, W.S., Jones, N.: The response of wire rope strands to axial tensile loads. Int. J. Mech. Sci. **29**(9), 605–636 (1987)
Verreet, R.: Steel wire ropes with variable lay lengths for mining application. OIPEEC Bull. **81**, 63–70. ISSN 1018–8819 (2001)
Vogel, W.: Prüf—Überwachungs—und Zertifizierungsstelle IFT… 2nd International Stuttgart Rope Day, Institut für Fördertechnik und Logistik, Universität Stuttgart, 17–18 Feb 2005
Wang, N.: Spannungen in einem geraden Rundlitzenseil. Studien-arbeit. Inst. Fördertechnik, Universität Stuttgart (1989)
Wehking, K.-H., Vogel, W., Schulz, R.: Dämpfungsverhalten von Drahtseilen. Fördern und Heben **49**(1/2), S60–S61 (1999)
Wehking, K.-H., Klöpfer, A.: Lebensdauer und Ablegereife von Draht-seilen unter Zugschwell-beanspruchung. Abschlussbericht d. Forschungsprojekts AVIF und DRAHT **51**(2), S138–S144 (2000)
Wehking, K.-H.: Zukunftsausrichtung des IFT im Bereich der Seiltechnik. 1. Internationaler Stuttgarter Seiltag. **21**, S1–S14 (2002)
Wehking, K.-H., Ziegler, S.: Berechnung eines einfachen Seils mit Hilfe der Finite-Element-Methode. Fördern u. Heben **53** (12), S753–S754 (2003) und **54**(1/2), S58–S60 (2004)
Wiek, L.: Strain gauge measurements at multistrand non spinning ropes. OIPEEC Bull. **37**, 30–53 (1980)
Wiek, L.: Stress deviations in steel wire ropes. OIPEEC Round Table, Cracow (1981)
Wiek, L.: Experiments with shock loads on steel wire ropes. OIPEEC Bull. **70**, 75–91 (1995)
Woernle, R.: Ein Beitrag zur Klärung der Drahtseilfrage. Z. VDI **72**(4), S9–S17 (1929)
Wolf, R.: Zur Beschreibung der vollständigen Seilkinetik. Forsch. Ing.-Wes. **50** (3), S81–S86 (1984)
Wyss, Th.: Stahldrahtseile der Transport- und Förderanlagen. Schweizer Druck—und Verlags-haus AG Zürich (1957)
Yeung, Y.T., Walton, J.M.: Accelerated block tension fatigue testing of wire ropes for offshore use. OIPEEC Round Table, East Kilbride Glasgow, Scotland (1985)
Ziegler, S.: Einfluss der Drahtschwingfestigkeit auf die Lebensdauer von Seilen. Diss. Universität Stuttgart (2007)
Zweifel, O.: Zugkraftmessung in Drahtseilen mit Transversalwellen. Schweiz-erische Bauzeitung **79**, 21 (1961)

http://www.springer.com/978-3-642-54995-3

Wire Ropes
Tension, Endurance, Reliability
Feyrer, K.
2015, IX, 336 p. 201 illus., Hardcover
ISBN: 978-3-642-54995-3